



LIFT! More LIFT!

AHS STUDENT DESIGN COMPETITION REPORT



UNIVERSITY OF
MARYLAND



SWIFT
100% READY TO FLY



University of Maryland
 Alfred Gessow Rotorcraft Center
 Department of Aerospace Engineering
 A. James Clark School of Engineering
 College Park, Maryland 20742



GOLIATH TWIN-LIFT SYSTEM FEATURING SMART-TRUSS TECHNOLOGY

In Response to the 27th Annual American Helicopter Society
 Student Design Competition – Graduate Student Category
 LIFT! More LIFT!
 June 1, 2010

Benjamin Berry, Graduate Student (Team Leader)

David Mayo, Graduate Student

Vincent Posbic, Graduate Student

Dr. Inderjit Chopra, Faculty Advisor

Dr. V.T. Nagaraj, Faculty Advisor

Graham Bowen-Davies, Graduate Student

David Pfeifer, Graduate Student

Ananth Sridharan, Graduate Student

Dr. J. Gordon Leishman, Faculty Advisor

Acknowledgements

The *Goliath* design team wishes to acknowledge the following people and thank them for their guidance and assistance.

Dr. Vengalattore T. Nagaraj - Senior Research Scientist, Dept. of Aerospace Engineering, University of Maryland, College Park.

Dr. Inderjit Chopra - Interim Chair, Gessow Professor, and Director of Gessow Rotorcraft Center (AGRC), Dept. of Aerospace Engineering, University of Maryland, College Park.

Dr. J. Gordon Leishman - Minta Martin Professor of Engineering, Dept. of Aerospace Engineering, University of Maryland, College Park.

Dr. Roberto Celi - Professor, Dept. of Aerospace Engineering, University of Maryland, College Park.

Dr. Darryll J. Pines - Dean, Clark School of Engineering and Professor, Dept. of Aerospace Engineering, University of Maryland, College Park.

Dr. Norman Wereley - Professor, Dept. of Aerospace Engineering, University of Maryland, College Park.

Special thanks to **Rajan Sharma** for his immense and extremely appreciated assistance with the Experimentation Task.

Students of the Department of Aerospace Engineering University of Maryland, College Park:

Brandon Bush, Anand Saxena, Brandon Bush, John Tritschler, Aaron Harrington, Robert Vocke III, David McKearin, Shane Boyer, Nick Wilson, Ria Malhan, Peter Copp, Vikram Hrishikeshavan, Daniel C. Sargent, Ben King Sutton Woods.

Special thanks to

Wilco van Zonneveld – Sales Engineer, FibreMax for his invaluable advice regarding Aramid cables.

Paul Samuel – President & CEO, Daedalus Flight Systems.

David Taylor - Denied Geolocation & Navigation, ENSCO Geo/Nav.

Cindy Lokken Kator – Senior Project Coordinator, Solid Concepts, Inc.

Kim Konya – Wirerope Works, Inc.

Executive Summary

Introduction to the Twin-Lift Concept: Two is better than one...

The *Goliath* twin-lift system has been designed in response to the 2010 American Helicopter Society Student Design Competition (sponsored by The Boeing Company). The Request For Proposal (RFP) identified the need for the utilization of a twin-lift system for vertical lift of payloads that exceed the current capacity of individual rotorcraft. Significant technical challenges and high RDT&E costs are associated with developing a single heavy-lift rotorcraft of equivalent payload capacity. A twin-lift concept using certified in-service rotorcraft is highly cost-efficient. Multi-aircraft coordination, elevated pilot workload levels and increased logistical complexity have historically presented challenges towards practical realization of the twin-lift concept.

This design addresses these challenges by developing a load handling system and control architecture which takes advantage of developments in control theory, modern materials and especially the miniaturization of wireless sensing to provide real time information about the twin-lift system. The key operational challenges that have been addressed are namely:

- Multi-aircraft stability.
- Load sharing between aircraft.
- Control coordination, and
- Takeoff and landing techniques.

To meet these challenges and provide a new heavy lift service to the armed forces, the *Goliath* twin-lift system has been designed around:

- Innovative control synchronization techniques.
- Lightweight load sharing structure.
- Robust wireless communication.
- Modularity and streamlined logistics.

The resulting concept is capable of transporting greater payloads, further than any other helicopter available. This is achieved while maintaining operational safety during all stages of the flight. A comprehensive operational procedure has been developed to show the feasibility and suitability of the take-off and landing procedures.

Proven technology has been employed in innovative ways, resulting in a robust concept with a path to production projected to be only 30 months, taking into account the technology readiness levels of the system.





UNRIVALED VTOL HEAVY LIFT CAPABILITY



AFFORDABLE

- Uses existing helicopter assets
- Acquisition cost of system is a fraction of an equivalent heavy-lift helicopter

SAFE

- Innovative control system coordinates helicopter movements to prevent accidents
- Ducted rotor thrusters stabilize load swinging

LOAD STABILITY

- Vertical fins on attachment frame orient container for least drag

SMART-TRUSS

- Relays position of truss and load to helicopter controllers
- Detects and damps load oscillations using ducted rotor thrusters
- Modular and portable

PORTABLE

Modular *Smart-Truss* design breaks down into six man-portable sections and fits in the cargo hold of one CH-53E

MISSION CAPABLE

- Fulfills the US Navy Operational Maneuver From The Sea (OMFTS) mission profile
- Delivers 40,000 lb container payloads 100 nm under hot-day conditions

Design features

- Cross-platform adaptability *Minimal hardware modifications to the helicopter.
Low cost and multi-use.*
- Lightweight materials *High-strength Aluminum alloys used in spreader bar.
Improved payload capacity to 187% compared to one CH-53E.
Disassembled sections can be lifted by four personnel.*
- Modular design *Spreader bar disassembled into six sections.
Transported in the cargo hold of one CH-53E.
Ease of replacement and repair.*
- Air crew safety *Input synchronization and position regulation control system.*
- Ground crew safety *Stabilizing anti-swing mechanisms for spreader bar.*
- Streamlined logistics *Reduced payload pick-up and alignment time.*
- Payload flexibility *Swivel hook suspension can accommodate various payloads.*
- Payload dynamic stability *Dual vertical fins expand forward speed range to 90 knots.*
- User-friendly interface *Dedicated twin-lift avionics display/control module.*
- Intuitive control *Pilot control inputs automatically synchronized.*
- Real-time measurements *Sensor suite on spreader bar.
Wireless transmission network.
Interface with AFCS to utilize onboard helicopter sensors.*
- System redundancy and robustness *Stand-alone doubly redundant twin-lift avionics modules.
Multiple measurement and transmission/reception paths.
Resistance to interference/jamming.
All weather capability.*



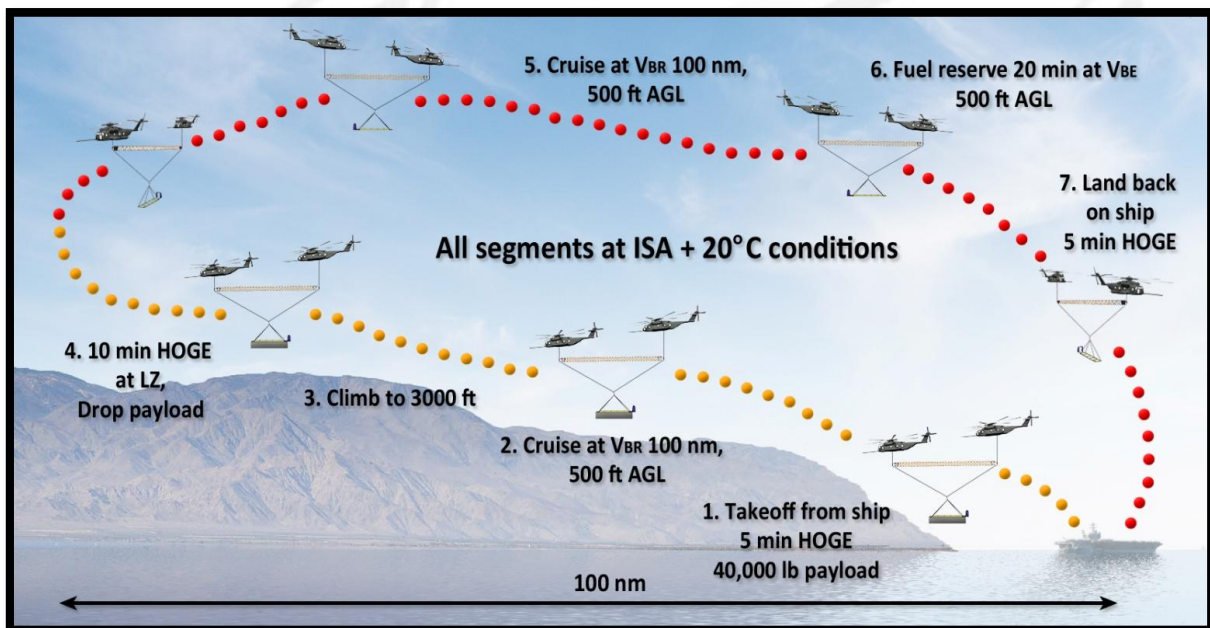
Mission Capability and Performance

The University of Maryland's *Goliath* twin-lift system utilizes existing assets to provide VTOL heavy-lift capability unrivaled by current or planned rotorcraft systems. While the *Goliath* concept remains versatile in its application, it has been designed specifically to meet the stringent requirements of the U.S. Navy's seabasing and Operational Maneuver from the Sea (OMFTS) missions.

These missions involve rapidly deploying troops, ground vehicles, and logistics equipment from the fleet directly to the inland objective point. This eliminates the reliance on traditional port infrastructure or beach-head staging areas to transport heavy cargo to inland locations.

The mission requirements from the RFP —were met and expanded to match the the OMFTS mission as outlined in the mission profile shown below. In addition the following logistical challenges of shipborne operations have been satisfied.

- Storage within a candidate ship.
- Rapid deployment.
- Transportable without specialized equipment.



Y

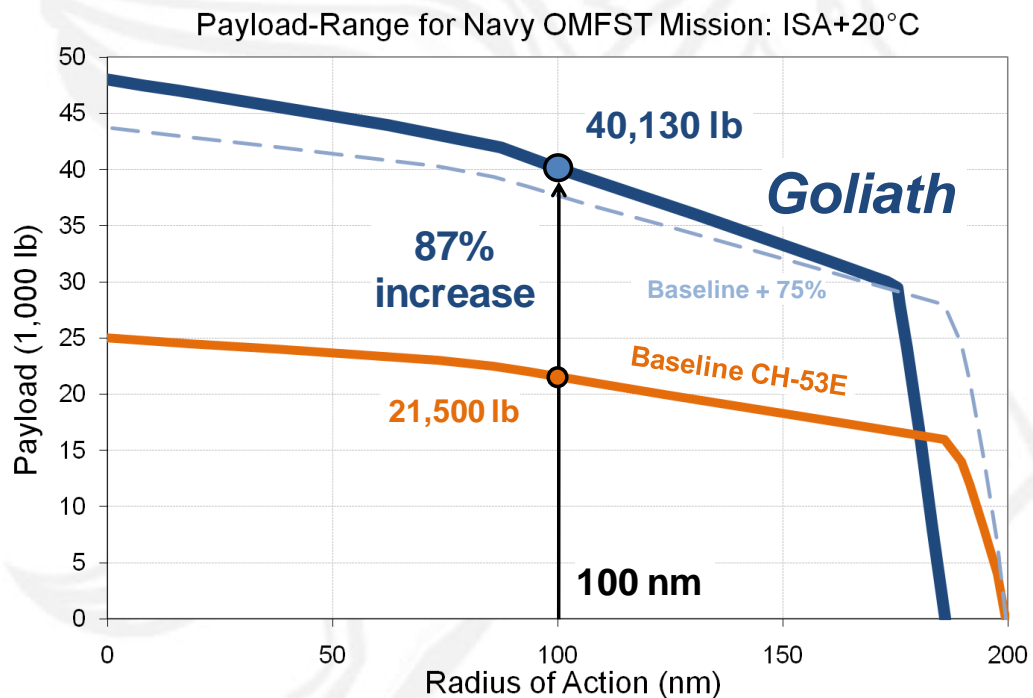
OMFTS primary mission profile using two CH-53E Super Stallions



Goliath Twin-Lift Performance

The *Goliath* twin-lift system uses two U.S. Marine Corps CH-53E helicopters to cooperatively lift and safely deliver a single external payload at best-range cruise speeds. Performing the primary Navy OMFTS mission, the *Goliath* capabilities are:

- Hot-day: Deliver a 40,000 lb ISO container to a distance of 100 nautical miles in 65 minutes and return without refueling.
- Standard-day: Deliver 51,500 lb the specified 100 nm delivery distance.



This represents an **87% payload increase** compared to a single CH-53E, the Navy's current option for lifting heavy cargo. This meets and exceeds the RFP requirement of a 75% increase in payload capability over the baseline.

The increased payload capability greatly widens the operational flexibility of military units. For example, commanders using the *Goliath* system could deploy armored tactical vehicles such as the LAV-25, Stryker, and the Buffalo MRAP, as well as heavy logistics and construction vehicles.

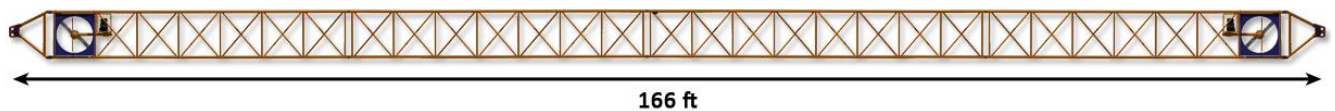


Spreader Bar – Designed for Logistics

The key focus of the *Goliath* Smart Truss was to make the logistics of the twin-lift concept a manageable reality. The operation of the twin-lift resource in a theater of war would be crippled if the logistical realities—transportation, ground handling, and storage—are not integral in its design. The *Goliath* Smart Truss has been designed from the bottom up with these in mind. The result is a twin-lift concept that:

- Can be rapidly and economically deployed on strategic missions that deliver more payload at less cost.
- Minimizes dependence on specialized aircraft.
- Demands the least possible ground support.
- Ready to be deployed at a moment's notice.

The *Goliath* Smart Truss achieves this without sacrificing payload capability. The control and stability of a twin-lift system demands a robust, accurate, and safe sensing network. This system is seamlessly designed into the *Goliath* Smart Truss, taking advantage of the unique geometry of the spreader bar to leverage state of the art, but proven, technology to provide real-time and dependable positional awareness.



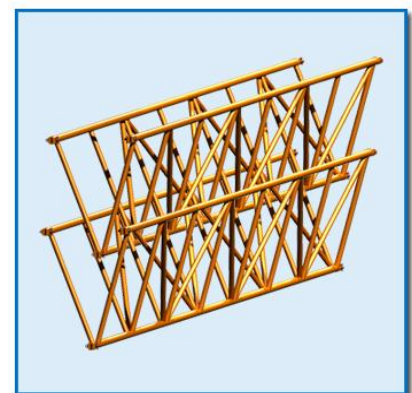
The spreader bar truss is essential for:

- Reacting lateral payload cable tensions.
- Maintaining safe helicopter separation.
- Load sharing.
- Relaying payload dynamics to the control system.

To maximize payload efficiency the spreader bar is designed from lightweight aluminum alloys.

Ground handling:

- Every element of the spreader bar is optimized around modularity and handling.
- The spreader bar consists of six identical truss elements, routinely moved by a team of four men.

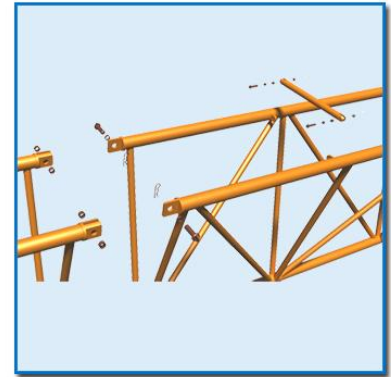


Stackable truss sections



Assembly:

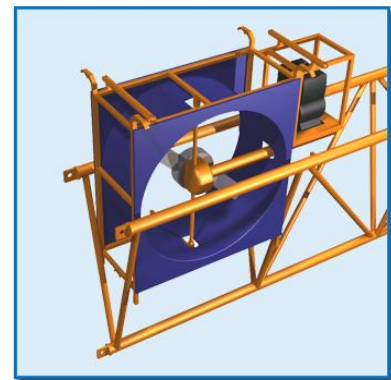
- Pin joints allow for rapid assembly of the spreader bar and minimum logistical downtime.
- Minimum unique parts provide for fast and economic repairs.
- Disassembled spreader bar elements can be stacked to reduce storage requirements and allow for greater logistical flexibility.



Easy disassembly

Modularity:

- Thrusters, sensors and spreader bar elements have been developed in coordination to maximize dual functionality, minimize weight, expedite assembly and minimize footprint.
- The vertical fin is simply bolted to the container attachment frame.
- Spreader bar elements are each identical for efficient manufacture, maintenance and repair with minimal training.



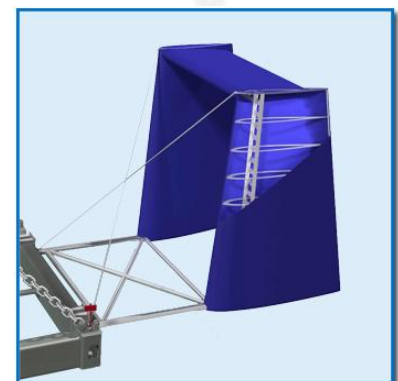
Removable ducted rotors

Transportability

- The disassembled spreader bar and all auxiliary components can be stored in the cargo hold of a single CH-53E.



Entire truss and ducted rotors fit in cargo hold of a CH-53E



Stabilizing Vertical Fins



Control of the twin-lift system

Previous attempts at utilizing a twin-lift system were thwarted by high pilot workloads at speeds as low as 20 knots. The need for control augmentation has been well-recognized, and stabilization is considered crucial to overcoming operational restrictions imposed by the system dynamics. The Goliath twin-lift design incorporates an automatic controller that features the following functions.

Multi-function twin-lift avionics module:

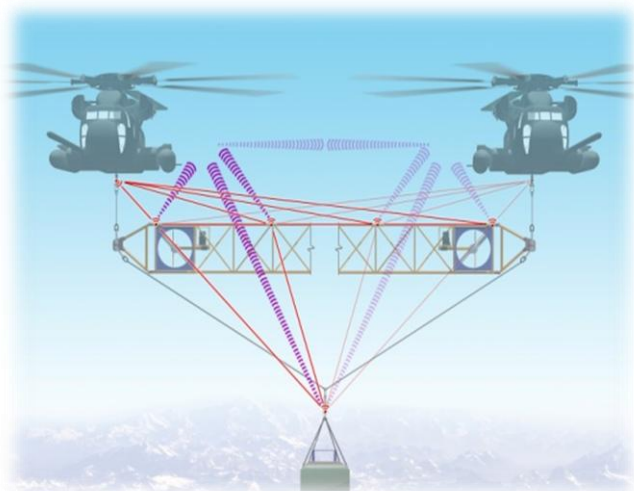
The Goliath twin-lift controller features an all-in-one pilot interface that provides real-time display and control, featuring:

- Visual cues for ease of hook-up
- Spreader bar sensor diagnostics
- Helicopter avionics monitoring
- Twin-lift control processing
- System heading dial
- Emergency jettison and synchronization disengage switch
- Immediate control transfer during emergency



Real-time measurement and separation regulation:

A sophisticated sensor suite is utilized in conjunction with the existing AFCS sensors to measure and then transmit the system states using a wireless network to two twin-lift avionics modules, one in each helicopter. These processors generate analog signals that are fed to the AFCS outer loop servos to produce the desired helicopter control changes, maintaining system stability and complete operational safety.



Instant conversion to twin-lift mode

The CH-53E helicopters are operable as fully functional independent aircraft.

- Transition to the twin-lift configuration is actuated through a simple pilot interface.
- The Goliath twin-lift system is commanded by a single Master pilot.
- The slave pilot is hands-off, the controller interprets Master pilot commands for both helicopters.
- The twin-lift system can be disengaged at anytime in case of emergency. Both pilot input and failure sensors are monitored for disengagement and/or jettison commands.
- The simple electrical interface requires no structural modifications.

Motion synchronization for single pilot control

When twin-lift synchronization is engaged:

- The master pilot's control inputs are modified by the controller
- Modified commands are transmitted wirelessly to both helicopters.
- The avionics module installed on both helicopters interprets the commands before actuating the helicopter controls.

Twin-lift specific control inputs for pilot intuition

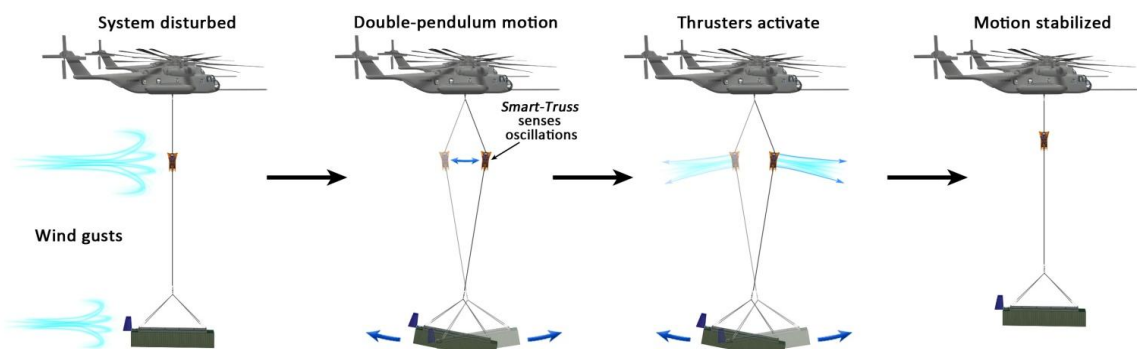
Coordinated turns require unique control architecture:

- The avionics module has a dial interface for heading commands.
- This interface preserves pilot yaw flexibility.



Active ducted rotors for stabilization

- Active thrusters damp spreader bar oscillations from helicopter motions or wind gusts.
- Wireless signals from the controller variably actuate the thrusters.
- Active damping eliminates oscillations that delay hook-up time of payload and endangers life.



Equal helicopter workload enforced

- Cargo hook load sensors provide dynamic updates to the controller for load sharing

Sequence of Operations: Carrier-Based Mission

The logistics of ground and air operations at every stage of the mission have been incorporated into the design of the *Goliath*. The following sequence of operations gives a step-by-step overview of the carrier-based mission profile.

To succeed in Seabasing operations the *Goliath* twin-lift system has been tailored to excel in the most demanding shipboard environment. Key features are:

- **Compact storage:** the *Goliath* Smart truss can be stored compactly and within the limitations of an aircraft carrier and within the cargo hold of a single CH-53E
- **Requires no specialized equipment:** Each component of the disassembled spreader bar can be carried just four people.
- **Rapid assembly:** Simple assembly and fast set up times are imperative for time critical shipboard operations.

Spreader bar hook-up

- The spreader bar is assembled, straddling the ship deck.
- Each helicopter is piloted to the ends of the spreader bar.
- Immediately after the attachment of the spreader bar cables to the helicopters the pilots initiate twin-lift control synchronization.
- The master pilot takes command of the *Goliath* Twin-Lift system.



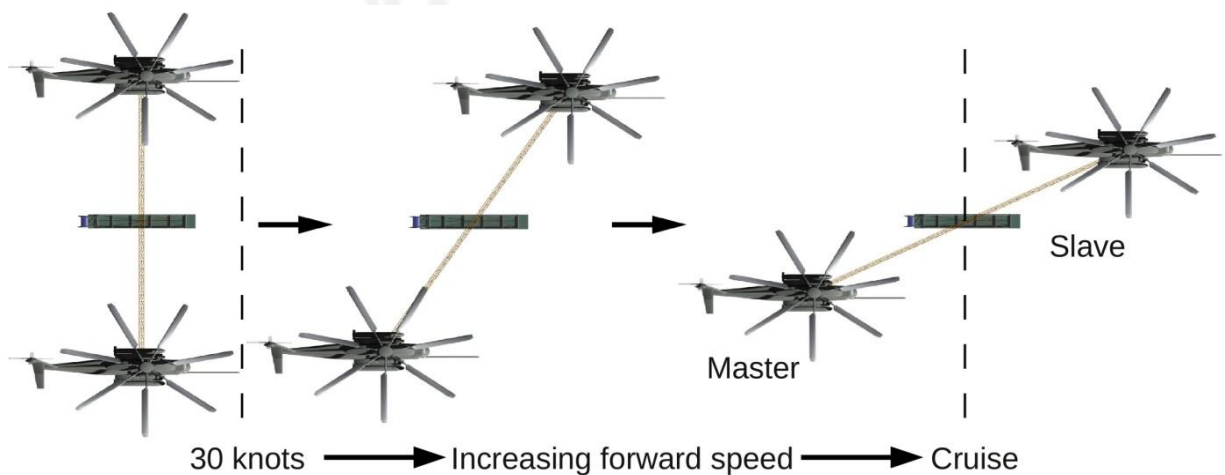
Payload pick-up

- The master pilot maneuvers the *Goliath* Twin-Lift configuration to the container payload.
- Thrusters on the spreader bar remove any oscillations and allow for precise maneuvering of the container attachment frame.
- A mechanical linkage mechanism automatically locks onto the container.
- The *Goliath* Twin-Lift system is cleared for lift off.



Transition to cruise

- The avionics module, core to the control architecture of the *Goliath* Twin-Lift system, initiates transition to cruise flight helicopter configuration.
- In cruise the master pilot trails behind and above the slave helicopter
 - This affords pilot visual cues for maneuvering and control.
 - Parasitic drag is reduced on the spreader bar at the acute, 30°, sweep angle.



Cruise flight

- The master pilot commands maneuvers in flight.
- The avionics module reinterprets the pilot's commands to coordinate both helicopters while maintaining payload stability.
- Robust failure mode analysis ensures crew safety at all times with double redundant jettison procedures.



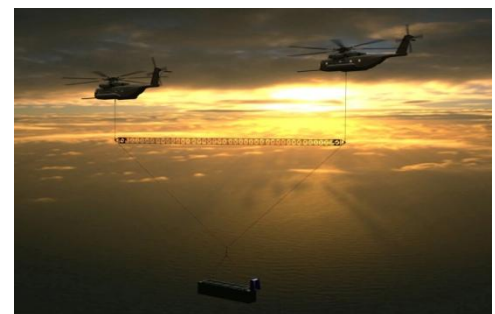
Payload drop off

- On approach, the configuration swing back into the hover orientation (airspeed trigger).
- Master pilot engages hover hold and allows controller to stabilize any oscillations.
- On touchdown, mechanical links automatically release container to allow quick egress.



Configuration return

- Return in swept configuration.
- Lightly loaded spreader bar is more susceptible to oscillations.
- Thrusters on spreader bar maintain load stability.



Ensuring Safety of Flight

The *Goliath* concept prioritizes the safety of both air and ground crews.

- The *Goliath* is a robust package involving explicit safety procedures and a network of sensors.
- Reliable inner-loop controllers run diagnostics to detect disparities in sensor information in real-time.
- In flight safety is maintained by robust controllers that coordinate helicopter positions during maneuvers.
- Ducted rotors remove potentially unstable oscillation modes from the slung load.
- Emergency hooks, located at the container, and at each helicopter are simultaneously release should a safety threatening fault be detected.
- In the event of emergency load jettison the helicopters default to heading hold to allow recovery time.
- Ground operations assume, where possible, standard slung load procedures. This requires minimum specialized training.
- Spreader bar and auxiliary equipment were designed with ground handling in mind to ensure safe assembly procedures.

The Affordable Heavy Lift Solution

Heavy lift option	Acquisition cost (mil. US\$)
New build – heavy lift	100
The <i>Goliath</i> twin-lift with 2 CH-53E	45
A single CH-53E	22
The <i>Goliath</i> twin-lift concept	0.2

The economic advantage of the *Goliath* twin-lift concept is amplified by its near zero dependence on any one particular rotorcraft. Without requiring any structural modifications the *Goliath* twin-lift system can be extended and applied to any two rotorcraft after integration to the flight controls and provide lift that is unmatched by any other single platform.

Another critical application of the *Goliath* Smart-Truss technology is in combining two medium-lift helicopters to provide heavy-lift utility on an as-needed basis without expensive procurement of specialized heavy rotorcraft and the associated overhead.



Conclusion

Goliath is a revolutionary scalable twin-lift concept that, when fully implemented, would realize enormous advancements in both civil and military vertical-lift capability. The modular design of system components reduces implementation costs, while minimizing overall system footprint. The innovative use of proven technologies ensures complete operational safety, while robust and redundant sensor suites enable precision position control. Ultimately, it is the scalability of the *Goliath* to both heavy-lift and lighter helicopters, applicability to current and next-generation rotorcraft, and adaptability to a wide variety of payloads, that gives this versatile system an unrivaled edge over most, if not all, other vertical-lift platforms.



Executive Summary for the Experimentation Task

Model Helicopter Hover Testing, Prediction, and Modification

Before bringing the concept to production, the *Goliath* twin-lift system would have to undergo a flight test program. The experimentation task of this design competition was meant to act as an analog through hover testing of a small-scale model helicopter.

The RFP requirements were as follows:

- Purchase an off-the-shelf (COTS) model helicopter of at least 30-in rotor diameter.
- Measure the hover lift-to-power capability of the baseline helicopter.
- Correlate an analysis to the baseline test data.
- Design a modification to improve lift-to-power and predict its improvement.
- Implement the modification and measure the actual improvement.

Baseline helicopter selection: the Century *Swift* electric-powered helicopter



Specifications of the Century *Swift* model helicopter

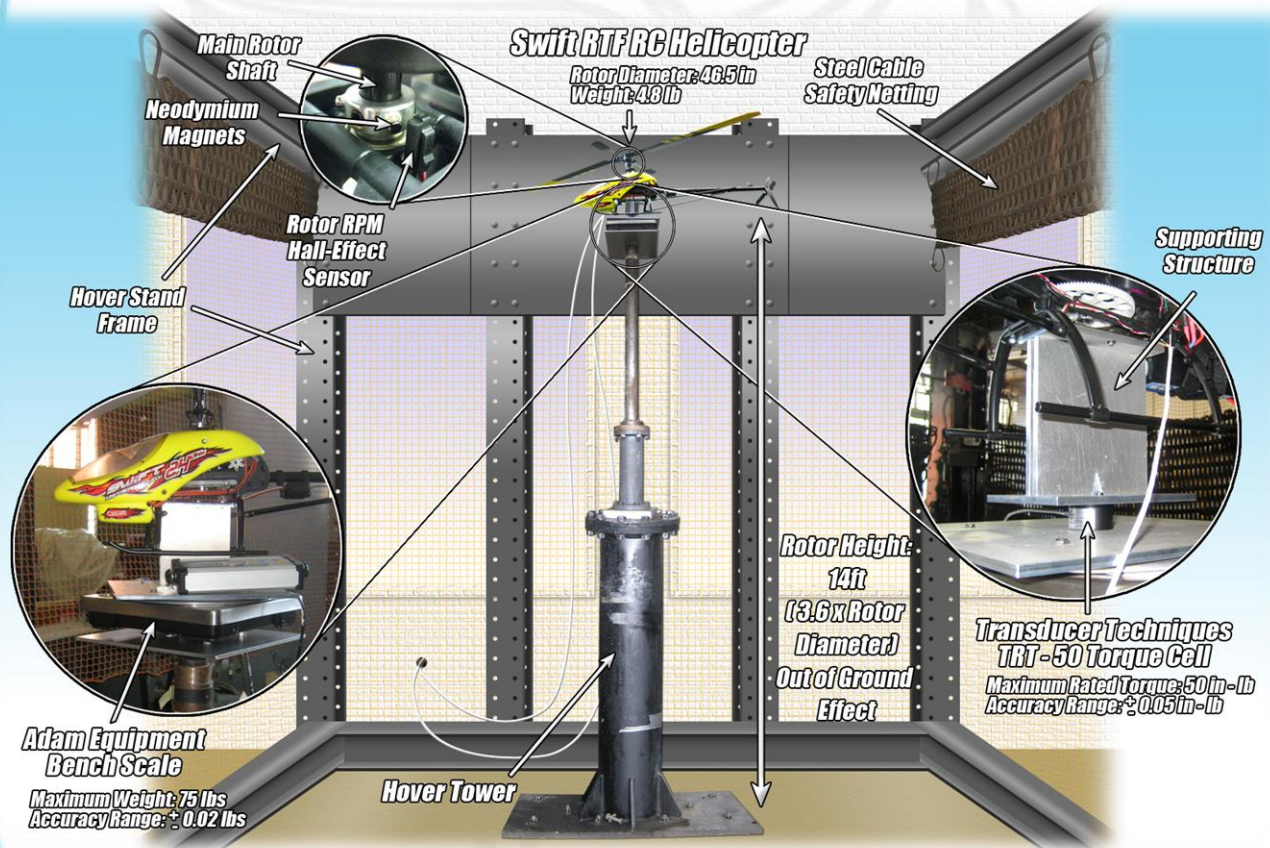
Total weight (lb)	4.8
Main rotor diameter (in)	46.5
Nominal rotor RPM	1,600-2,100
Number of blades	2
Hover disk loading (lb ft ²)	0.41
Tail rotor diameter (in)	8.5
Power system	Electric
Maximum continuous power (hp)	0.80



Measuring Lift and Power on the University of Maryland Hover Tower

The hover performance of the model helicopter was tested on the University of Maryland's Alfred Gessow Rotorcraft Center Hover Tower.

- Helicopter tested well out-of-ground-effect (3.6 rotor diameters).
- Heavy-gauge steel netting in plane of rotor for test safety.
- Adjacent control room behind thick glass windows for test observation.

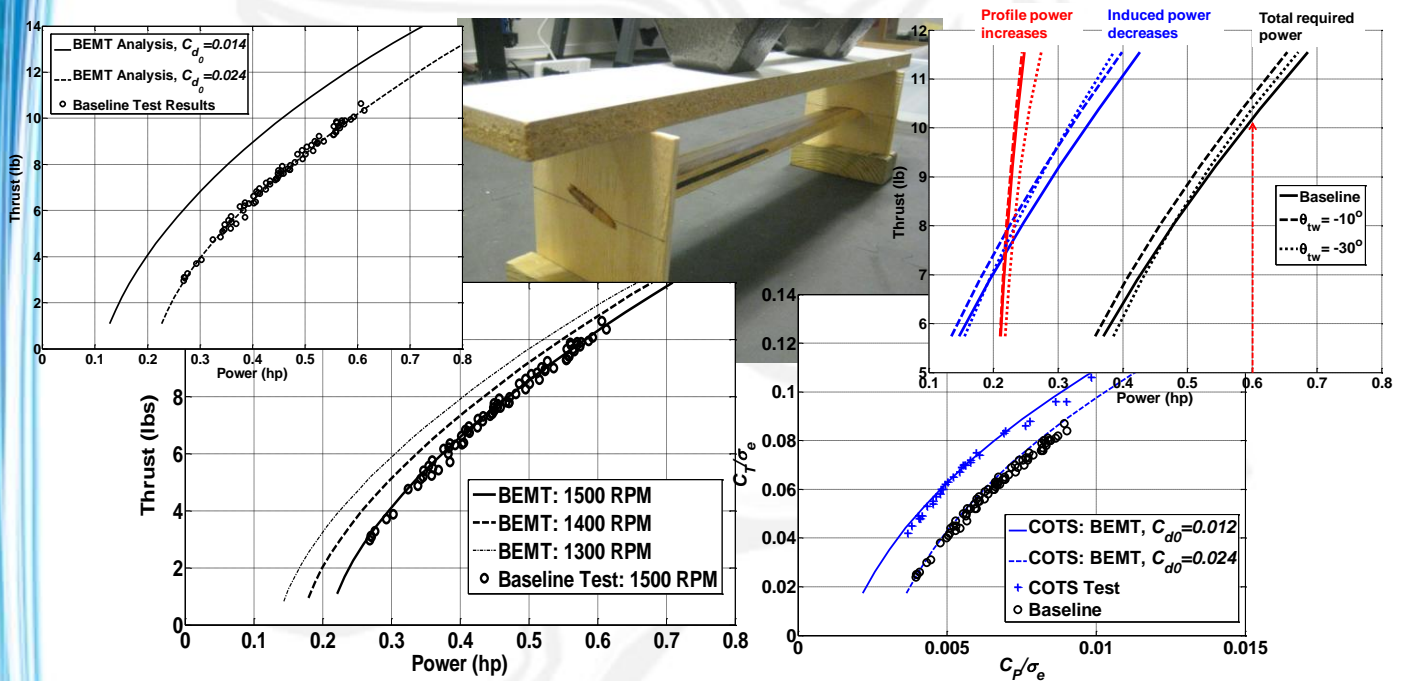


- Thrust measured with precision bench scale, accurate to 0.02 lb.
- Rotor reaction torque measured with a 50 in-lb torque cell, accurate to 0.05 in-lb.
- Rotor shaft RPM measured with a Hall-effect sensor and neodymium magnets.
- Data acquisition through a National Instruments DAQ and LABVIEW software™.



Trade Studies and Analysis Correlations

- A code was written based on Blade Element Momentum Theory (BEMT) to predict main rotor thrust and power.
- Analysis included corrections for:
 - Downwash on fuselage and measuring scale.
 - Tare profile power consumption of non-rotor blade components.
- Trade studies conducted for airfoil section, rotor RPM, blade pre-twist, and taper.
 - Experimental and model-based trade studies performed.

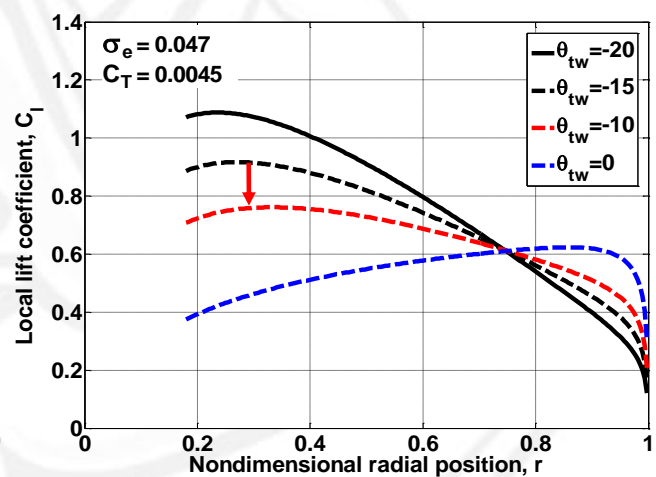
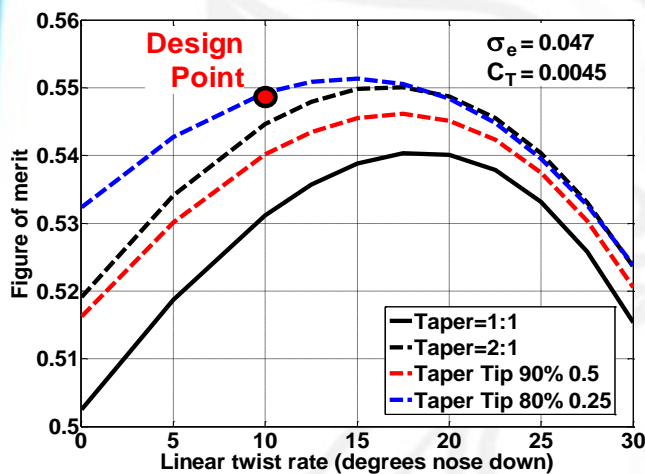


Rotor Blades Tested



Design, Prediction and Manufacturing of Custom Optimized Rotor Blades

- Optimization was conducted based on BEMT code and lessons learned from the off-the-shelf blade tests.
- Optimized blades incorporated twist, taper, and thinner airfoil sections.
- Rapid-prototyped blade core was wrapped in a bi-weave carbon-fiber sleeve for torsional rigidity.
- **Custom optimized blades increased thrust by 17% and helicopter lift by 14%**



	Custom	Baseline
Rotor diameter (in)	46.5	46.5
Number of blades	2	2
Blade chord (in), root to 0.80 R	2.16	1.71
Rotor solidity, thrust-weighted	.047	0.047
Hover disk loading (lb ft ⁻²)	0.41	0.41
Max airfoil thickness (inches, % chord)	0.22, 10%	0.25, 15%
Airfoil profile	Eppler 387	NACA 0015
Tip Reynolds number (at 1,500 RPM)	275,000	275,000
Finished blade weight, per blade (lb)	0.31	0.14



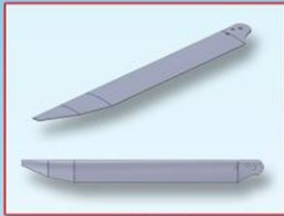


IN-HOUSE DESIGN. OUT-OF-THIS-WORLD PERFORMANCE.



Design of Optimized RC Helicopter Blades

Airfoil: Eppler 387
Twist: -10°
Taper: 4:1 Tip Taper



CAD Design



Rapid Prototype Core and Plastic Clamshell Mold



B1-Weave Carbon Fiber Sleeve

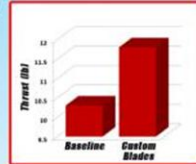
Provides Exceptional Torsional Rigidity

Wet Lay-Up Process



Mounting of Helicopter on UMD Alfred Gessow ROTORcraft Center Hover Stand

Result: 17% Increase in Thrust for Same Power Setting



10° Linearly Twisted Female Foam Mold Enforces Blade Twist



Finished Blade Mounted on Helicopter

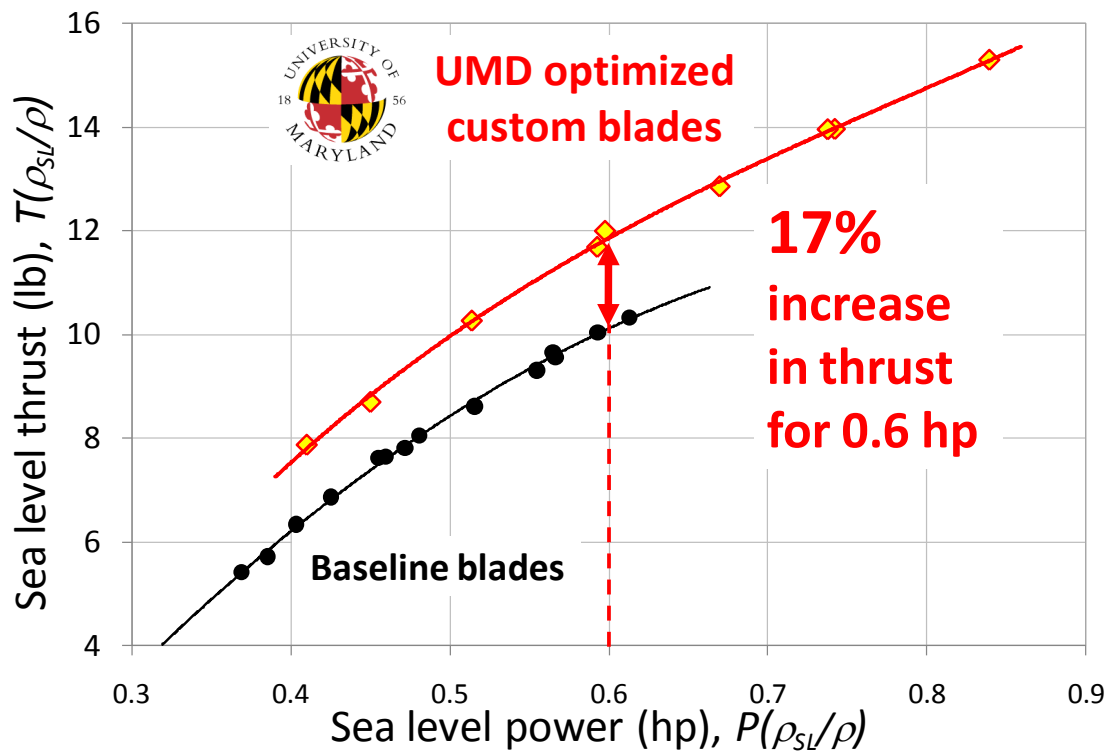


Removal from Vacuum Bag



12 Hours Under Vacuum

Custom Blade Design, Construction, and Testing



GOLIATH TWIN-LIFT SYSTEM

FEATURING SMART-TRUSS TECHNOLOGY



UNIVERSITY OF
MARYLAND

**ALL BRAWN.
ALL BRAINS.**



Table of Contents: Experimentation Task

ACKNOWLEDGEMENTS 3

LIST OF FIGURES VIII

LIST OF TABLES: DESIGN TASKXI

LIST OF TABLES: EXPERIMENTATION TASK.....ERROR! BOOKMARK NOT DEFINED.

LIST OF SYMBOLS.....XII

RFP COMPLIANCE 1

1 INTRODUCTION..... 2

2 BASELINE HELICOPTER SELECTION 3

 2.1 CANDIDATE HELICOPTER SELECTION 3

 2.2 COMPARISON METRICS 4

 2.3 ANALYTICAL HIERARCHY PROCESS 5

 2.4 TWIN-LIFT HELICOPTER SELECTION 6

3 TWIN-LIFT CONFIGURATION SELECTION 7

 3.1 DESIGN REQUIREMENTS 7

 3.2 TWIN-LIFT CONFIGURATION CONCEPTS 8

 3.3 TWIN-LIFT ORIENTATION AND SEPARATION STUDIES 11

 3.4 TWIN-LIFT CONFIGURATION SUMMARY 12

4 LOAD HANDLING SYSTEM 15

 4.1 THE SPREADER BAR 16

 4.2 DUCTED ROTOR 25

 4.3 CONTAINER ATTACHMENT FRAME 28

 4.4 VERTICAL FIN 29

 4.5 SENSOR AND COMMUNICATION SUITE 32

 4.6 CABLE SELECTION 35

 4.7 SYSTEM WEIGHT SUMMARY 36

 4.8 SYSTEM DRAG ESTIMATES 36

5 MISSION PERFORMANCE ANALYSIS 37

 5.1 PERFORMANCE CODE DEVELOPMENT 37

 5.2 MISSION PERFORMANCE ESTIMATES 39

 5.3 PERFORMANCE SUMMARY 42

6 TWIN-LIFT SLING LOAD DYNAMICS 42

 6.1 PERSPECTIVE ON HELICOPTER SLING LOADS 42

 6.2 DYNAMICS OF THE ISOLATED HELICOPTER 44

 6.3 TWIN-LIFT DYNAMICS 44

7 TWIN-LIFT HANDLING QUALITIES 48

 7.1 SURGE RESPONSE CRITERIA 48

 7.2 EVALUATION OF SURGE BANDWIDTHS 48

 7.3 MODEL DESCRIPTION 49

 7.4 RESULTS FROM ANALYSIS 51

 7.5 CONCLUSIONS 52

8	TWIN-LIFT CONTROL COORDINATION	52
8.1	CONTRIBUTIONS OF PREVIOUS WORK	52
8.2	CH-53E AUTOMATIC FLIGHT CONTROL SYSTEM (AFCS).....	53
8.3	TWIN-LIFT CONTROL DESCRIPTION	55
8.4	TWIN-LIFT STATE MEASUREMENTS.....	56
8.5	TWIN-LIFT CONTROLLER FUNCTION	57
9	TWIN-LIFT SEQUENCE OF OPERATION.....	61
9.1	ASSEMBLY AND PAYLOAD PICKUP	62
9.2	FORWARD FLIGHT	65
9.3	PAYLOAD DROP OFF AND DISASSEMBLY.....	70
9.4	RETURN JOURNEY	73
10	TWIN-LIFT COST COMPARISON	74
10.1	BASELINE PRICE COMPARISON.....	74
10.2	GOLIATH SMART TRUSS SYSTEM COMPARISON	75
11	FEASIBILITY AND PATH TO PRODUCTION	76
11.1	FEASIBILITY	76
11.2	PATH TO PRODUCTION	77
12	ALTERNATE MISSIONS.....	77
12.1	MILITARY MISSIONS.....	77
12.2	CIVILIAN MISSIONS	78
13	BASELINE HELICOPTER MODIFICATIONS.....	79
14	CONCLUSIONS.....	79

Table of Contents: Experimentation Task

1	INTRODUCTION.....	81
2	BASELINE HELICOPTER DESCRIPTION	82
3	EXPERIMENTAL SETUP	83
4	EXPERIMENTAL PROCEDURES	86
5	HOVER PERFORMANCE PREDICTION METHOD.....	87
5.1	TARE PROFILE POWER ESTIMATION	87
5.2	VALIDATION OF ANALYSIS METHOD.....	87
6	BASELINE ROTOR TESTING	88
6.1	ROTOR DESCRIPTION.....	88
6.2	TESTING RESULTS	88
6.3	CORRELATION	89
7	EXPERIMENTAL TRADE STUDIES.....	90
7.1	INCREASED BLADE LOADING COEFFICIENT	90
7.2	TWISTED BASELINE BLADES.....	93
7.3	ALTERNATE COTS BLADES	94
8	MODIFICATIONS: UMD OPTIMIZED BLADES.....	96



8.1	BLADE GEOMETRY DESIGN STUDIES	96
8.2	MANUFACTURING	97
8.3	TESTING RESULTS	99
9	TEST PROGRAM CONCLUSIONS.....	99
10	TEST PROGRAM CONCLUSIONS	100

List of Figures: Design Task

Figure 1: List of all helicopters that achieve the RFP payload requirements [Jane's 2009]	3
Figure 2: Payload-range with extended fuel, sea level hot day, slung load drag 80 ft ²	5
Figure 3: Baseline helicopter comparison weightings	5
Figure 4: AHP baseline helicopter comparison	6
Figure 5: Proposed load sharing configuration	7
Figure 6: Finally selected twin-lift configuration	13
Figure 7: Twin-lift configuration	15
Figure 8: Army studies of twin-lift using spreader bars	17
Figure 9: Military spreader bar	17
Figure 10: Telescoping spreader bar	18
Figure 11: Folding space truss	18
Figure 12: Free-body diagram of loading conditions on the spreader bar	19
Figure 13: Spreader bar "tube" optimization	19
Figure 14: Spreader bar "I-Beam" optimization	19
Figure 15: Truss optimization algorithm	20
Figure 16: Results of design trade studies for the truss	22
Figure 17: Summary of truss design	23
Figure 18: Spreader bar elements stacked within the cargo hold of the CH-53E	24
Figure 19: Assembly and modularity of spreader bar	24
Figure 20: Modular ducted rotor	25
Figure 21: Ducted rotor concepts for modularity	26
Figure 22: Exploded view of thruster assembly	27
Figure 23: Features of the load attachment frame	28
Figure 24: Construction and features of vertical fin	29
Figure 25: Remote-instrumented cargo hook	34
Figure 26: Pilot interface to control box	35
Figure 27: CH-53E fuselage drag as a function of fuselage angle of attack from wind tunnel data [Sturgeon 1993]	38
Figure 28: CH-53E power requirement validation plot at various gross weights	38
Figure 29: Specific range correlation for the CH-53E at weight of 50,000 lb	39
Figure 30: Payload-range curve for primary mission profile with 48 ft ISO container payload	40
Figure 31: Payload-range curve for an ISO container with structure internally stored on return cruise	40
Figure 32: Sensitivity of maximum payload to radius of action and payload drag for generic payload	41
Figure 33: Payload-range curves for varying ambient temperature conditions	42
Figure 34: CH-53E carrying a UH-60 on a sling	43
Figure 35: Ch-54B on a twin-lift mission	43
Figure 36: Prediction of CH53-D natural modes versus flight test data for various speeds: hover to 100 knots	44
Figure 37: Twin-lift symmetric modes	45
Figure 38: Twin-lift anti-symmetric modes	45
Figure 39: Double pendulum symmetric mode (left) and anti-symmetric mode (right)	46
Figure 40: Double pendulum symmetric mode simulation	46
Figure 41: Double pendulum anti-symmetric mode simulation	46
Figure 44: Spreader bar yawing mode	47
Figure 42: Symmetric mode frequency versus suspension length	47
Figure 43: Anti-symmetric mode frequency versus suspension length	47
Figure 45: Finding phase and pendulum bandwidths from a bode plot	49
Figure 46: Finding gain bandwidth from a bode plot	49
Figure 47: Equivalent sling load model for lateral and longitudinal modes	50
Figure 48: Longitudinal surge gain and phase	51
Figure 49: Lateral surge gain and phase	51

Figure 50: CH-53E onboard sensors available to AFCS 53

Figure 51: CH-53E control architecture 54

Figure 52: Controller for the twin-lift subsystems 57

Figure 54: Longitudinal time-history of the lower spreader bar in response to an initial disturbance 58

Figure 55: Thruster time-history for damping of pendulum asymmetric mode 58

Figure 53: Spreader bar stabilization subsystems 58

Figure 56: Vertical position of the lower spreader bar in response to an initial condition 59

Figure 57: Thruster force time-history for yaw damping 59

Figure 58: Separation regulation flow diagram 59

Figure 59: LBA and MU compensations 60

Figure 60: AFCS signal additions 60

Figure 61: Oscillation time-history of container attachment frame 61

Figure 62: Support point motion time-history 61

Figure 63: Aircraft carrier layout 62

Figure 64: Assembly of spreader bar 62

Figure 65: Approach of the helicopter to the spreader bar 63

Figure 66: Avionics box display during approach 63

Figure 67: Positioning of helicopters before hook-up 63

Figure 68: Avionics display before hook-up 63

Figure 69: Spreader bar attachment 64

Figure 70: Avionics display for lock on 64

Figure 71: Coupled helicopters in climb 64

Figure 72: Configuration layout for payload pick-up 65

Figure 73: Twin-lift turn coordination in hover 66

Figure 74: Avionics display for turn coordination 66

Figure 75: Illustration of swing maneuver 67

Figure 76: Minimum system turn radius versus airspeed 67

Figure 77: Payload path 71

Figure 78: Helicopter lateral position time-history 71

Figure 79: Helicopter vertical position time-history 71

Figure 80: Helicopter roll angle time-history 71

Figure 81: Helicopter lateral position time-histories 72

Figure 82: Helicopter longitudinal position time-histories 72

Figure 83: Payload fore-aft oscillation time-history 72

Figure 84: Payload lateral oscillation time-history 72

List of Figures: Experimentation Task

Figure 85: Century *Swift* ready-to-fly RC helicopter 82

Figure 86: Adam equipment CPWplus bench scale modifications 85

Figure 87: Torque cell mounted to capture reaction torque 85

Figure 88: Hall-effect sensor to measure rotor speed 85

Figure 89: Comparison of hover theory with NACA experiment [Harrington 1951] 87

Figure 90: Baseline rotor power polars to show effect of rotor RPM 88

Figure 91: Correlation of baseline rotor results with predictions for sea-level density and 1,500 RPM rotor speed 90

Figure 92: Predicted effect of rotor speed changes 91

Figure 93: Results for the baseline rotor with increased blade loading coefficient at 1,500 RPM 92

Figure 94: Blade loading coefficients for the baseline rotor with increased collective pitch biasing 92

Figure 95: Effect of twist on hovering performance of baseline blades 93

Figure 96: Jig built to impart nose-down twist to the baseline blades 93

Figure 97: Results for baseline blades with added twist for 1,500 RPM 94

Figure 98: Alternative OTS carbon fiber blades 95

Figure 99: Power polar for the alternate COTS blades with BEMT correlation 95
Figure 100: Twist and taper trade study results 96
Figure 101: Prediction of custom optimized blade performance 97
Figure 102: Blade root of optimized custom blades 97
Figure 103: Custom blade results, sea level thrust vs. power 99
Figure 104: Baseline and modified rotor blades 99
Figure 105: Power polar of the UMD optimized blades compared to the baseline blades 100

List of Tables: Design Task

Table 1: Comparison attributes for baseline selection	4
Table 2: Summary of baseline helicopter comparison	6
Table 3: AHP matrix comparing configuration concepts	9
Table 4: The effect of helicopter spacing and orientation on twin-lift dynamics	11
Table 5: Design specification summary	17
Table 6: Material properties	18
Table 7: Thruster specifications	25
Table 8: Thruster design parameters	27
Table 9: Design parameters of the vertical fin	30
Table 10: Comparison of available sensors	32
Table 11: Cable selection	35
Table 12: System weight summary	36
Table 13: System drag summary	36
Table 14: Estimated CH-53E parameters	37
Table 15: Sling load literature summary	43
Table 16: Twin-lift literature summary	44
Table 17: Surge bandwidth requirements for rotorcraft operating with external loads	48
Table 18: Summary of literature on twin-lift controls	53
Table 19: CH-53E AFCS components	53
Table 20: CH-53E control couplings	55
Table 21: CH-53E AFCS capabilities	55
Table 22: Twin-lift control comparison	56
Table 23: System parameter measurements	57
Table 24: Separation regulation controller gains	61
Table 25: Sensor failure during payload transportation	68
Table 26: Sensor failure during return phase	69
Table 27: Actuator failure during return flight	69
Table 28: Communication loss	70
Table 29: Controller malfunction	70
Table 30: List of <i>Goliath Smart Truss</i> components and prices	75
Table 31: Feasibility assessment	76
Table 32: Timeline to production	77
Table 33: Potential military payloads for CH-53E twin-lift concept	78
Table 34: Potential civilian payloads for CH-53E twin-lift concept	78

List of Tables: Experimentation Task

Table 35: Specifications of the Century Swift helicopter	82
Table 36: Specifications of the Outrunner 550 Plus motor	82
Table 37: Baseline rotor geometry	88
Table 38: Alternate OTS rotor geometry	95
Table 39: UMD custom rotor blade geometry	97
Table 40: Lift increase of modified blades (0.6 hp)	100

List of Symbols

$C_{l\alpha}$	Lift curve slope	σ	Solidity
C_d	Drag coefficient	σ_{max}	Maximum bending stress
C_{d0}	Profile drag coefficient	θ_c, ϕ_c	Cable deflection angles from vertical
DL	Disk loading	θ_H, ϕ_H	Helicopter pitch and roll attitude
EI	Bending stiffness	$\dot{\phi}_H, \dot{\theta}_H$	Helicopter fuselage pitch rate
F_c	Nominal compression force	ρ	Density
F_{crit}	Critical force	r	Hook to CG distance
FM	Figure of Merit	UL	Useful load
g	Acceleration due to gravity	V_{BE}	Velocity, best endurance
GW	Gross weight	V_{BR}	Velocity, best range
H	Harris and Scully's function	W_o	Empty weight
I_{xx}, I_y	Helicopter roll and pitch inertia	x_H, y_H	Helicopter longitudinal translation
κ	Induced power factor	\dot{x}_H, \dot{y}_H	Helicopter surge velocities
l_{c1}, l_{c2}	Equivalent cable lengths	$X_w, Y_v,$	Force stability derivatives
L/D	Lift-to-Drag	$X_q, Y_p,$	
M_H	Helicopter mass	$X_{\delta lon}, Y_{\delta lat}$	
m_L	Payload mass	$L_v, M_w,$	Moment stability derivatives
N_b	Number of blades	$L_p, M_q,$	
η	Design factors	$M_\delta, L_\delta,$	
P	Power	M_{θ_H}, L_{ϕ_H}	

RFP Compliance

Design Requirement	Compliance	Reference
In-service rotorcraft, 5000 lb useful load	✓	Section 2
Control system design	✓	Section 3
Design of load handling device	✓	Section 4
100nm delivery distance with reserves	✓	Section 5
Cooperatively lift 75% more payload	✓	Section 5
Twin lift maneuvers	✓	Section 9

Design criteria

Goliath	Design features
Load handling structure	<ul style="list-style-type: none"> • Modularity and Portability • Cost-efficiency
Load sharing between aircraft	<ul style="list-style-type: none"> • Operational safety • Equal workload sharing
Multi-aircraft stability	<ul style="list-style-type: none"> • Active thrusters • Separation regulation architecture
Multi-aircraft coordination and take-off/landing	<ul style="list-style-type: none"> • Avionics display/control module • Control synchronization scheme • System sensor suite • Interface with helicopter AFCS
Mechanical/electronic modifications	<ul style="list-style-type: none"> • No hardware changes • AFCS servo signal augmentation • Utilization of AFCS sensors • FAS alteration for anti-swing cuing
System redundancy	<ul style="list-style-type: none"> • Duplicate processing/sensing units • Instantaneous control transfer
Safety considerations	<ul style="list-style-type: none"> • Enforced rotor separations • Spreader bar anti-swing mechanisms • Intuitive single pilot control • Emergency jettison system • Individual AFCS activation

1 Introduction

The *Goliath* twin-lift proposal is submitted in response to the 27th Annual AHS Graduate Student Design Competition “Lift! More LIFT!”. The RFP addresses the rotorcraft community's requirement for a solution to the heavy-lift vertical takeoff and landing (HL-VTOL) challenge.

Heavy-lift helicopters have become indispensable assets to the military for fulfilling multiple roles, especially troop transport and field resupply operations. The heavy-lift helicopter is a powerful asset that has been, and is currently being, used to provide a tactical edge in the battlefield. This type of asset is particularly important when the infrastructure required to deploy conventional fixed-wing aircraft is unavailable in the theater of operations. The ability of rotorcraft to deliver personnel, cargo, and equipment is a crucial capability in overcoming natural and man-made obstacles in a timely and efficient manner.

The requirement for transporting increasingly larger payloads over greater distances has been met, so far, by designing heavy-lift rotorcraft with correspondingly expanded capabilities. Recently, the growing emphasis on armored vehicles with enhanced personnel protection to combat a determined and well-equipped adversary, has spawned the next generation of ground troop transports with offensive and defensive capabilities. The need for repeated heavy-explosive fire (IED and RPG) survivability during counter-insurgency conflict resolution, has led to the widespread use of heavily armored land vehicles for troop transport, such as the Mine-Resistant Ambush Protected (MRAP) vehicles.

Until recently, the UH-60A was rated to carry an HMMWV (light-assault vehicle) from the external cargo hook, which is rated at 9,000 lb. However, additional armor plating has resulted in increased vehicle weight, rendering the existing fleet of UH-60As incapable of transporting the next-generation of troop transports.

To date, greater payload requirements have been addressed, to some extent, through utilization of the performance margins incorporated in existing rotorcraft designs, while simultaneously upgrading or redesigning the heavy-lift helicopter fleet to match the projected vertical-lift capability for future missions. During such upgrade and redesign procedures, the technical issues associated with heavy-lift helicopters must be considered. Scaling-up transmission and engine power may be prohibitive in terms of development and operational testing, and as such the payload fraction may be severely reduced. Large rotor diameters, increased noise levels, and downwash velocities pose logistical problems and restrict the range of operating environments and increase the footprint of the rotorcraft. Finally, airframe fatigue because of higher levels of vibration result in increased service costs.

The RDT&E costs and life-cycle costs associated with a heavy-lift helicopter increase significantly with the payload capacity. Because such heavy-lift systems will not be used frequently, it is difficult to justify such high investments.

Therefore, an alternate configuration is proposed, in which two identical helicopters are used to lift a payload together, which is termed “twin-lift.” The advantages of using a twin-lift system instead of a single heavy-lift helicopter of equal capacity are multifold. First, an existing rotorcraft fleet may be modified to deliver the same payload, resulting in reduced concept implementation time. Second, the design and development costs are largely eliminated by using a current, certified, in-service rotorcraft. Thirdly, the twin-lift concept may be scaled up or down to transport a wide variety of payloads using different rotorcraft, depending on the vertical-lift capability of helicopters that are available in theater. Fourthly, the individual helicopters may be replaced with upgraded versions to expand the capacity of the twin-lift concept. Finally, the twin-lift configuration may be disassembled at any time during the working life of the individual helicopters, thereby reverting back to normal operation of the helicopter fleet. This versatility can be leveraged to reduce the twin-lift system footprint, which is of vital importance to naval operations.

To ensure the versatility of the twin-lift system, the hardware modifications to the existing helicopters must be kept to a minimum. This reduces the implementation costs of the concept, while simultaneously ensuring upgradability. Further, system modularization enables ease of component replacement and repair. A control system that regulates helicopter positions and payload oscillations reduces pilot workload for maneuvering the heavy externally slung loads, while maintaining complete operational safety. Payload pick-up and low-speed maneuvering tasks are simplified by augmentation of this control system with additional thrusters mounted on the spreader bar. Scalability and payload flexibility of the

concept is accommodated in the control system and load handling system design, allowing the twin-lift concept to be optimized for a specific set of rotorcraft, and therefore, payload weights. This capability allows the concept to be tailored for different needs depending on local availability of lifting platforms.

A multi-helicopter payload transportation system design utilizing two CH-53E Super Stallions and incorporating all these features is presented below, entitled *Goliath* twin-lift.

2 Baseline Helicopter Selection

This section describes the selection process for the baseline helicopter used for the twin-lift slung load concept. Although the focus of the RFP was on the structure and control of the load handling system, the choice of the baseline helicopter is critical to the justification of the design decisions. The RFP stipulated the following requirements of the baseline helicopter:

- The baseline helicopter should be a current, in-service rotorcraft.
- The baseline helicopter should have a useful payload of at least 5,000 lb at sea level ISA + 20°C.

2.1 Candidate helicopter selection

Figure 1 lists all the rotorcraft for which information was readily available [Jane’s 2009] that could achieve the requirements of the RFP.

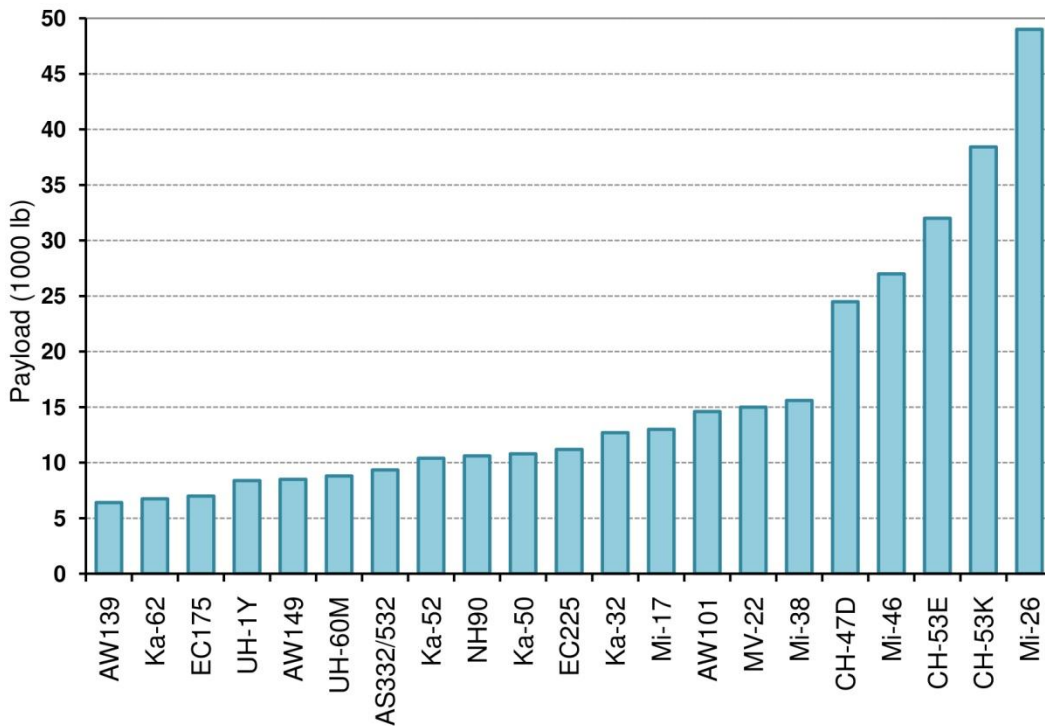


Figure 1: List of all helicopters that achieve the RFP payload requirements [Jane's 2009]

The chart in Figure 1 comprises twenty seven helicopters. The mission profile defined for this twin-lift concept is in compliance with the RFP and assumes military operations. The twin-lift concept offers a relatively inexpensive and viable option to answer the question of the next-generation heavy-lift rotorcraft to serve the U.S. armed forces. This decision lends itself to the selection of American rotorcraft only, and more specifically to rotorcraft commonly used for sling load operations. The four rotorcraft down-selected on the basis of these criteria are the UH-60M/L, the CH-53E, the CH-47D, and the MV-22

2.2 Comparison metrics

The reduced set of candidate helicopters that met the demands of the RFP was evaluated using the following list of technical and non-technical attributes. These attributes were determined by the design team to be representative criteria characteristics for the challenges faced by a twin-lift concept.

- **Maximum mission external payload:** This metric is defined as the maximum external load with which a single rotorcraft can complete the proposed mission. This metric takes into account both the helicopter’s payload capability as well as its ability to deliver the payload a specified distance. This mission payload is the baseline used to show compliance with the RFP (lift 75% greater payload than either helicopter alone). Figure 2 shows this important distinction in terms of payload carried for a given radius of action.
- **Data availability:** The availability of published data required for the accurate evaluation of performance, stability, and the control scheme of the whole system. Greater data availability affords greater confidence in the evaluation for the designed capability of each rotorcraft.
- **Inventory:** The number of aircraft currently in service in the U.S. armed forces is an important factor in the decision making. Higher availability of a rotorcraft gives a twin-lift system based on that rotorcraft greater utility and logistical flexibility, both of which translate to improved payload delivery efficiency.
- **Reliability:** Maintenance man-hours per flight-hour were used as a metric to quantify reliability.
- **Modeling complexity:** This metric compares how difficult each baseline concept is to model for performance and flight mechanics assessments. Pertinent to the time constraints of this project, this metric stresses the robustness of the helicopter simulation.
- **Hover performance in hot and high conditions:** The hover-out-of-ground-effect (HOGE) ceiling was used to compare abilities in high density altitude environments. The mission profile, defined to bring the mission in-line with a typical naval seaborne operation, demands payload performance in hot and high conditions.
- **Operating cost:** The cost per flight hour provides an economic assessment of the twin-lift system.
- **Downwash characteristics:** Rotor disk loading was used as an indication of the severity of the downwash. This metric indicated the effect of wake impingement on the load-handling structure during flight, on ground crew operation in the rotor downwash, and susceptibility to brownout.

The condensed list of attributes was assigned values shown in Table 1. Whenever applicable, published data on each rotorcraft was used to complete the table. Maximum mission external payload was calculated after modeling the power requirements and fuel burn for each rotorcraft. Figure 2 shows the relationship between maximum external payload versus radius of action for the candidate helicopters. The figure assumes a slung load drag area of 80 ft² and sea level, hot day conditions. Numeric values were assigned to qualitative attributes based on experience and preliminary research to indicate their relative importance.

Table 1: Comparison attributes for baseline selection

Attribute	Metric	UH-60L	CH-53E	CH-47D	MV-22
Payload	Max external payload (lb)	9,000	32,000	25,500	15,000
	Max mission payload (lb)	9,000	31,250	20,200	12,600
Hover hot and high	HOGE ceiling (ft)	10,600	9,500	5,500	5,400
Downwash	Disk loading (psf)	10.4	15	8.8	26.7
Data availability	-	1	1	1	1
Modeling complexity	-	1	1	1.5	1.5
Reliability	MMHPFH	15	44.1	25	15
Availability	Total proposed order	1217	227	472	360
Operating cost	Cost per flight hour (\$/hr)	2,000	15,000	2,700	11,000

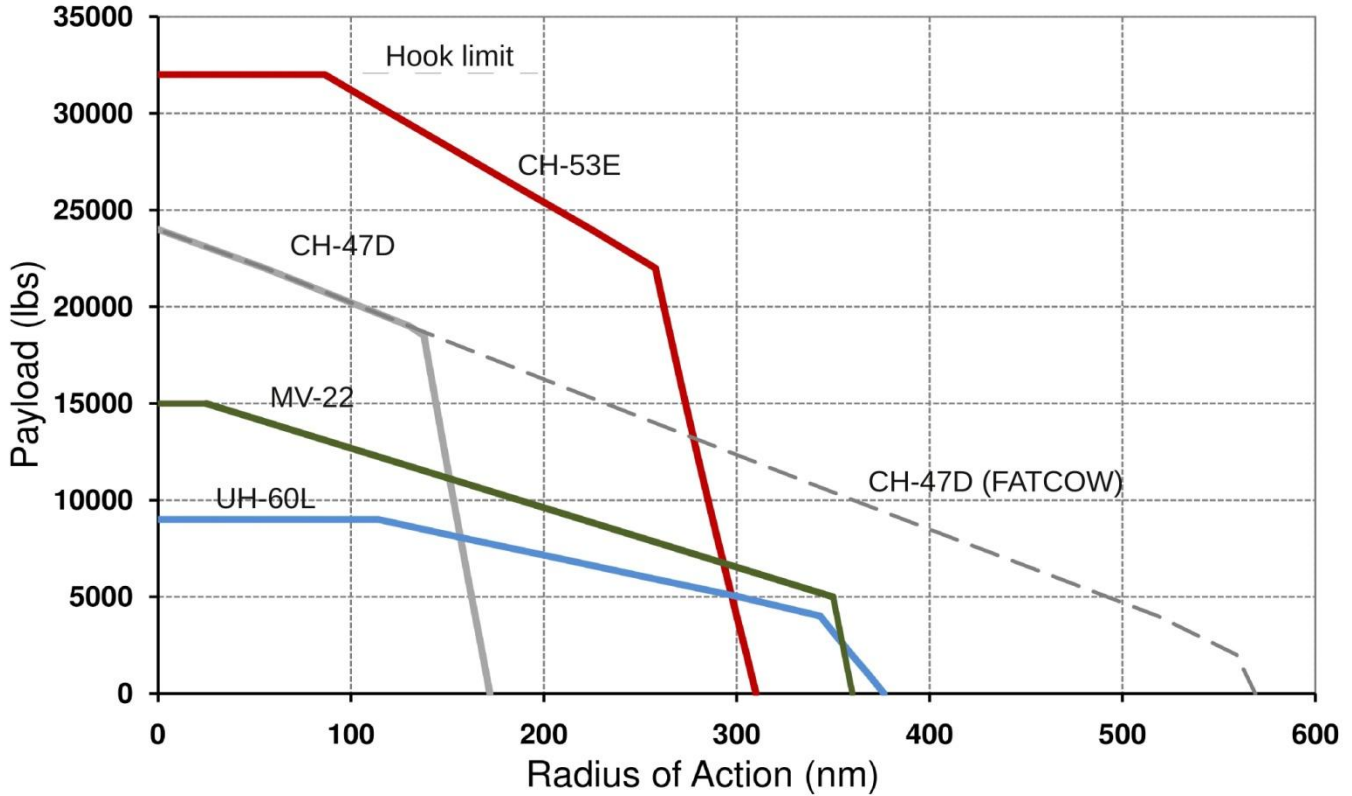


Figure 2: Payload-range with extended fuel, sea level hot day, slung load drag 80 ft²

2.3 Analytical hierarchy process

The relative importance of each of the attributes to the baseline helicopter selection was determined using an Analytical Hierarchy Process (AHP). This method is designed to assist in the comparison of several conflicting system attributes. The method achieves this goal by assigning numerical weightings to each attribute as a function of their relative importance. The relative importance of each attribute is determined by one-to-one comparison between attributes, as carried out by the designer.

Each member of the design team performed an AHP analysis of the attributes. These results were collated and then averaged. Figure 3 shows the ranked relative importance of each attribute. The maximum mission payload of the baseline helicopter was shown to be the most important attribute in comparison.

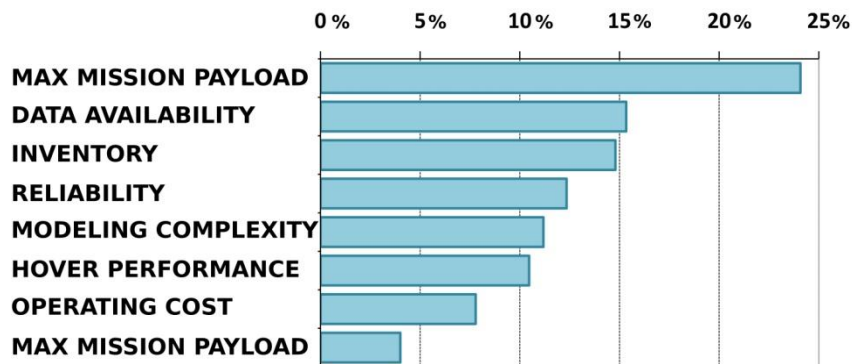


Figure 3: Baseline helicopter comparison weightings

2.4 Twin-lift helicopter selection

The attribute values were weighted with the results of the AHP process to incorporate their relative importance into the comparison study. Figure 4 shows the normalized relative scores by the candidate helicopters for each attribute. These scores were then summed to give the overall score of each helicopter, as shown in Table 2

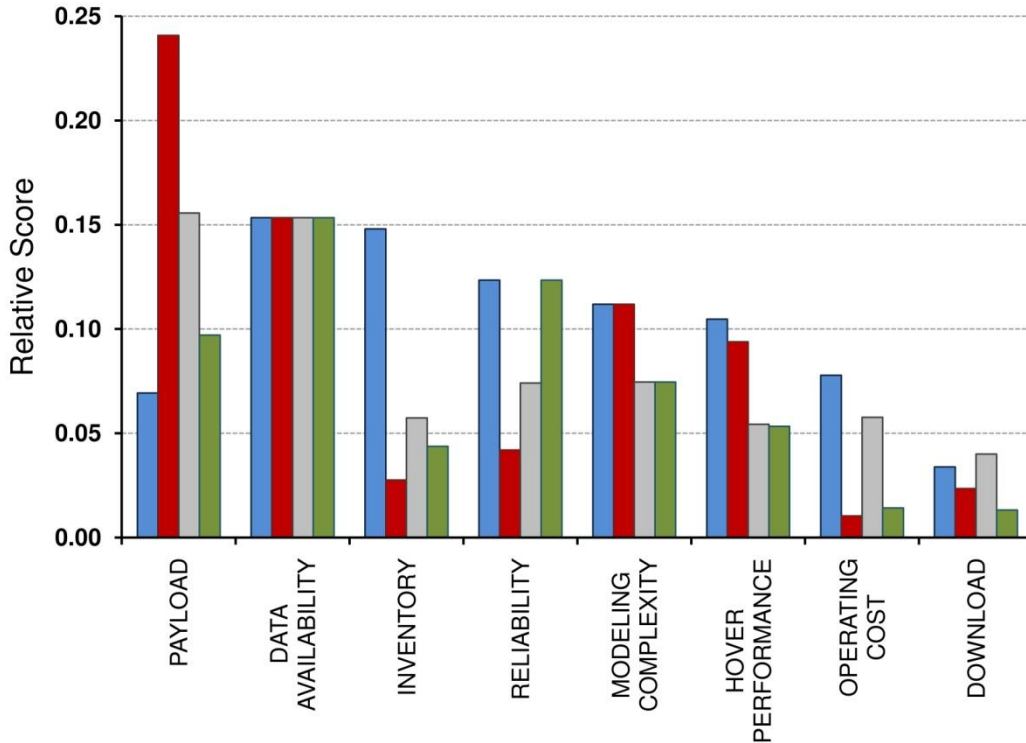


Figure 4: AHP baseline helicopter comparison

Table 2: Summary of baseline helicopter comparison

Overall Scores	
UH-60L	100.0%
CH-53E	85.5%
CH-47D	81.1%
MV-22	69.7%

The final weighted scores of the candidate baseline helicopters show that the UH-60L scores highest despite having the lowest payload capability. This outcome is bolstered largely by the huge availability advantage that the UH-60L offers.

Despite the result that the UH-60L shows best suitability for the system concept according to the AHP process, this outcome does not account for some practical concerns. There are several helicopters, and two used in this comparison, that have a greater payload capability operating alone than the combined payload of two UH-60Ls. While the RFP stressed that the helicopter and payload capability were secondary to the structural configuration and controls, it was decided that a helicopter with a higher payload posed greater technical challenges as well as a greater potential utility of the twin-lift concept. The UH-60L is not a suitable technology demonstrator because it does not overcome the challenges posed by a heavy-lift handling system. Therefore the CH-53E was chosen as the baseline helicopter around which to design the twin-lift system. Furthermore, the CH-53E is a Marine heavy-lift helicopter, suitable to the ship borne mission profile. Finally, the next generation CH-53K is currently in development and it is expected that the availability of this aircraft will further extend the capability of the twin-lift system. The modifications required to adapt the current design to the CH-53K are expected to be minimal because of the similarities across the two platforms.

3 Twin-Lift Configuration Selection

The central design decision was to find the configuration that would best achieve the desired load sharing between the two helicopters. Figure 5 shows a sketch of the final concept that was selected. This concept incorporates a spreader bar suspended between the two helicopters that enforce the nominal separation between the helicopters. The payload is itself suspended by two cables from each end of the spreader bar.

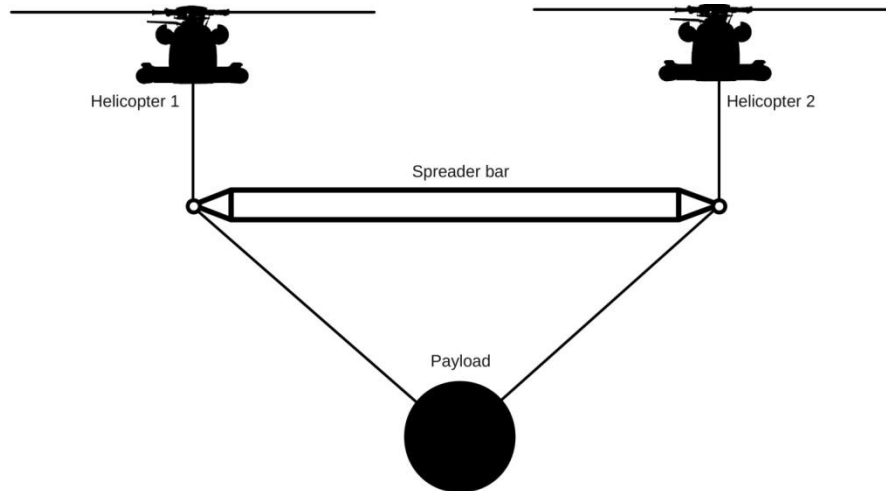


Figure 5: Proposed load sharing configuration

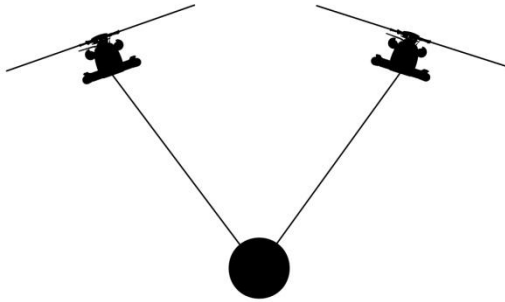
3.1 Design requirements

Concepts were developed, including several that have previously been suggested by the rotorcraft industry, for lifting configurations that take advantage of the unique requirements of the design specification. These concepts were compared qualitatively in terms of the requirements stated in the RFP and the constraints listed below. The decision process was aided by the use of the AHP decision matrix, which ranks the concepts for their suitability to the design goals. The design constraints considered were:

- **Safety:** The chosen configuration must ensure the safety of the aircrew at all times.
- **Payload adaptability:** The configuration should be easily adaptable to different scales and weights of payloads.
- **Payload efficiency:** The greatest efficiency is achieved when payload weight is maximized and the structural weight of the auxiliary load is minimized.
- **Drag:** Parasitic power requirements must be minimized to achieve the mission goals with best efficiency.
- **Helicopter modifications:** The RFP requires that the load sharing be between helicopters that are currently in use. The concept that requires the least number of modifications will be the most economic and feasible to implement. Furthermore, this provides benefits in terms of reduced maintenance and fewer specialized personnel and training, as well as allowing for the greatest fleet adaptability to the concept.
- **Modular components:** This metric considers the modularity of the concept between different aircraft and for the system in terms of component replacement and repair.
- **Maintenance:** This metric considers extra maintenance required by each concept over normal aircraft operations.
- **Download:** This considers the reduction in lifting capability from aerodynamic download on structural elements.
- **Logistics:** The ground handling, transportation and storage associated with each new concept must be considered.
- **Independent return:** This capability ranks the flexibility of the concept to perform the return portion of a mission with the helicopters now operating independently of each other. This attribute is advantageous for flight speed, efficiency, and dual mission capability.
- **Unit cost:** Considers the cost implications of each concept.

3.2 Twin-lift configuration concepts

The concepts that were compared, along with a brief description and relative advantages and disadvantages of each, are as follows:



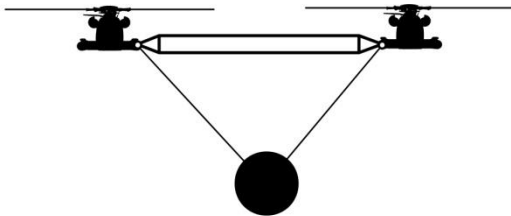
Pendant concept (PC): This is the simplest configuration possible. The payload is suspended by two cables connected directly to each helicopter.

Advantages:

- Simple with no structural development required.
- Minimum parasitic weight/drag.
- Fast hook up time.
- Minimal logistics/handling/transport of components.
- Straightforward jettison procedure.
- No download penalty on spreader bar.

Disadvantages:

- Difficult to maintain load sharing.
- Imparts a roll angle to the helicopters.
- Long cables required to maintain separation.



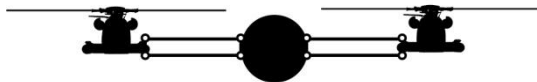
Joined pendant concept (JPC): A spreader bar is cantilevered from either helicopter. The payload is slung from the ends of the spreader bar.

Advantages:

- Enforcement of rotor and aircraft separation.
- Allows for smaller tip clearance.
- Single pendulum response.

Disadvantages:

- Forces transferred between helicopters.
- Structural modifications to airframes required.
- Jettison procedure complex. Safety concern.
- Significant download penalty on spreader bar.



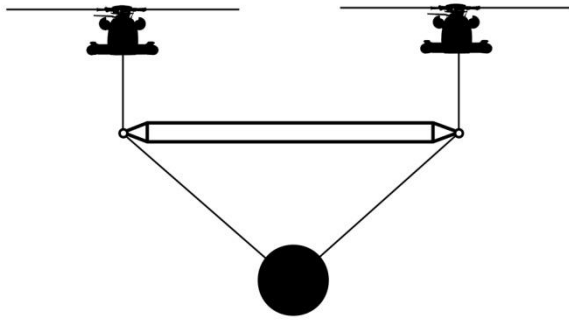
Joined loaded concept (JLC): Similar to JPC, but the pendulum is removed by supporting the payload directly on the spreader bar.

Advantages:

- Enforced rotor separation.
- Allows for smaller tip clearance.
- No pendulum stabilization required.
- Less drag (than the JPC).

Disadvantages:

- Forces transferred between helicopters.
- Structural modifications required to airframe.
- Aerodynamic download penalty on spreader bar.
- Jettison procedure complex. Safety concern.
- Difficult to adapt to different size loads.
- Large stresses on spreader bar. Increased weight.



Slung spreader bar concept (SSC): A spreader bar is slung between the helicopters with the payload suspended beneath the spreader bar.

Advantages:

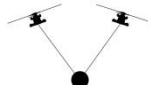
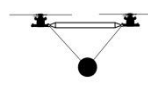
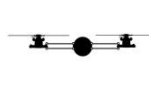
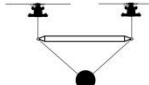
- Load sharing enforced.
- Nominal rotor clearance enforced.
- No structural modifications to airframes.
- Jettison procedure maintained. Safer.
- Independent return adaptable.
- Little or no download penalty from rotor wake.

Disadvantages:

- Larger parasitic drag area of concept.
- Larger structural weight of concepts.

Table 3 shows the results of the AHP comparison of the various concepts considered for the overall twin-lift configuration. The conclusion from the AHP selection analysis is that two concepts, the pendant concept and the spreader bar concept, are the best designs to meet the objectives of the RFP. Although the spreader bar concept scores marginally higher, the qualitative and subjective nature of the comparison calls for a more rigorous study of the values provided by each concept

Table 3: AHP matrix comparing configuration concepts

					
Attributes	Importance (%)	Pendant	Joined Pendant	Joined Loaded	Slung Spreader Bar
Safety	24.3	1	1	1	7
Adaptable to loads	14.8	7	7	1	7
Weight	13.0	9	5	1	5
Drag	10.8	7	5	7	5
Modifications to airframe	7.5	9	1	1	9
Modular components	5.9	9	5	7	7
Maintenance	5.4	9	5	5	7
Download	5.2	1	1	1	1
Ease of ground handling	5.5	10	2	2	5
Independent return	4.9	9	1	1	7
Unit cost	2.6	9	1	1	5
Overall ranking		99%	54%	37%	100%

Pendant configuration:

The advantages of the pendant configuration are time and payload efficiency. This system is suited to lifting loads of relatively small dimensions in comparison to the rotor diameter of the helicopter. The concept requires no special modifications or equipment with none of the associated logistical complications. The pendant configuration is not susceptible to the unstable divergent mode of the open-loop twin-lift system (see SECTION 6). Furthermore, studies of this concept [Prasad 1987] showed that load path tracking, while maintaining a constant

helicopter separation between the helicopters, gave a superior response with the pendant configuration compared to a spreader bar configuration with little or no degraded controller operation.

The disadvantages of the concept are the non-zero trim roll angles and large tether lengths required to maintain an acceptable separation between the helicopters. The large roll angles also require excess rotor thrust to maintain helicopter separation, which offsets some of the payload benefits compared to the spreader bar configuration. Furthermore, pilot disorientation and discomfort when enduring sustained roll angles has to be considered. To reduce the roll angle, a long pendant tether length may be used. This approach, however, comes with drag penalties as well as practical issues. For example, to limit the roll angle to 10° with a full payload and a one diameter rotor tip clearance requires a tether length of 600 ft. This issue results in an additional 150ft^2 of parasitic drag area, which then more severely limits payload-specific range characteristics.

Spreader bar configuration:

The advantages of the spreader bar configuration are that it does not suffer from altered trim roll angles, and load sharing is more even between the aircraft compared to using the pendant configuration [Prasad, 1989]. This configuration allows for shorter tethers and, in turn, better compactness. Prasad [Prasad 1989] also showed that the control travel, and hence pilot workload, for load path tracking is reduced compared to the pendant configuration.

The disadvantages of the concept include the additional parasitic drag of the spreader bar and the introduction of the oscillatory, unstable modes of helicopter lateral separations (see SECTION 6). These undamped modes also require careful tuning of the control system feedback. Ground handling and pick up operations are more complicated with this concept, and the return phase of the mission incurs additional drag of the spreader bar and cables. This drag will not be present with the pendant concept if the cable is winched up.

Conclusions:

The spreader bar configuration was ultimately chosen as the best solution to meet the design requirements. This concept offers a relatively compact configuration, a more neutral roll attitude, and reduced control travel to perform the candidate maneuvers. Robust controllers, in conjunction with real-time system state sensors, are capable of maintaining helicopter stability and control and, if operated in a redundant manner, can ensure complete crew safety. The trim roll angles and large cable drag of the pendant configuration were deemed to be unacceptable, and this deficiency overshadowed the improved natural stability characteristics of this configuration.



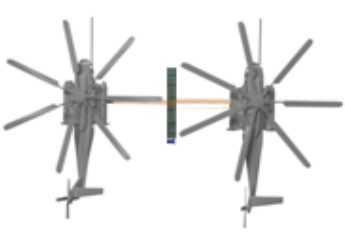
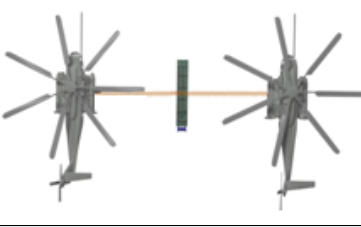
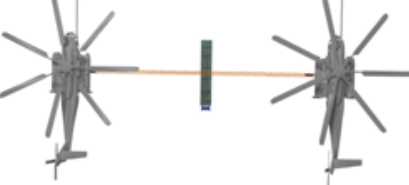
The following are the important features of the chosen spreader bar twin-lift configuration:

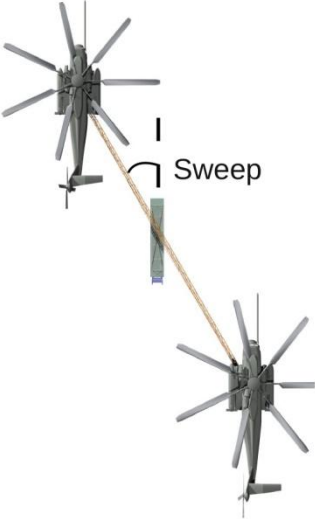
- **Safety:** The separation of the helicopters is held to a defined distance, maintaining rotor tip clearances.
- **Emergency jettison:** The independent aircraft allows for greatest flexibility in load jettisoning in the event of the malfunctioning of a single aircraft, thus offering the greatest safety of the configurations considered.
- **Aircraft adaptability:** The spreader bar is carried from the cargo hooks that are normally used by the helicopter, which requires no structural modifications to the helicopter, rendering the configuration readily and economically adaptable to the available aircraft.
- **Payload flexibility:** Load suspension is ultimately from a single point that is adaptable to different sizes and shapes of payload, and so offers a payload hookup interface that is common to current external payload rigging procedures.
- **Flexible return:** The configuration easily adapts to independent return of the helicopters, or return with the spreader bar slung between helicopters, or even with a single helicopter supporting the spreader bar.
- **Load sharing:** The spreader bar shares the payload between the two aircraft, which is a minimum weight configuration that maximizes payload efficiency.
- **Minimal rotor wake effects:** The spreader bar is suspended mostly out of the main rotor wake effects to minimize aerodynamic download penalties.

3.3 Twin-lift orientation and separation studies

The effect of different tether lengths and helicopter lateral and vertical spacing are summarized in Table 4

Table 4: The effect of helicopter spacing and orientation on twin-lift dynamics

Criterion	Impact
Zero vertical offset	
	<ul style="list-style-type: none"> • Download on spreader bar in cruise flight offsets payload capacity. • Low speed forward flight: unequal load sharing. • Sling sets interchangeable (helps ground crew operations).
One fuselage depth (20 feet) vertical offset	
	<ul style="list-style-type: none"> • No significant download in forward flight. • No impact on lateral-vertical dynamics. • No adverse effects on yawing of spreader bar.
Zero rotor tip separation	
	<ul style="list-style-type: none"> • No in-plane rotor tip clearance. • Small allowances for helicopter position drift. • Tight tolerances lead to unattainably fast sensor signal processing requirements. • Safety concerns.
0.5 diameter (40 ft) tip separation	
	<ul style="list-style-type: none"> • More clearance – safer. • Allows for some time delay in detecting relative position drift. • Used in combination with vertical offset at low speeds. • Helicopters cannot execute individual yaw attitude changes without colliding.
1 diameter (80 ft) tip separation	
	<ul style="list-style-type: none"> • Additional safety margins when used with fuselage vertical offset. • Increased spreader bar drag in forward flight. • Helicopters can yaw relative to spreader bar without colliding.

Spreader bar sweep	
	<ul style="list-style-type: none"> • A significant decrease in drag for sweep angles beyond 45°. • Trail helicopter pilot has visual cues (attitude and tip-path-plane) of the lead helicopter.

Conclusions:

Based on the comparisons summarized in Table 4, the following configuration was selected to ensure operational safety. The features of the selected configuration are:

1. One diameter (80 ft) clearance between the rotor tips of the two helicopters.
2. The longitudinal axis of the spreader bar is oriented at 30° to the direction of flight.
3. Vertical offset of one helicopter depth vertical offset (with the trail helicopter above the lead helicopter).

The foregoing configuration enables the pilot of the trail helicopter to observe the attitude and rotor tip-path-plane of the lead helicopter with better situational awareness. A vertical offset can be introduced through different spreader bar tether lengths.

3.4 Twin-lift configuration summary

Figure 6 shows the selected twin-lift concept. The configuration consists of two helicopters separated by a spreader bar suspended from the cargo hook of each helicopter. The length of the spreader bar is equal to two rotor diameters for a first-order design. This length is evaluated further in the detailed design of the spreader bar (see SECTION 4). The payload is suspended by cables from the ends of the spreader. The spreader bar is swept back 60° from the direction of flight and the trailing helicopter is raised by one fuselage height above the lead helicopter.

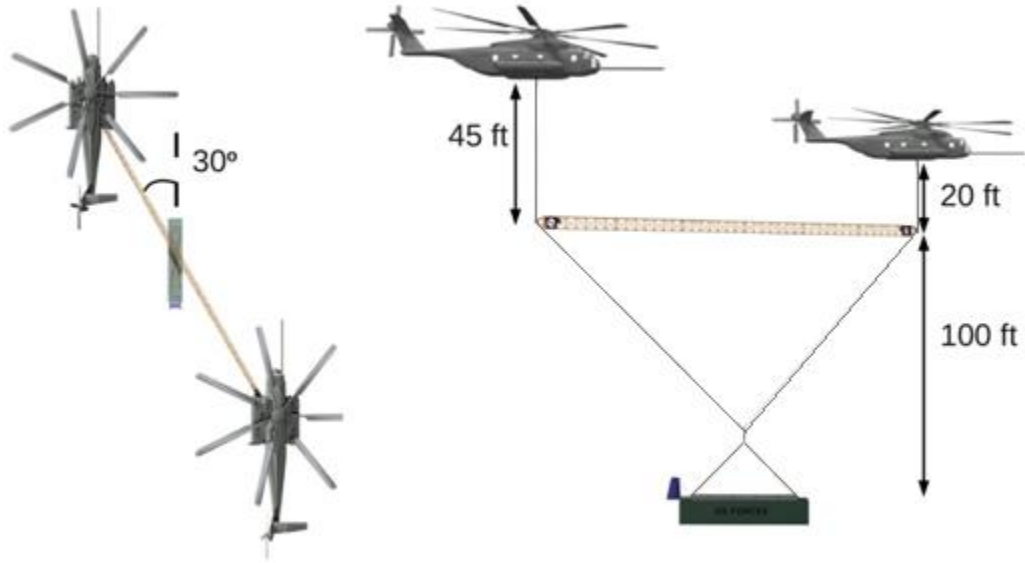


Figure 6: Finally selected twin-lift configuration



Spreader Bar Detail

Modularity

Avionics Module



Wireless Sensor Unit x 4



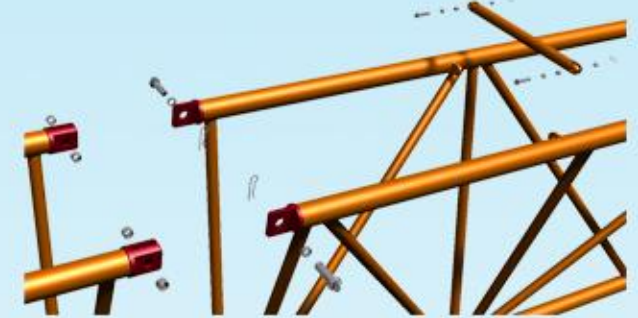
Rear View



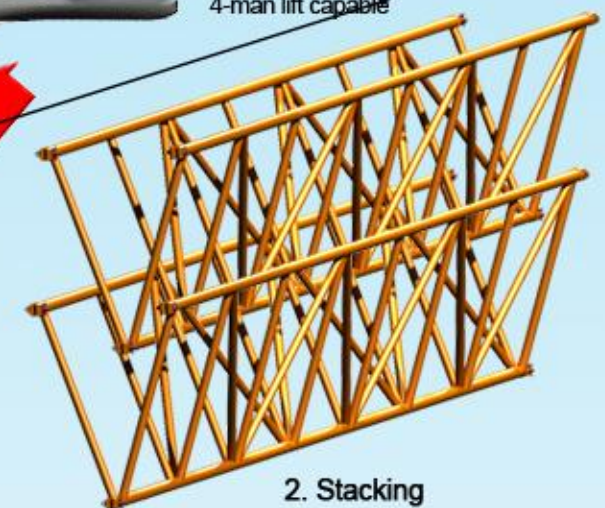
Side View

26.4 ft, 236 lb
4-man lift capable

3. Storage for Transport



1. Disassembly

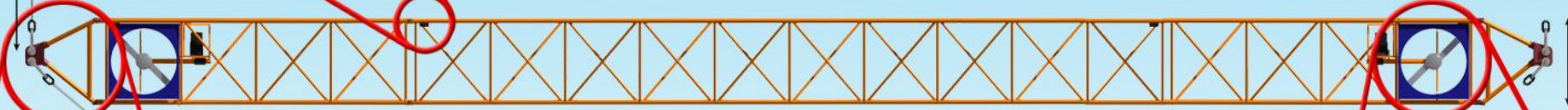


2. Stacking

166 ft, 1950 lb



20 ft



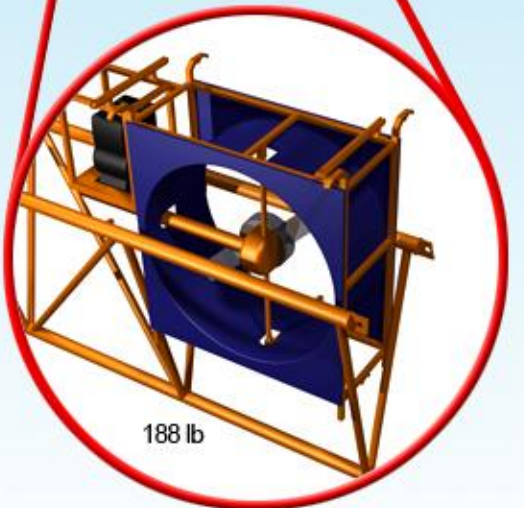
4 ft

Remote Instrumented Cargo Hook



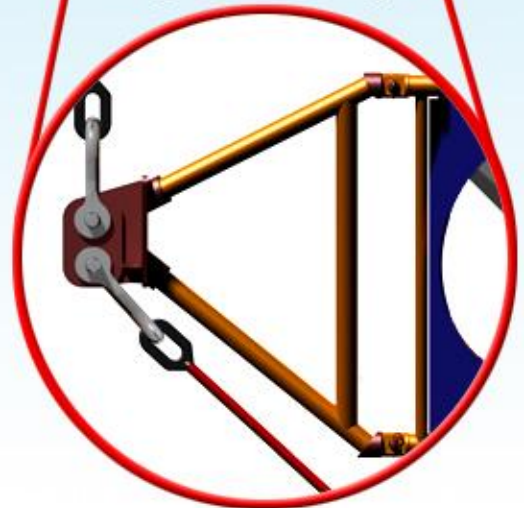
2.8 ft
180 lb

Ducted Rotor for Active Stabilization



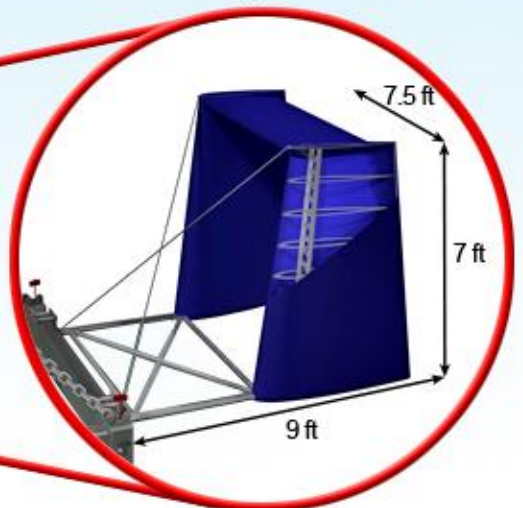
188 lb

Hinged End Fitting



4.5 ft

Stabilizing Vertical Fin



7.5 ft

7 ft

9 ft

100 ft

4 Load Handling System

This section describes the structural components of the twin-lift concept. The key components that are considered in this section, as shown in Figure 7 are as follows:

- 1) The spreader bar, which distributes the payload and enforces separation between the aircraft. Control thrusters are positioned on the spreader bar to assist with the stability and control of the system.
- 2) The container attachment frame, which distributes the payload weight to the support cables and houses the vertical fin.
- 3) The vertical fin, which orients and gives directional stability to the payload.
- 4) The sensor suite, which provides the system information required by the pilot and on board computer to both control and stabilize the configuration.
- 5) The miscellaneous fittings and cables, which are unique to this configuration.

Each section is organized as follows:

- a) The specification of the design requirements of each component.
- b) Conceptual evaluation.
- c) Design methodology and implementation.
- d) The resulting design.

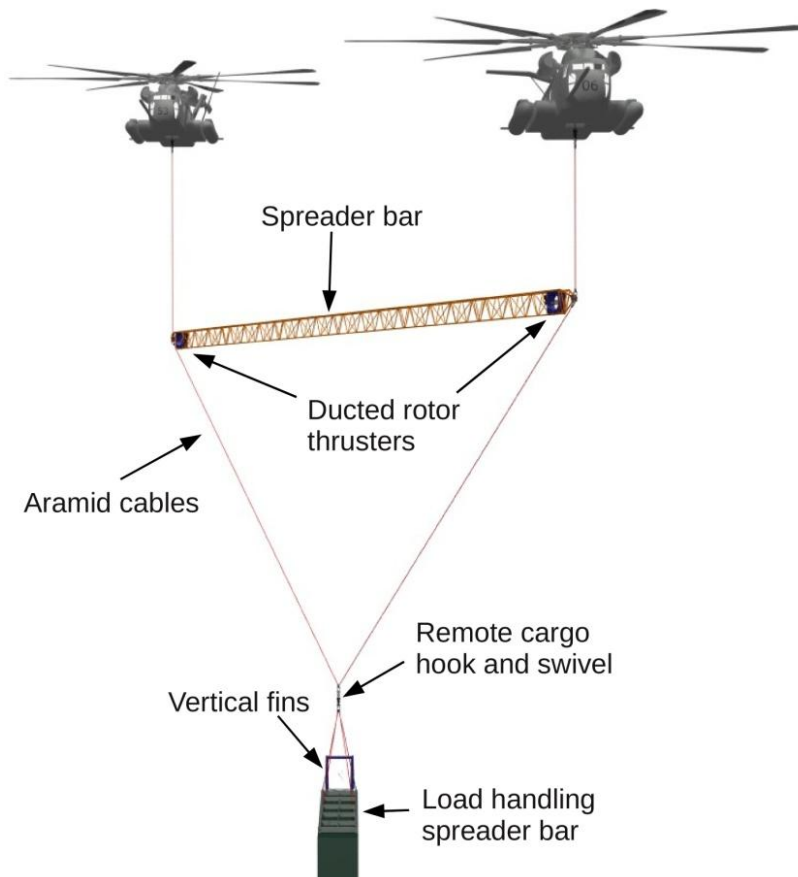


Figure 7: Twin-lift configuration

The unique features of this design are:

- **Modularity:** Great emphasis has been placed on maintaining the modularity of all components. The entire load handling structure can be disassembled and stored in a 7-by-7-by-30 ft volume within half-an-hour. This modularity allows the designed load handling structure to fit within the cargo hold of a CH-53E, the candidate aircraft.
- **Proven technologies:** All technologies employed in this configuration are tested and proven. The sensor suite has been carefully chosen to be robust and fully operational in all weather conditions. Redundant modular components are available OTS for economic integration into the system.
- **Logistics:** The modular components of the configuration have been sized to consider the logistics of ground handling, transportation, and storage. No element of the configuration requires more than four people without special tools to maneuver and assemble.
- **Passive and active stability:** The configuration incorporates both active and passive stability measures that allow for the controller to maintain the stability of the load throughout the mission.

4.1 The spreader bar

4.1.1 Design specifications and requirements

SECTION 3 has detailed the configuration selection and showed that the spreader bar concept provided the best combination of safety, controllability, and efficiency for the given mission. The design specifications that must be met to achieve this configuration are the following:

Spreader bar length: The spreader bar enforces the separation between the two helicopters. The rotor diameter of the CH-53E is 78 ft. The minimum separation required of the spreader bar is, therefore, 78 ft assuming the helicopters remain in the same horizontal plane. However, to maintain the safe operation of both helicopters, a design factor was used to increase the horizontal tip clearance between the helicopters. Expressed in terms of rotor diameters, a design factor of two indicates a separation between rotor tips of one diameter or two diameters between the fuselages. However, increased safety by a greater tip clearance means increased system weight. First-order trade studies assume a design factor of two, or a spreader bar length of 160 ft, to be investigated further in the subsequent studies.

Maximum payload: The theoretical maximum payload was used as the design point. The CH-53E has a maximum payload capability of 32,000 lb on its external hook and the RFP calls for a shared payload of 1.75 times this value. The resulting design load for the spreader bar, therefore, is 58,000 lb. The actual mission payload will be smaller to meet the requirements of the RFP. However, this “over design” is intentional to ensure the spreader bar configuration remains fully capable for alternate missions.

Compressive loading: The compressive loading on the spreader bar is a function of the maximum payload and of the cable angle to the slung load. Assuming a nominal cable angle of 45° and the specified payload, these values result in a compressive force on the spreader bar of 29,000 lb.

Weight: To maximize the efficiency of this particular configuration, the structural weight was kept to a minimum. Furthermore, a minimum weight will reduce the bending loading on the spreader bar. This outcome is in competition with safety and operational considerations, which are functions of spreader bar length and cable angle. Safety factors, consistent with industry standards, are built into each component of the configuration.

Parasitic drag: To maximize efficiency of the helicopters and to achieve the mission range requirements, parasitic drag calculations were carried out during the design process.

Storage and transport: The logistics of the spreader bar operation are considered in differentiating between the concepts. These logistics included ground handling, transportation to the operational theater and storage of the spreader bar.

Alternative usage: The potential to use the spreader bar in secondary roles when not required for heavy lift operations. Possibilities may include radio antennae and building supply materials. This capability assumes limited application for the configuration, or long periods between its deployments, and may not be applicable in some situations.

Scalable: Assuming that aircraft demand may not at all times allow for the designed aircraft to be available, a capability to scale the load handling system to different aircraft offers versatility, economy, and potential time savings.

Priority in design given to helicopter safety: Safety of both helicopters and their crew must be a design priority if the configuration is to succeed.

Table 5 summarizes the design specifications where Need (N) stands for “Must have” and Want (W) stands for “Good to have.”

Table 5: Design specification summary

Description	Requirement	Need/Want
Spreader bar length	160 ft	N
Maximum payload	58,000 lb	N
Compressive loading	29,000 lb	N
Weight	Minimum	N
Parasitic Drag	Minimum	N
Storage and Transport	Yes	W
Alternative uses	Yes	W
Scalable to different helicopters	Yes	W
Enforced helicopter safety	Yes	N

4.1.2 Review of spreader bar technology

To determine if there is a preexisting structure that would serve as the spreader bar giving a technologically ready and economic solution, a review of the published literature on spreader bars was conducted.



Figure 8: Army studies of twin-lift using spreader bars
[Meek 1970]

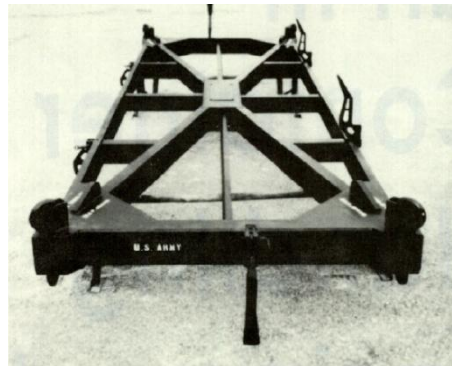


Figure 9: Military spreader bar

This twin-lift configuration is not a new one. The twin-lift concept was investigated using two CH-54B helicopters [Meek 1970], shown in Figure 8. In this exercise, the spreader bar is constructed as a linearly tapered truss structure. This idea takes advantage of the high specific stiffness of a truss structure, together with the aerodynamic drag benefits of several slim members compared to a single bluff body. The effect of structural taper on weight was further investigated in the trade studies shown later in this document.

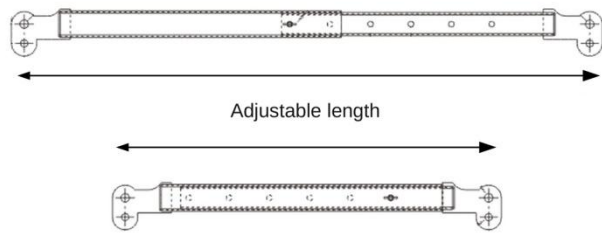


Figure 10: Telescoping spreader bar

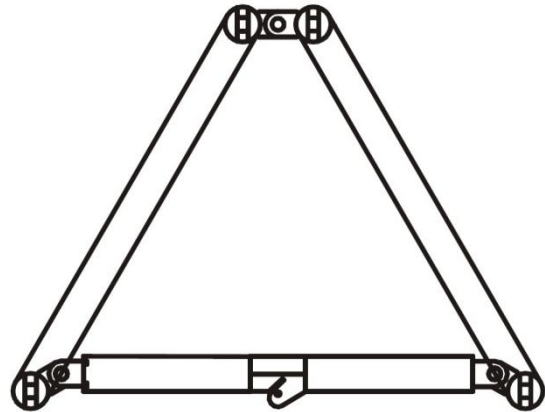


Figure 11: Folding space truss

In industry, container spreader bars are used by overhead cranes for lifting heavy, large, or irregularly shaped loads. Figure 9 is a typical container handling spreader bar used for port operations that spans 40 ft. Longer spreader bars, with a typical use being for the laying of long lengths of pipe work in construction, are available up to lengths of 140 ft. However these concepts are designed for nominally distributed loading and would be unsuitable for the compressive loading experienced on a twin-lift spreader bar. Companies like TANDEMLOC [Tandemloc 2010] offer telescoping spreader bars up to 90 ft long, such as shown in Figure 10. These concepts offer a viable design to relieve storage and transportation concerns. However, this option weighs 8,000 lb and the expectation is that a potential 160 ft length would be prohibitively heavy.

A final concept for the ground handling of the spreader bar is taken from stage truss design. These are designed to be light weight, easily stored and transported, and quickly assembled. The example shown in Figure 11, made by James Thomas [Thomas 2010], achieves this goal by making the truss foldable, and thus stackable. However, these modifications for adaptability come at the cost of increases in weight for a given load-bearing capability.

4.1.3 Design and analysis

Figure 12 shows the free body diagram and the design parameters considered for the spreader bar analysis. The design parameters are:

- 1) The length of the spreader bar.
- 2) The cross-sectional shape of the spreader bar and its dimensions.
- 3) The cable angles to the load handling frame.
- 4) The material properties of the spreader bar material.

The design analysis considers the spreader bar strength in compression and tension, buckling stiffness of the global structure, buckling stiffness of the elements for the truss structure, and fatigue strength.

Table 6: Material properties

Material	Steel	Aluminum	Titanium	CFRP	GFRP
Alloy Grade	1144	2095 (Weldalite)	Beta (weldable)	E-Glass (90/90)	Thornel (90/90)
Young's modulus (ksi)	26,000	10,000	15,900	1,600	1,600
Ultimate strength (ksi)	115	73	195	20	33
Density (lb/in ³)	0.283	0.194	0.162	0.061	0.058
Cost (2008 \$/ton)	700	1,800	23,000	54,000	9,100

The potential construction materials considered were steel, aluminum, titanium, glass composites and graphite composites. However, composites were immediately eliminated on the grounds of the compressive nature of the loading, relative expense, and difficulty of field repairs. Titanium was eliminated because it is expensive. The aluminum alloy 2095 or Weldalite, overcomes the innate weakness of aluminum in welding. This high-strength aluminum alloy has been designed to maintain 90% of its strength after welding, making it suitable for structural applications where welding offers weight advantages over other joining methods. Table 6 gives approximate values of the costs of these candidate materials along with their material properties used for the evaluation.

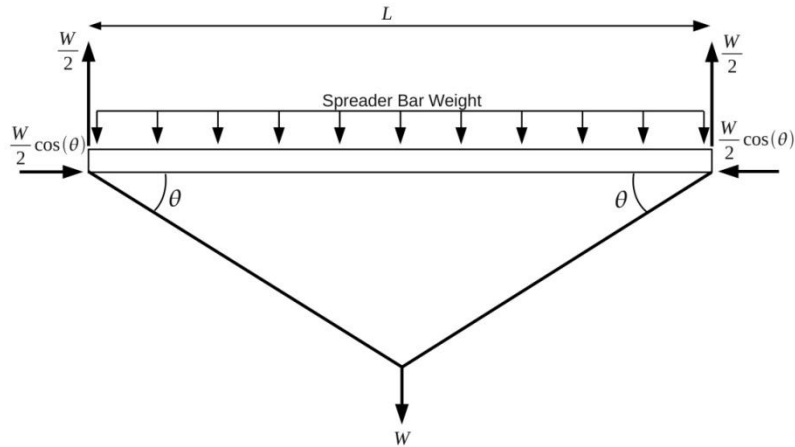


Figure 12: Free-body diagram of loading conditions on the spreader bar

Three different spreader bar configurations were considered. Two baseline results were obtained by considering the spreader bar as a simple I-beam, and then as a tube section, followed by the analysis of a truss like structure. A basic algorithm was used to evaluate the I-beam and the tube configurations. The material properties and loading conditions were initialized with the nominal compression force, F_c , and design factors, η . The iteration loop then steps through viable geometries by varying tube diameters and thickness, and web to flange ratios for the I-beam. The resulting geometries are tested against the buckling criteria, F_{crit} and bending stress limits, σ_{max} . Successful configurations are stored before the loop restarts. The graphs in Figure 13 and Figure 14 show the results for aluminum and steel for a selection of cross-sections. For both the I-beam and tube cross-sections, aluminum performed better than steel. The optimized weight in either case proved to be the same at about 6,000 lb, showing the importance of bending stiffness in this problem.

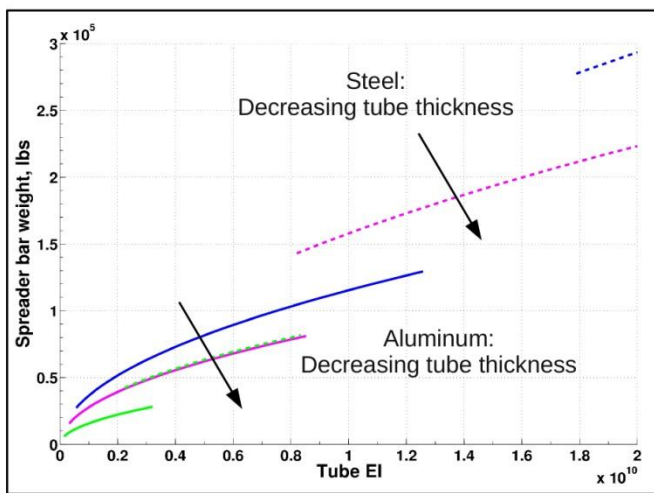


Figure 13: Spreader bar "tube" optimization

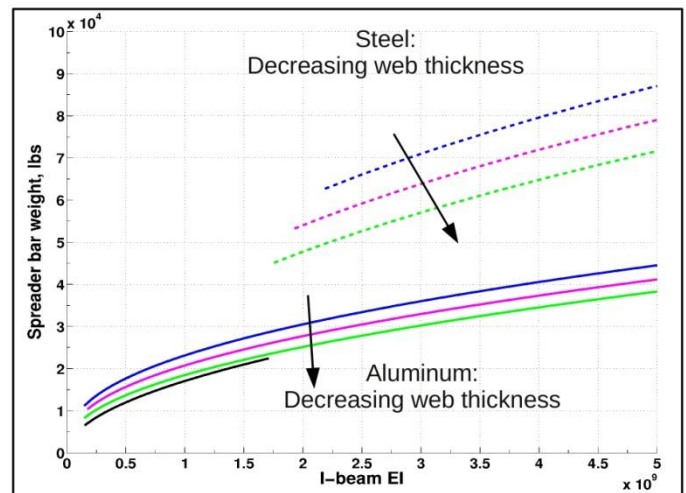


Figure 14: Spreader bar "I-Beam" optimization

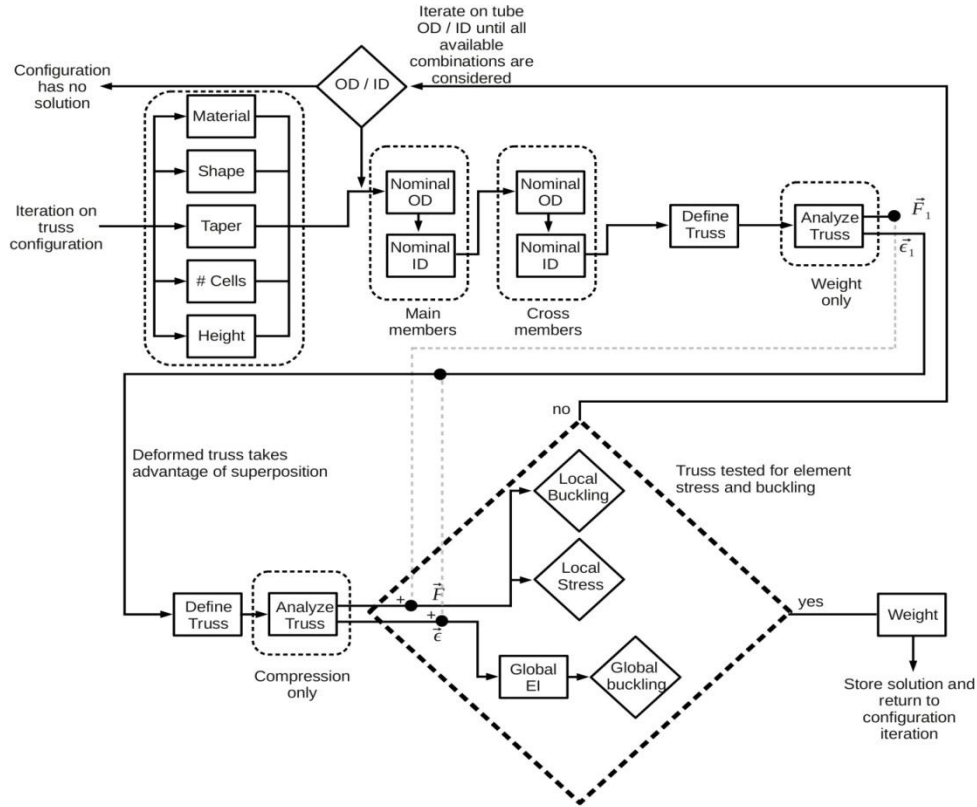


Figure 15: Truss optimization algorithm

The truss analysis was performed using a finite-element program that was developed in-house to analyze space trusses. This program allowed for an efficient interface to conduct parametric studies of several different configurations. This core program was incorporated into the wrapper algorithm shown in Figure 15, which was designed to carry out a parametric study while optimizing for weight. Two loops of the iteration were performed: The first loop iterated on a unique combination of truss material, shape, taper, number of cells and height, while the second loop optimized the weight of the unique truss configuration by evaluating the stresses for different tube outer and inner diameters. The evaluation of stresses accounts for bending stresses under self-weight and by superposition of forces, buckling under compressive loading for local cell elements, as well as for the global truss, and finally for compressive and tensile stresses developed within the truss members under all expected loads. Factors of safety were incorporated into each stage of the design process.

Simplifying assumptions in the truss analysis: 1) The truss elements were assumed to be industry standard tubes as they are most economical; 2) Nominal torsional stability was ensured with a truss width ratio of 50% of height; 3) A finite number of truss shapes were assumed.

4.1.4 Trade study

Figure 16 shows the results of the trade studies conducted during the truss design and the optimization process. The results are given in this section.

Number of truss cells: All the cases that were run showed a trend of decreasing weight with number of truss cells. Figure 16a shows that the limit of this trend is about 50 cells, beyond which the trend shows increased truss weight.

Truss materials: Figure 16b Shows that the superior strength-to-weight of aluminum offsets the higher strength of steel.

Truss shape/configuration: Figure 16b also shows that the truss design is relatively insensitive to any of the shapes and configurations considered. Generally neither square nor triangular shapes offered a preferred trend.

Truss height: The dependence on truss weight to height is shown in Figure 16c. The results indicate that the least weight is achieved when the truss height was around 5 ft, though there is little weight penalty for using heights of either 4 ft or 6 ft.

Truss taper: Figure 16d shows how truss taper affects truss weight. The results indicate that a large amount of taper gives a significantly greater weight penalty compared to using small or no taper. Below 50% taper there was no distinction between the optimum weight configurations.

Tip clearance: Tip clearance between rotors was investigated, as shown in Figure 16e, and gives the expected trend that greater tip clearance increases structural weight. However, this comes at the cost of reduced safety. The weight penalty between a 60% tip clearance and 100% clearance is 600 lb or an 80% increase in weight. However considering that this weight remains less than 2% of the configuration payload, as well as having the increased safety margins, this was considered an acceptable penalty.

Cable angle: The effect of cable angle to the payload is shown in Figure 16f. The trade study shows a dramatic increase in weight for cable angles below 45° . However, dynamic considerations and flight stability (see SECTION 6) govern optimal cable lengths, which dictate the cable angles.

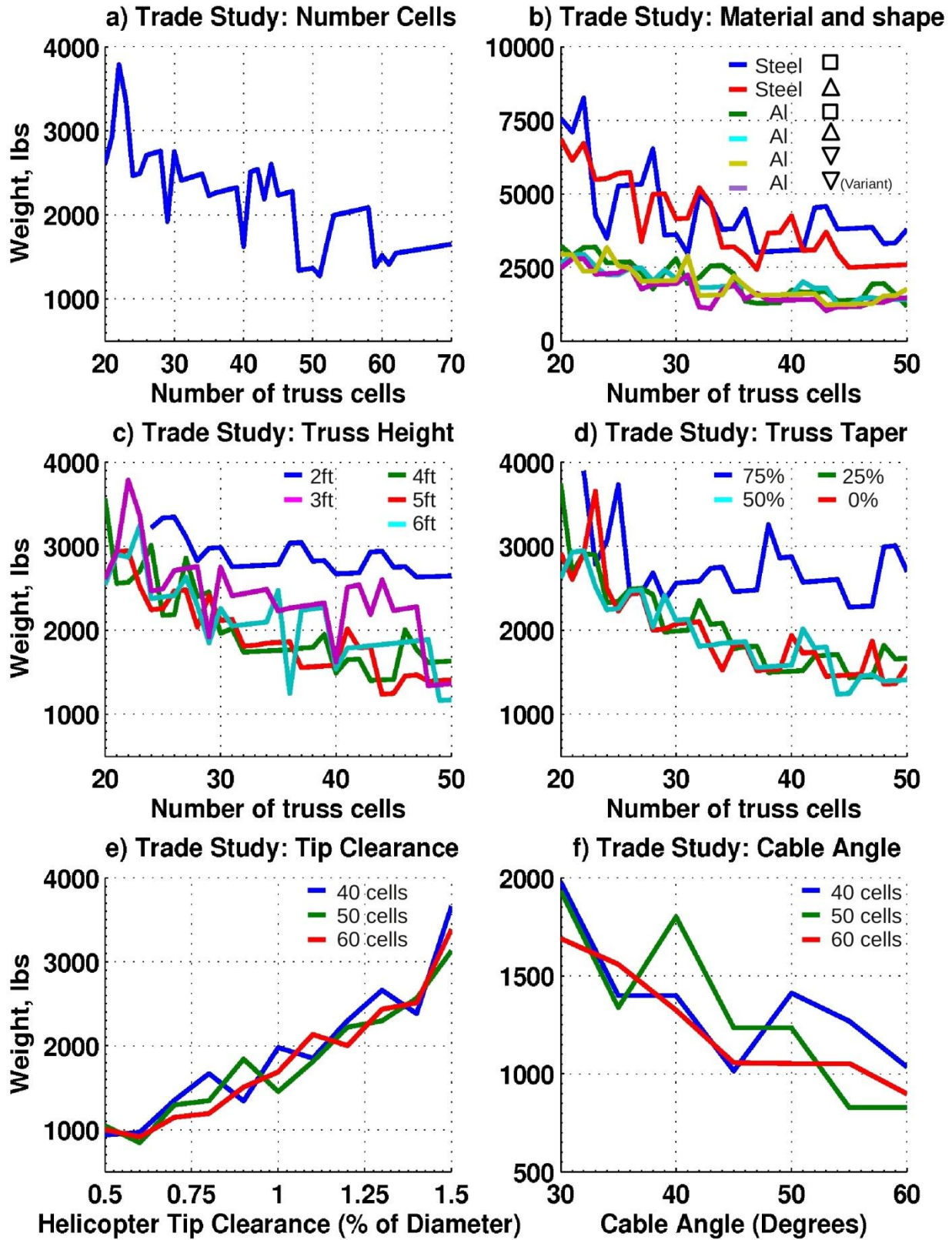


Figure 16: Results of design trade studies for the truss

4.1.5 Concepts

Operational logistics is a central feature of this design concept. Versatility in ground handling, transportation and storage of the structure, nominally the spreader bar, can only be achieved by making the spreader bar separable into a number of smaller components that can be easily handled and transported. These considerations gave rise to concepts concerning the spreader bar structure:

- Modular components minimizes training, spare parts, and expense. This goal can be achieved by designing the spreader bar as an assembly of several identical cells.
- Transportation space availability for the spreader bar and the entire load sharing structure limits overall dimensions. This attribute is a consideration for ship and airborne transportation. An obvious concept is to make the spreader bar transportable within the cargo hold of a single helicopter. This capability increases options for mission planning, allows flexibility for mission return, and offers faster, more efficient transportation of the off-loaded load sharing configuration.
- To allow for operation in remote theaters, ground handling should make use of no specialized equipment and should require a minimum number of persons.

4.1.6 Design conclusions

The final optimized truss is summarized in Figure 17. This design was readied with consideration for the results of the trade study and the configuration concepts. The design adopted a tip clearance of one rotor diameter, giving a spreader bar length of 160 ft. The triangular truss shape allows for truss modularity and storage (as outlined in SECTION 4.1.2), while maintaining good structural properties. A truss height of 4 ft trades a small weight penalty from the optimum of 5 ft in favor of compact storage options. The number of truss cells was optimized, giving a final design weight of 1,430 lb.

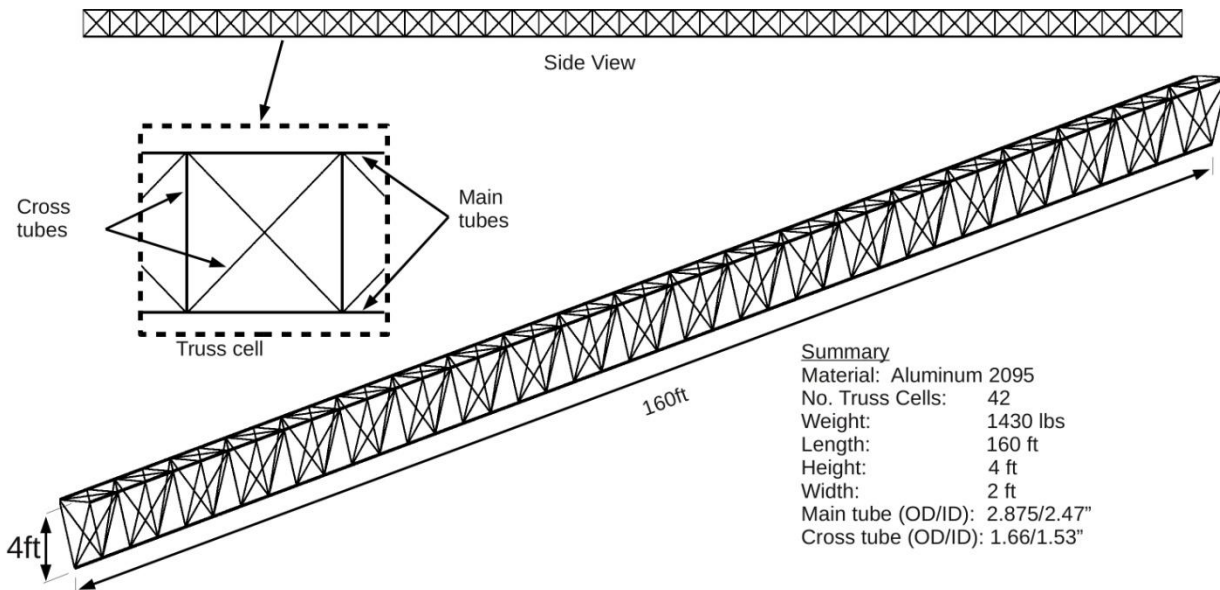


Figure 17: Summary of truss design

4.1.7 Design features

Transportability: The spreader bar was designed to fit into the cargo hold of a single CH-53E with excess space available for accessory parts and crew. Figure 18 shows the spreader bar disassembled into six truss elements and then stacking them so as to fit in the cargo hold of a CH-53E. The cargo hold dimensions are 37.5 x 7.5 x 6 ft, which allows for six truss elements stacked two high and three wide. The total stored footprint is 27 x 7 ft with a total height of 5.2 ft. Figure 18 shows that this stacking is easily achieved with sufficient clearance for loading and unloading operations, as well as retaining floor space for accessory parts or crew.

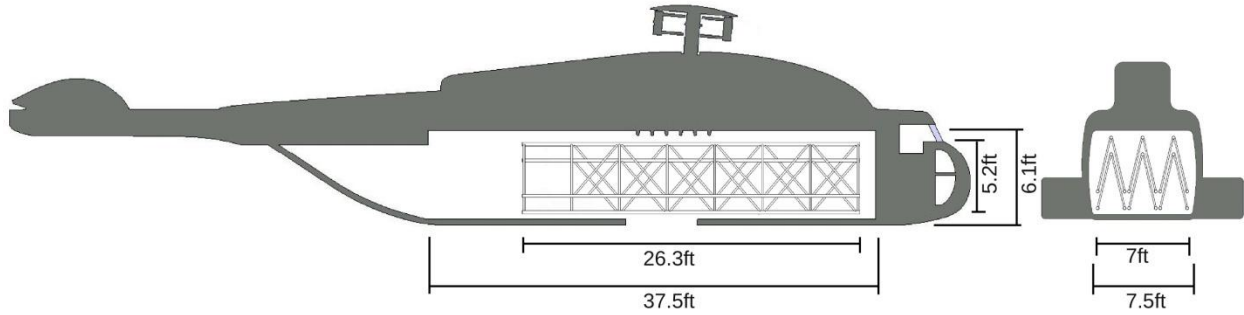


Figure 18: Spreader bar elements stacked within the cargo hold of the CH-53E

Ground handling: Ground handling of the spreader bar requires no special equipment and can be conducted by four personnel. The final total weight of the spreader bar was 1,950 lb after incorporating the fittings and joints required to accommodate modularity and storage. However, the weight of each truss element was just 236 lb, which can easily be carried by four personnel.

Modularity: The spreader bar is partitioned into six identical elements, each 27 ft long. These elements are interchangeable, thus minimizing the total number of parts required. Damaged truss elements can be easily replaced. Two standard tube sizes are used in the truss elements for ease of manufacturing and economy. The spreader bar can be easily adapted for use on smaller helicopters by removing a single truss element.

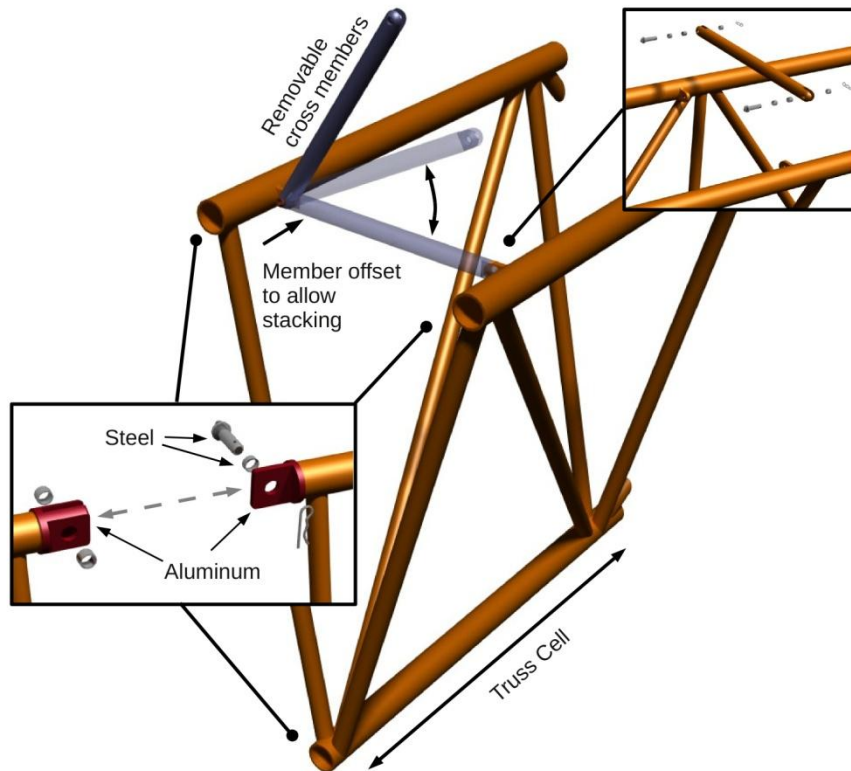


Figure 19: Assembly and modularity of spreader bar

Assembly: To maintain modularity of the truss elements, a simple pin connection mechanism is used to join the truss elements, as shown in Figure 19. Either end of each element has a female or male coupling, as highlighted in the insert. High-strength steel pins carry the joint stresses within cadmium-plated bushings for wear and corrosion prevention. This

method facilitates rapid assembly of the spreader bar, this attribute being critical for shipboard operations. The second insert in Figure 19 shows how the cross members of the truss are removable in a similar fashion, which allows for stacking of the truss elements.

Minimum weight: The truss optimization allowed for minimization of the spreader bar weight, for greater payload efficiency, while maintaining all safety considerations.

Cable connections: To transfer the cable tension to the helicopters requires unique end fittings on the truss to accommodate the cable linkages. The geometry of these fittings is taken directly from industry standard end fittings for spreader bars to ensure standard cable fittings are accommodated.

Drag reduction: To reduce parasitic drag on the cylindrical members of the spreader bar, the surface finish is roughened to ensure the boundary layer is always fully turbulent. The parasitic drag breakdown is given later in this section (Table 13).

4.2 Ducted rotor

Simulation of the double pendulum configuration (discussed in SECTION 8) demonstrated that the configuration requires some augmentation to achieve acceptable control and response characteristics. The analysis predicted that a controlled, time-varying, bidirectional force of up to 112 lb, applied at the spreader bar would augment the system response to acceptable levels. A small ducted rotor is capable of supplying the thrust required with sufficient control authority, while maintaining modularity of the concept, as is shown in Figure 20. The following describes the design of this ducted rotor.

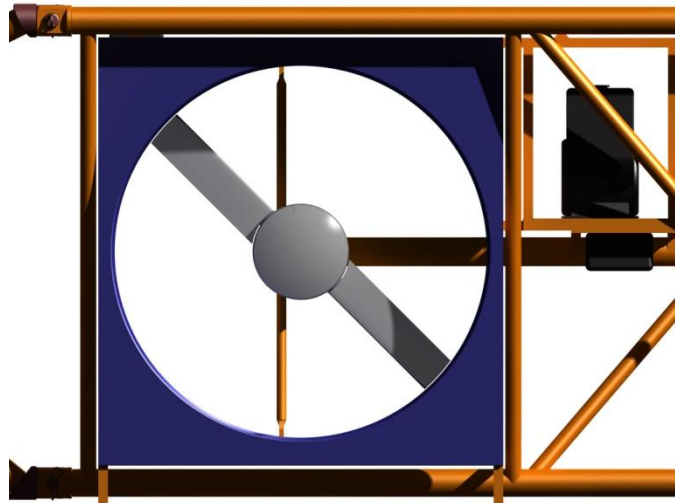


Figure 20: Modular ducted rotor

4.2.1 Specifications and design requirements

The specifications of the thruster are given in Table 7.

Table 7: Thruster specifications

Actuation required (lb)	112, variable
Flight speed	Primarily hover
Direction	Bi-directional, yaw control required
Modularity	Yes
Weight	Minimum
Safety	Yes

4.2.2 Thruster concepts and modeling

The following concepts were considered to provide the actuation at the spreader bar:

- **Compressed air jets:** These concepts have only a few moving parts and no hot exhaust. Thrust and directional control can be obtained easily through throttling and turning the thrust nozzle. However, simple gas calculations predicted that either large mass flow rates or high pressures were required. A typical mission required more than 250 ft³ of compressed air. Because a 5 ft³ storage cylinder weighs about 150 lb, this concept is not feasible.
- **Small jet turbine engine:** These engines have a compact, liquid energy store, and scale well to provide the thrust requirements. Thrust vectoring, or antagonistic pairs of thrusters, can provide bi-directional control. However, jet turbines are more complicated to operate and maintain, especially in dusty environments. Feasibility is further reduced by relatively higher noise and reduced safety from the hot exhaust.
- **Ducted rotor:** This system offers a proven, simple and robust technology. Variable thrust is achieved through pitch and RPM variations. Bi-directional operation can be achieved with antagonistic pairs of rotors or pitch control of blades with symmetric airfoils. The power source offers flexibility and can adapt to small engines, electric motors, as well as hydraulic or pneumatic motors. However, ducted rotors require larger cross sectional areas for a given thrust than for the other concepts, although by maintaining modularity this trade is considered acceptable.
- **Active support:** Pendulum modes can be stabilized by actuating the suspension point. In this case, the attachment point of the payload to the spreader bar is moved so as to counteract the pendulum motion. While this concept is suitable for a single pendulum, it has not been proven capable of stabilizing a double pendulum.

A ducted rotor concept appears as the most practical solution to provide the thrust at the spreader bar in a robust and safe manner. However, special consideration had to be given to maintaining the modularity of the concept to take advantage of the spreader bar structure and common interfaces. To provide bi-directional control, variable thrust and yaw control of the spreader bar necessitated that at least two ducted rotors be used, one at either end of the spreader bar. The position and size of the ducted rotor was determined after considering two additional concepts, namely the location and attachment of the ducted rotor to the spreader bar.

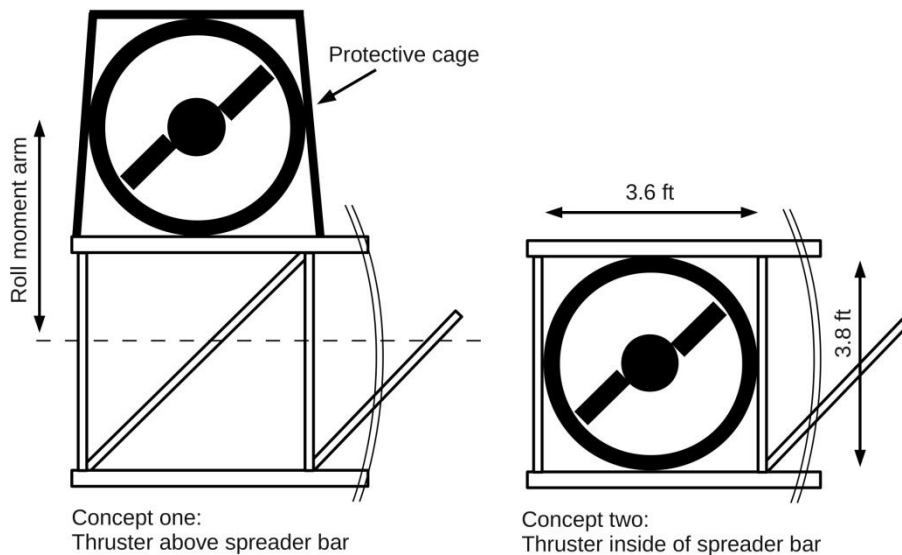


Figure 21: Ducted rotor concepts for modularity

The first concept shown in Figure 21 considered the rotor as a modular component that attaches to the top tubes of the spreader bar, which allows for unconstrained sizing and simple modularity. However, the exposed rotor requires additional structural reinforcement and the raised rotor imparts a roll moment on the spreader bar. The second concept shown in Figure 21 considers the rotor constrained to the dimensions of a single cell of the spreader bar truss. This concept leverages the spreader bar structure for rotor protection and reduced additional weight, maintains modularity and simple assembly,

and ensures that the thrust acts close to the centroid of the spreader bar. The restriction on diameter imposed by the internal truss cell dimensions of 3.7-by-3.6 ft was shown not to limit the design.

Table 8: Thruster design parameters

Design thrust (lb)	56
Rotor radius (ft)	1.6
Blade loading (C_T/σ)	0.12
Solidity	0.08
Rotor RPM	3,000
Blade geometry	NACA 0012 untwisted
Number of blades	2
Power required	4.6 hp

Table 8 summarizes the results of the analysis and validation of the ducted rotor design. At a maximum design thrust of 112 lb using two rotors, a rotor radius of 1.6 ft is capable of achieving this thrust at a blade loading coefficient of 0.12, which is within the stall boundaries of the rotor at this scale, including Reynolds number considerations. The design RPM was set after consideration of suitable small engines, which showed peak efficiencies and torque at 3000 RPM. NACA 0012 symmetric airfoils were selected to allow for bi-directional pitch actuation.

4.2.3 Design features

Modularity: Figure 22 shows the modularity of the ducted rotor. The ducted rotor, drive shaft, engine block and gearbox, pitch servos, battery and communications link to the rotor controller are all in a single container unit. This unit is supported by a cage that fits into the cell structure of the spreader bar. The figure shows how the thruster cage is lowered into the spreader bar. The cage is secured making use of the fittings already used for the cross members of the truss previously highlighted in Figure 19. The load path through the thruster cage ensures that the removal of the last diagonal truss members to incorporate this concept does not compromise the structural integrity of the spreader bar.

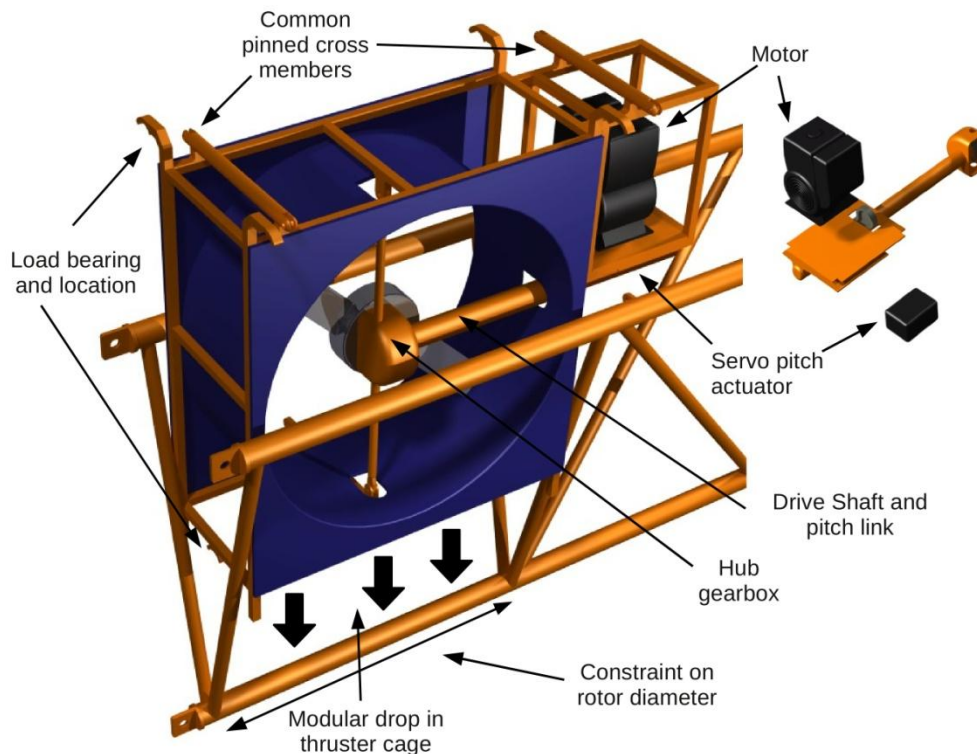


Figure 22: Exploded view of thruster assembly

Ease of assembly: Assembly of the ducted rotor cage requires only four pinned joints. These four joints allow for rapid assembly of the spreader bar or for the removal and storage or repair of the critical control unit of the twin-lift configuration.

Thrust control: The motor throttle and pitch links are driven from servo motors attached to the underside of the motor mount. These servo motors are battery powered, sharing the battery and alternator of the electric start motor to ensure in-flight charging of the battery. Control of the servo motors takes place through wireless links with the flight computers housed on the helicopters. This system is described in detail in SECTION 4.5. The control logic is discussed in the SECTION 8.

Safety: Although not shown in the figure for clarity, a mesh grid over the duct ingress and egress prevents unsafe handling of the rotor at all times.

Motor: A Kohler CS6 gasoline engine with electric start and throttle control was chosen to provide the power to the rotor. This motor weighs 35 lb dry and has a nominal power rating of 6 hp at 3,600 RPM. The torque produced at 3,000 RPM was matched to the rotor characteristics. Fuel consumption estimates of 0.1 gallons/hp/hr mean that the factory fuel tank of one gallon of gasoline is sufficient for a typical mission.

Final weights: The final weight of the modular thruster, including the rotor, duct, motor, fuel, gearbox, servos and electronics, was approximately 188 lb.

4.3 Container attachment frame

A second spreader bar, called the container attachment frame, is required to lift containers or otherwise large loads. This spreader bar serves the purposes of evenly distributing the weight of the payload, mitigating any compressive loading on the container, and separating the sling points so that the cables are not damaged against the payload structure. In this configuration, the spreader bar also provides a convenient location to attach the vertical tail, which was shown to reduce payload fishtailing for long slender bodies such as containers. The design of the load handling frame is driven by the need to reduce weight.

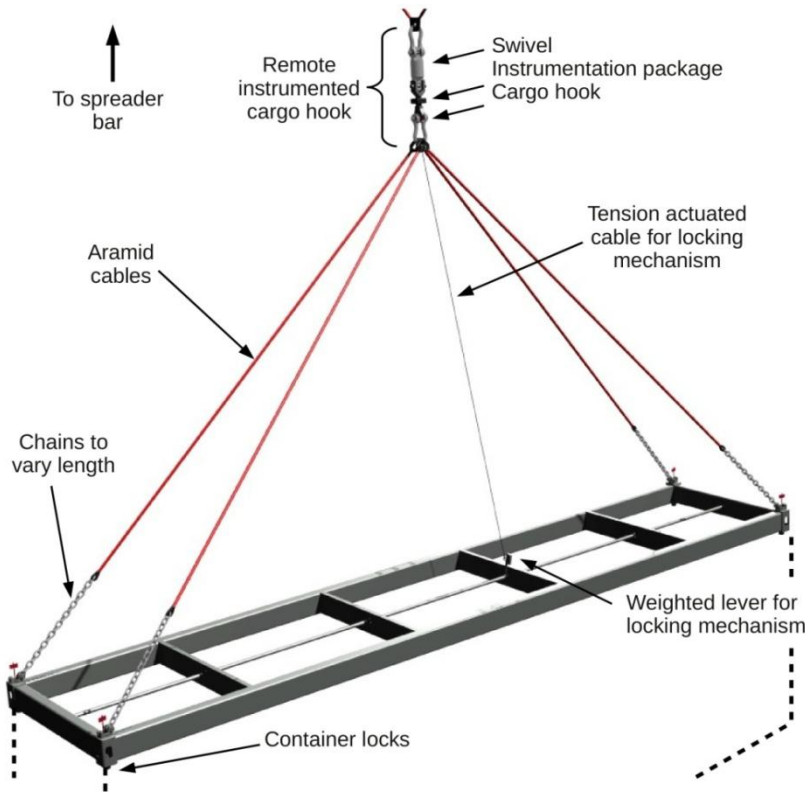


Figure 23: Features of the load attachment frame

4.3.1 Literature review and current technology

Industry and military container handling of 20 ft, 40 ft and 48 ft ISO containers is routinely performed using 20 ft and 40 ft spreader bars, the larger of which can accommodate 48 ft containers as well. A review of available container handling spreader bars showed that the 40 ft spreader bars have a gross weight of around 5,000 lb, i.e., 8% of the useful payload of the configuration under consideration. Lighter weight options of 800 lb are available, but these are unsuitable for the dynamic loading expected in flight. These reasons motivated the redesign of the container attachment frame to take advantage of lightweight materials and more aggressive structural safety factors.

4.3.2 Design and features

Maintaining the basic configuration of an industry standard spreader bar, but taking advantage of light weight aluminum (6075), safety factors applicable to aerospace applications, and optimized load carrying capability of 58,000 lb (reduced from 128,000 lb), allowed for a weight reduction for the new container attachment frame of nearly 4,000 lb. The final spreader bar weighed 1,320 lb, while still maintaining all the functionality of the original design. The additional cost attributed to this unique component of the configuration is justified in terms of increased payload and mission flexibility.

Figure 23 shows the spreader bar design, which incorporated an automatic container locking mechanism. The locking mechanism is a robust mechanical linkage that passively engages and disengages the container attachment locks depending on cable tension alone. Under tension, the weighted lever is raised to lock the container. When tension is removed, the weighted lever drops to release the container. This mechanism provides an efficient means of container drop off that is personal independent and adds system redundancy through electrical actuation of the external cargo hook.

4.4 Vertical fin

The section on payload dynamics discussed the benefits of a vertical fin used to stabilize and orient bluff body payloads, such as an ISO container, in forward flight. This section describes its design.

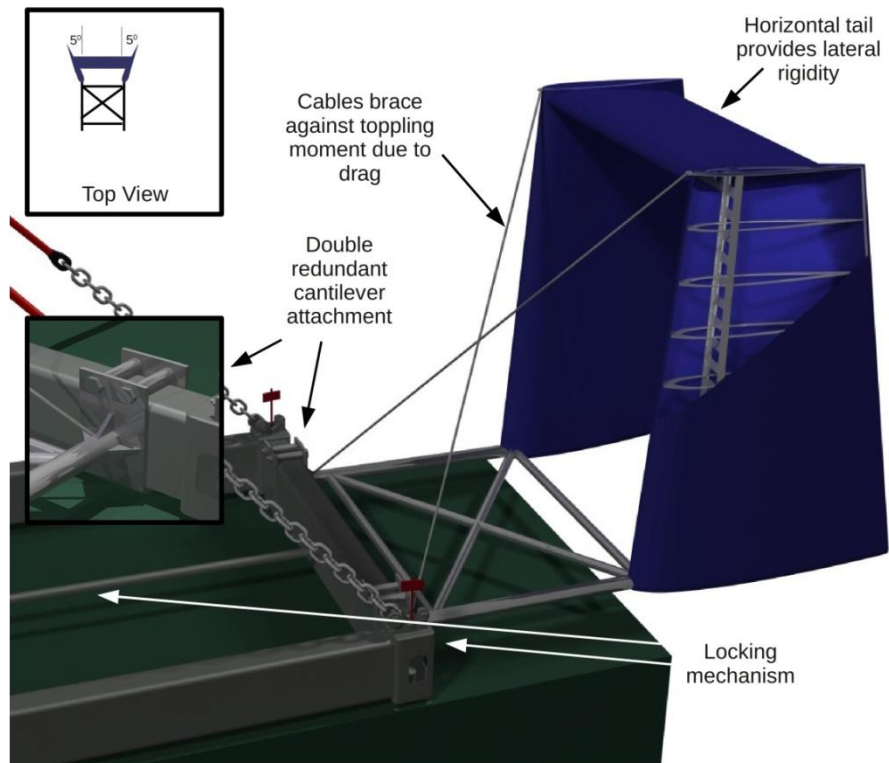


Figure 24: Construction and features of vertical fin

4.4.1 Specifications and design requirements

The container attachment frame provides a convenient attachment point for the vertical fin that does not require a special fitting to be made for the payload. This flexibility allows for the benefits of the vertical fin to be realized on payloads other than the 40 ft container. However the 40 ft container was chosen as the design condition for the vertical fin.

Table 9: Design parameters of the vertical fin

Yaw moment coefficient (ft ³)	700
Design airspeed (knots)	90
Mean lift coefficient	0.4
Moment arm (ft)	25
Determined tail area (ft ²)	70

Wind tunnel tests on 20 ft and 40 ft containers [Cicolani 1987, Sampath 1980] provide the yaw moments as a function of yaw angle. The wind tunnel test results for a 40 ft container showed a maximum yaw moment coefficient (yaw moment divided by dynamic pressure with units of ft³) of 700 ft³ for yaw angles below 20°.

The design of the vertical fin assumed that the moment arm extends 5 ft behind the container to give a total moment arm of 25 ft about the swivel. A design airspeed of 90 knots and a mean lift coefficient of 0.4 were assumed for the fin airfoil. This information is summarized in Table 9.

4.4.2 Features of the vertical fin

Dual vertical fins: Figure 24 shows the construction of the vertical fin. Structural complications of a single vertical fin with a 70 ft² of area necessitate the dual tail configuration, each with a surface area of 35 ft².

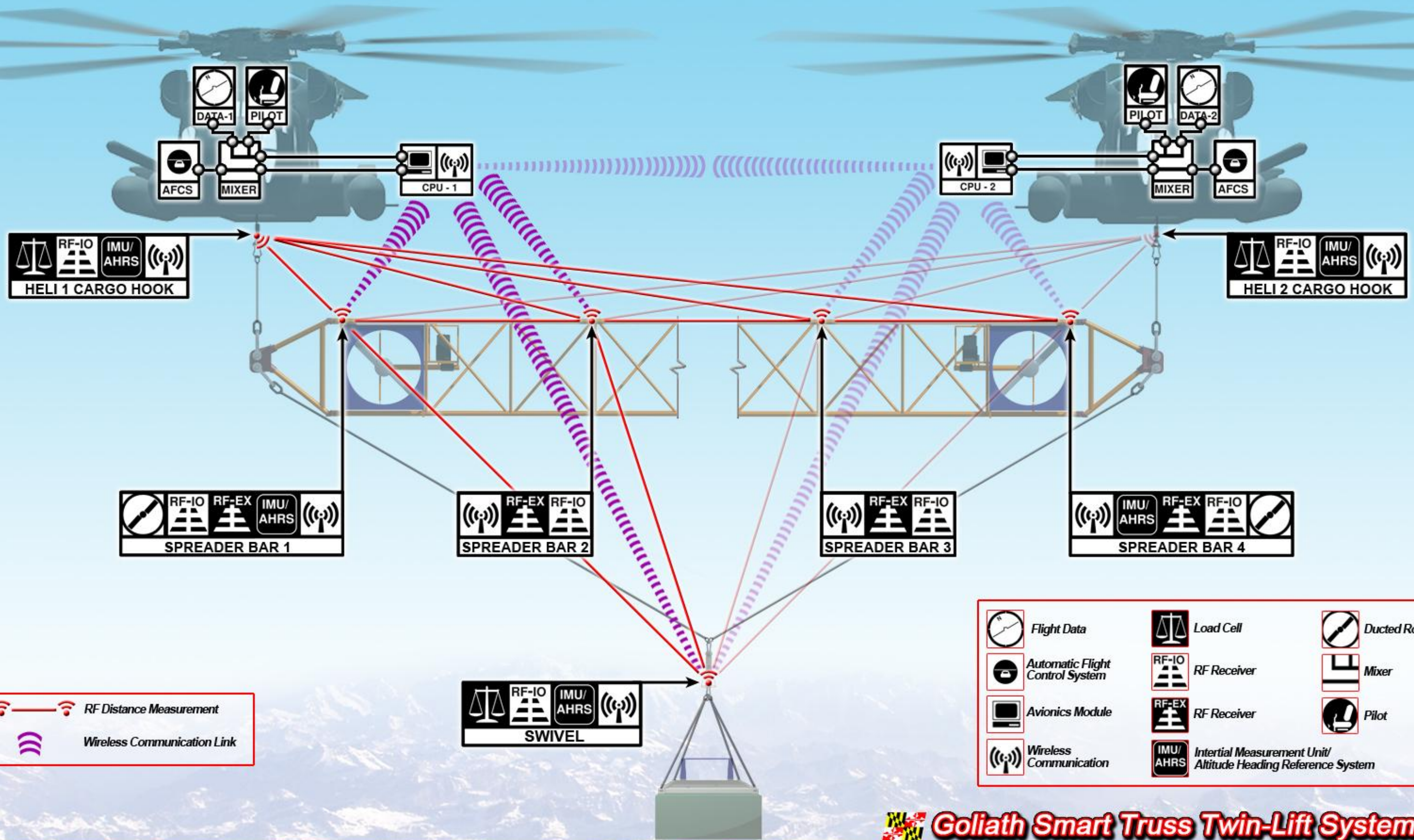
Redundant safety: The attachment of the vertical fin to the spreader frame is achieved using an under slung attachment bolted above the spreader bar beam, as shown in the figure insert. This system ensures that any one bolt failure will not degrade the mission because the vertical fin will remain attached between the spreader bar and the container.

Toe-in cant: The two fins have a toe-in cant of 5° to improve static and dynamic stability of the payload in forward flight [Cicolani 2007].

Weight: The weight of the vertical fin system was estimated to be 288 lb.



Sensor Arrangement Detail



4.5 Sensor and communication suite

4.5.1 Specifications and design requirements

The outer loop controller relies on information about the relative positions and orientations of each element of the system to ensure safety and coordination of the helicopters. This information must be available in real-time with high fidelity. The sensors and communication must be robust against weather variations and in degraded mission environments. To maintain modularity, the combination of sensors should require a minimum of modifications to the spreader bar, no modifications to the payload, and no modifications to the helicopters.

4.5.2 Concepts and comparison

Table 10 summarizes the sensors that are available and that maybe be suitable for use in the twin-lift configuration in terms of relative advantages and disadvantages.

Table 10: Comparison of available sensors

Sensor type	Advantages	Disadvantages
GPS/DGPS	Global positioning. Small and low power, reliable.	Limited accuracy of GPS (30 ft). DGPS relies on reference locations to increase accuracy to 1 ft.
RADAR	High accuracy.	No orientation information. Directional, require aiming.
LASER	High accuracy. Fast processing.	Affected by degraded visual environments (rain/dust). Directional.
LADAR	High accuracy. 2D and 3D scanning. Orientation capable.	Processing power intensive. May be slow for large viewing areas. Poor degraded visual performance. Resolution degrades with distance.
Inclinometer	Simple and robust. Lightweight and small.	Limited information when operated in isolation.
IMU	Gives orientations and rates. Can integrate to give relative positions and speeds. Fast processing.	Gyro drift limits positional accuracy.
AHRS/IMU units	Attitude and heading. Relative orientations and rates.	No relative position.
Image processing	Provide position. Very accurate.	No distance measurement on simple units. Distance requires increased computational overhead. Poor degraded visual performance.
Ultrasonic Position Sensor (USPS)	High accuracy (better than 1ft). Fast.	Cannot operate in high noise environments. Requires at least 4 sensors for a measurement.
Radio Frequency Position Sensor (RFPS)	Accurate distance measurements. Fast. Independent of visual conditions.	No orientation information. Requires at least 4 sensors for a measurement.

4.5.3 Conclusions

It was evident that no single sensor was capable of providing all of the required measurements in real-time and in all visual/weather environments. Therefore, an optimum combination of sensors was selected as follows:

RFPS: To evaluate the distance between each component of the configuration, the position of each helicopter and of the payload relative to the spreader bar can be determined by triangulation. This process requires four radio transmitters distributed along the spreader bar, one receiver radio located at each helicopter, and one at the payload. The cargo hooks provide a convenient reference location for the receiving radios. This system provides a robust, weather-independent and accurate positional awareness of the configuration in real-time. Precision is determined using the method of Dilution of Precision (DOP), which determines the accuracy of the triangulation methods, and shows that positional accuracy better than one foot can be achieved by this configuration of sensors. These units are available as palm sized units and are readily available with little or no technological risk.

AHRS/IMU: To augment the positional awareness, the heading and orientation of the spreader bar and payload are determined using AHRS/IMU units. These are similarly small components that can be incorporated into the radio transmitters and receivers. The high accuracy of these sensors is required by the system controller to maintain the stability of the configuration. Combined with the positional RFPS sensors, these sensors close the loop giving complete global positional information. At least one AHRS/IMU unit is required at the cargo hook on each helicopter, on the payload cargo hook, and on the spreader bar. Further AHRS/IMU information is required from the helicopter fuselage, but this is assumed to be already available from the on board flight system (AFCS).

Load cell: To ensure load sharing between aircraft, the cable tensions are determined through load cells placed in series with the cargo hooks at each helicopter. These load cells are available commercially and are rated to sufficient loads. This information is also used by the flight computer during maneuvers to ensure that the loads on the cargo hook are not exceeded.

Wireless communication: The remote layout of the twin-lift configuration is best suited to all communication via a high speed wireless connection. This system does away with wired connections that are prone to damage and are logistically difficult to implement along cables that span over 100 ft. Each sensor unit thus incorporates a wireless communication that links to the on board flight computers. The relatively short distances and clear line of sight is suited to high frequency wireless communication, which is less prone to interference and also allows for low energy transmission.

Onboard computer: All the sensor data is accumulated onto computers onboard each helicopter. These control computers are responsible for receiving all the sensor information and combining it with information from the flight computer (AFCS) on each helicopter to determine the states of the entire system. The computer then implements the control laws and swashplate commands are fed back to, and augment, the helicopter AFCS. Actuation commands are then broadcast back to the spreader bar to control the thrusters. The control logic is described in SECTION 8



Figure 25: Remote-instrumented cargo hook

4.5.4 Design features of the remote-instrumented cargo hook

The instrumentation of the twin-lift configuration is shown schematically in the truss sensor foldout. The sensing units, described schematically in the figure, are each stand alone units that form the network. Figure 25 shows the configuration of the instrumented external cargo hook from which the payload is suspended. The cargo hook at each helicopter has identical instrumentation, but is otherwise identical to the standard CH-53E cargo hook. The insert also shows a schematic of the sensor units that are installed to the spreader bar. These modular units attach to the cross members of the spreader bar. The features of the sensor suite are as follows.

Simple robust sensors: The sensor network is chosen to operate in a robust manner and in all weather conditions or visual environments. Information transfer is wireless, which minimizes maintenance and modes of failure.

No structural modifications to the helicopters: The underlying design concept of this design is that no structural modifications to the airframe of the helicopter are required. The load carrying system remains stand-alone and suitable for any helicopter with a suitable control architecture programmed into its controls.

Redundancy: All information has two sources of information and two paths to reach the control boxes on board the helicopters. Data is broadcast on separate frequencies to both control boxes to counter any interference or jamming that might be encountered. Communication between control boxes compares sensor information and check for erroneous data in the system, in which case corrupt information can be excluded.

Twin-lift control box: The on-board accumulation of data computing is carried out by the twin-lift control box. These are portable computing units that implement the control logic. They also provide a visual interface and interaction between the pilot and the slung load configuration. An identical control box is required on both helicopters in the configuration. Switches on each box identify which helicopter is the master or slave. All sensor information is broadcast to both control boxes and is

processed in real-time. Resulting control commands are compared between control boxes to check for system failures before they are sent to the respective helicopters. Failure of a single control box can be overridden by the other allowing for safe completion of the mission. The pilot interface on each control box provides pertinent information about the status of the twin-lift system. Figure 26 shows a conceptual view of the pilot interface. This interface provides the pilots with information concerning:

- The relative position of the helicopters to each other and the slung load.
- Real-time indication of the payload stability.
- System diagnostics.
- Control over the remote-instrumented cargo hook release and jettison in case of emergency.

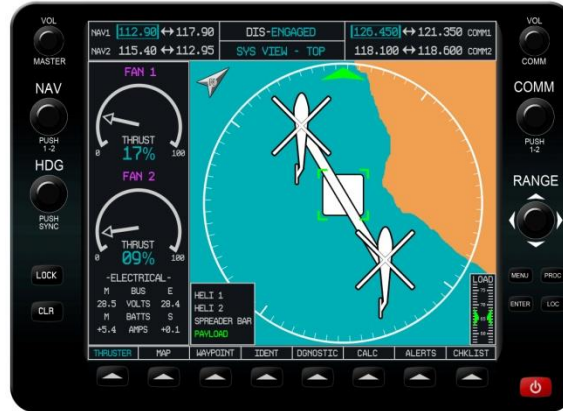


Figure 26: Pilot interface to control box

4.6 Cable selection

The present concept requires a total cable length of 400 ft, which makes its weight a significant consideration both for mission performance and ground handling. Table 11 compares the performance of the two cable materials considered in this design. Steel rope is a low cost solution and is used for most heavy lifting in industry, however it has a high weight penalty. Aramid cables offer five times greater strength-to-weight but are significantly more costly. Aramid type cables are already used in slung load operations. Aramid cable was chosen for this application because it allows for 1,400 lb of extra payload compared to using steel cables, and offers the only option that is feasible for ground handling in more remote areas without special equipment. The increased cost of the cables is partly recovered in the superior fatigue resistance, low maintenance, and more economical logistics.

Table 11: Cable selection

	Steel rope	ARAMID
Mission payload (lb)	58,000	
Maximum tension (lb)	49,000 / 20,000	
Design cable strength (tons)	102 / 50	
Cable length: Cable 1/Cable 2(ft)	290 / 110	
Available cable strength (tons)	132 / 51.7	110 / 55
Weight (lb/ft)	4.88 / 1.85	0.75 / 0.4
Total weight (lb)	1,620	261
Approximate cost (\$/ft)	9.20	45.70
Approximate cost (cables only, USD)	3,900	18,300

Maximum tension assumes 60/40 load sharing and 45° cable angle.
 Design cable length applies a design factor of five as per industry standard.
 Cable strength is the rated breaking strength of the cable.

4.7 System weight summary

Table 12 gives the total weight breakdown of the load handling system. It is seen that the miscellaneous fittings, which includes all cable end-fittings and attachments, including D-shackles, bolts and chains, contribute significantly to the overall weight to the system.

Table 12: System weight summary

	Weight (lb)	Percentage of useful load (58,000 lb)
Spreader bar	1,915	3.2%
Load handling frame	1,320	2.25
Thrusters (2 off)	188	0.7%
Vertical tail	260	0.4%
Cables	260	0.4%
Swivel and remote cargo hook	200	0.3%
Sensor suite and communications	10	~0%
Miscellaneous fittings	400	0.8%
Total	4,740	8.2%
Allowable for container	53,300	91%

The total parasitic drag of the configuration is summarized in Table 13. The drag of the container attachment frame is essentially that associated with the cargo container itself and is included in its estimate.

4.8 System drag estimates

Table 13 provides a drag summary of the main components of the twin-lift configuration. These are the cables and the truss elements. The cable drag is estimated by considering the cables as long cylinders in fully laminar flow. Their drag coefficients represent the worst case of bluff body flows. The reference dimension is the diameter of the cable. The two cables referred to are the main cables that run from the helicopters to the swivel, and the cables from the swivel to the payload.

Similarly, the two different truss tube sizes were considered independently. It was assumed that the surface finish on the spreader bar can be roughened so that the flow can be considered to be fully turbulent. This results in the decreased drag coefficient used in the calculations ($C_d = 0.3$). The cross sectional area assumes that the spreader bar travels perpendicular to the air flow. This is a worst case scenario that only exists in low-speed flight (< 30 knots). In cruise flight the spreader bar is at a 30° angle to the flow. As shown by Hoerner [Hoerner 1965], that a cylinder inclined beyond 45° to the flow would have significantly reduced drag.

The worst-case parasitic drag of the total load handling system, assuming flow perpendicular to the flow, was determined to be 104 ft².

Table 13: System drag summary

	Dimension (in.)	Length (ft)	C_d	Flat plate area (ft ²)
Main cables	1.4	110	1.0	13
Secondary cables	1.0	290	1.0	40
Truss main tubes	2.87	320	0.3	27
Truss cross tubes	1.66	590	0.3	24
Total drag				104 ft²

5 Mission Performance Analysis

To estimate the payload and range capabilities of the *Goliath*, a mission analysis code was coupled to an analysis that predicted the power required in hover and forward flight. Both analyses were developed for this project and the performance analysis was validated against available CH-53E flight test data. The mission analysis used the forward flight fuel flow results to calculate fuel weight for each mission segment of the primary mission profile.

The *Goliath* system was predicted to be capable of delivering a 40,130 lb ISO container 100 nm under ISA+20°C hot-day conditions. This represented an 86% increase in payload over the baseline CH-53E for the same mission profile, exceeding the requirements of the RFP by 11%.

5.1 Performance code development

A program was developed to calculate the engine fuel flow per hour for the CH-53E in forward flight. The fuel flow rate was fed into a mission analysis code that calculated the fuel burn over the mission segment. The approach used a blade-element propulsive trim procedure based on the harmonic balance method (developed by the design team). Rotor trim orientations for moment equilibrium were computed for each flight speed. Estimates of the CH-53E parameters used in the rotor trim calculations are shown in Table 14.

Table 14: Estimated CH-53E parameters

Parameter	Value
Number of main rotor blades	7
Main rotor blade radius (ft)	39.5
Main rotor chord (ft)	2.44
Main rotor solidity	0.137
Main rotor blade twist (°)	-20
Main rotor RPM	179
Height from ground to rotor hub (ft)	28.25
Longitudinal cg location from the shaft axis (ft)	-1.67
Distance of tail rotor from shaft axis (ft)	49.5

Published blade section airfoil and fuselage drag data were used to estimate the performance of the CH-53E. The aerodynamic characteristics of the SC-1095 main rotor airfoil were taken from Bousman (2003). Airfoil compressibility effects were accounted for using the Gessow and Crim correction to profile power [Leishman 2006].

Fuselage drag as a function of fuselage angle of attack was estimated using wind tunnel data from Sturgeon (1993). The data shown in Figure 27 was fit to the polynomial ($f = 0.0932\alpha_s^2 - 0.428\alpha_s + 48.6$) and incorporated into the performance analysis.

The rotor induced power factor (κ) and the average profile drag coefficient of the blades (C_{d0}) were estimated by using published hover flight test data from a fit in a least-squares regression sense to yield values of $C_{d0} = 0.009$ and $\kappa = 1.196$. With these data, the trim procedure computed the primary control displacements, blade flap responses and shaft angles, followed by the performance of the helicopter.

Flight test data for the CH-53E in hover, at best endurance, best range, and at maximum cruise speed were used for the validation. Maximum continuous power (9,600 hp) and military power (11,570 hp) ratings for the CH-53E are also shown in Figure 28. The analysis was found to be in good agreement with the flight test data.

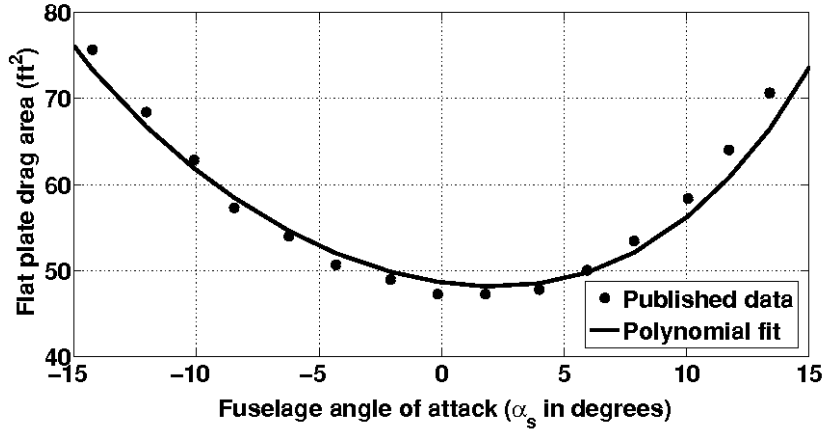


Figure 27: CH-53E fuselage drag as a function of fuselage angle of attack from wind tunnel data [Sturgeon 1993]

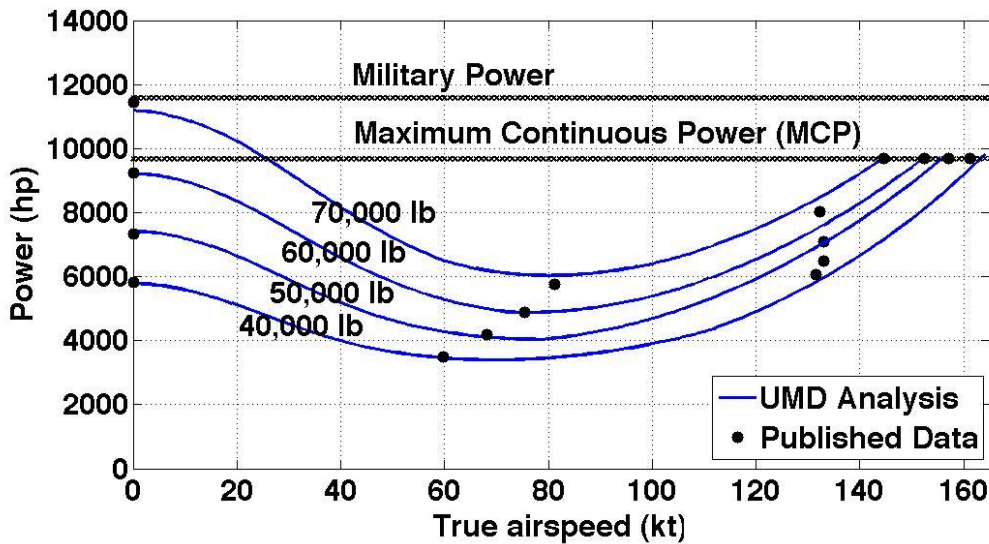


Figure 28: CH-53E power requirement validation plot at various gross weights

Using the published data, the specific fuel consumption (SFC) for the CH-53E as a function of relative power setting was also determined. With these data, the SFC was obtained as a function of power setting. Using the power settings for each airspeed, along with the corresponding SFC, the fuel flow was computed to calculate specific range (nautical miles per pound of fuel). In Figure 29, calculations of specific range are shown against published data for varying amounts of external load drag.

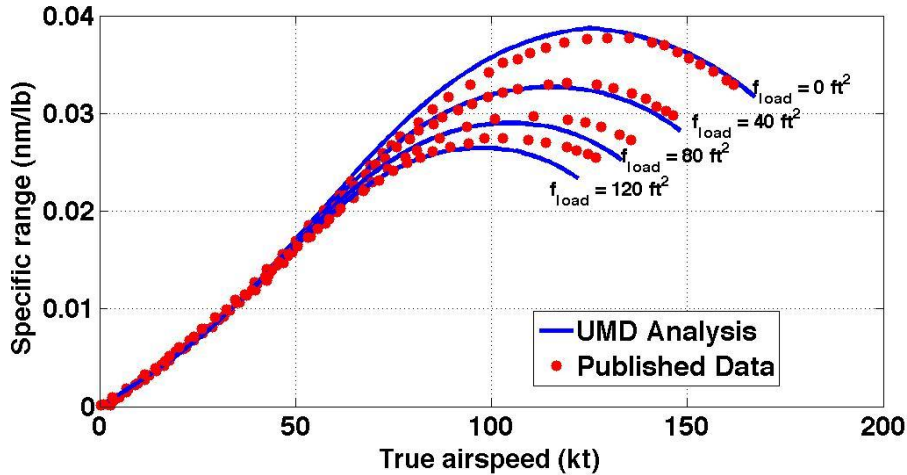


Figure 29: Specific range correlation for the CH-53E at weight of 50,000 lb

As external payload drag is increased, the correlation with published data decreases slightly at higher airspeeds. The under prediction of specific range is acceptable as it leads to conservative estimates of range for payloads with higher values of parasitic drag.

5.2 Mission performance estimates

The RFP required the twin-lift system to have a payload delivery capability that was 75% greater than a single baseline helicopter for the 100 nautical mile mission. A mission analysis code was developed to determine the payload capability of the CH-53E and the *Goliath* twin-lift system for varying delivery distances. The mission analysis program calculated fuel weight required for each mission segment using the validated rotor power required code developed in the previous section. Engine lapse rates for altitude and temperature were incorporated to incorporate realistic limits on available power for each mission segment.

The baseline single CH-53E and the *Goliath* twin-lift system were analyzed for the primary mission profile with varying delivery distance (radius of action). Both systems experienced an additional external payload drag of 70 ft², the estimate for a 48-ft ISO container. The *Goliath* system had additional drag and weight from the load-handling structure of 116 ft² and 4,750 lb, respectively.

The payload-range curve in Figure 30 compares the capabilities of a single CH-53E and the *Goliath* dual-CH-53E system when executing the primary mission profile with an ISO container. Figure 30 includes the conservative assumption that the helicopters remain joined and incur the drag penalties of the truss, cables, and container attachment frame on the return cruise. The payload capability of the *Goliath* is 40,130 lb for a 100 nm delivery distance, which is 87% greater than the baseline platform capability for the same mission. Therefore, the *Goliath* exceeds the RFP requirement of a 75% increase in payload delivery. **The *Goliath* can deliver a 40,130 lb payload 100 nm in only 65 minutes under hot-day conditions.**

Mission Profile
All segments ISA + 20°C

- Shipboard takeoff
- Hover OGE, 5 min, Sea Level
- Cruise ROA nm, 500 ft
- Climb to 3,000 ft
- Hover OGE, 10 min, 3,000 ft
- Drop payload
- Cruise ROA nm, 500 ft
- Fuel reserve: 20 min, 500 ft
- Hover OGE, 5 min, Sea Level
- Shipboard landing

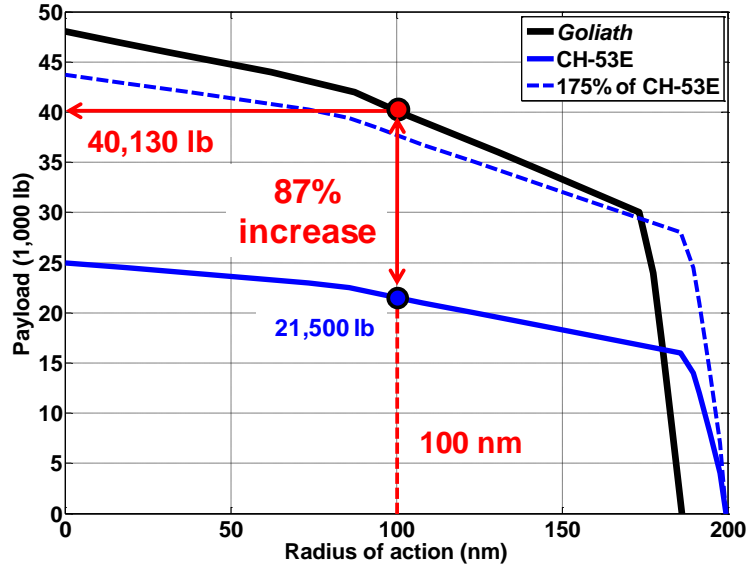


Figure 30: Payload-range curve for primary mission profile with 48 ft ISO container payload

5.2.1 Clean return performance

The modular and lightweight truss spreader bar system was specifically designed to easily breakdown and fit in the cargo hold of a single CH-53E. The lightweight aramid cables are also capable of being stowed by hand. Therefore, there is a possibility of the *Goliath* system being split into two separate helicopters on the return trip with all components being stored internally. This concept was referred to as a clean return, and can be implemented if the drop-off site conditions permit the landing and disassembling of the system. The performance benefits of this operation are increased payload capability for the 100 nm range mission or increased delivery distance for the same payload weight (see Figure 31). For a clean return mission, the ISO container payload capability can be increased by an additional 5% to 42,000 lb.

Mission Profile
All segments ISA + 20°C

- Shipboard takeoff
- Hover OGE, 5 min, Sea Level
- Cruise ROA nm, 500 ft
- Climb to 3,000 ft
- Hover OGE, 10 min, 3,000 ft
- Drop payload
- Cruise ROA nm, 500 ft
- Fuel reserve: 20 min, 500 ft
- Hover OGE, 5 min, Sea Level
- Shipboard landing

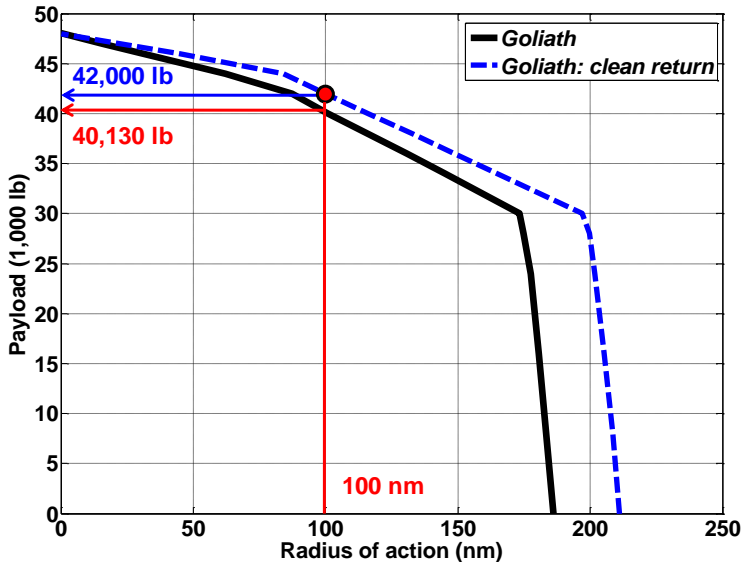


Figure 31: Payload-range curve for an ISO container with structure internally stored on return cruise

5.2.2 Payload sensitivity to external payload drag

The analyses shown in Figure 30 and Figure 31 were specifically for the ISO container mission and, therefore, included the container attachment frame drag and weight. The sensitivity of maximum payload capability to changes in delivery radius and payload drag were explored and plotted in Figure 32. The mission profile was the same, however but the external drag and weight of the container attachment frame (which was designed for ISO containers) was removed. The primary mission profile point with the ISO container is highlighted in Figure 32. Payload drag has a relatively minor effect on payload capability, i.e., a 1,800 lb reduction from 0 to 150 ft² payload drag. For a reduction in mission radius to 50 nm, the maximum payload capability increases 17% to a 47,000 lb ISO container at ISA+20°C.

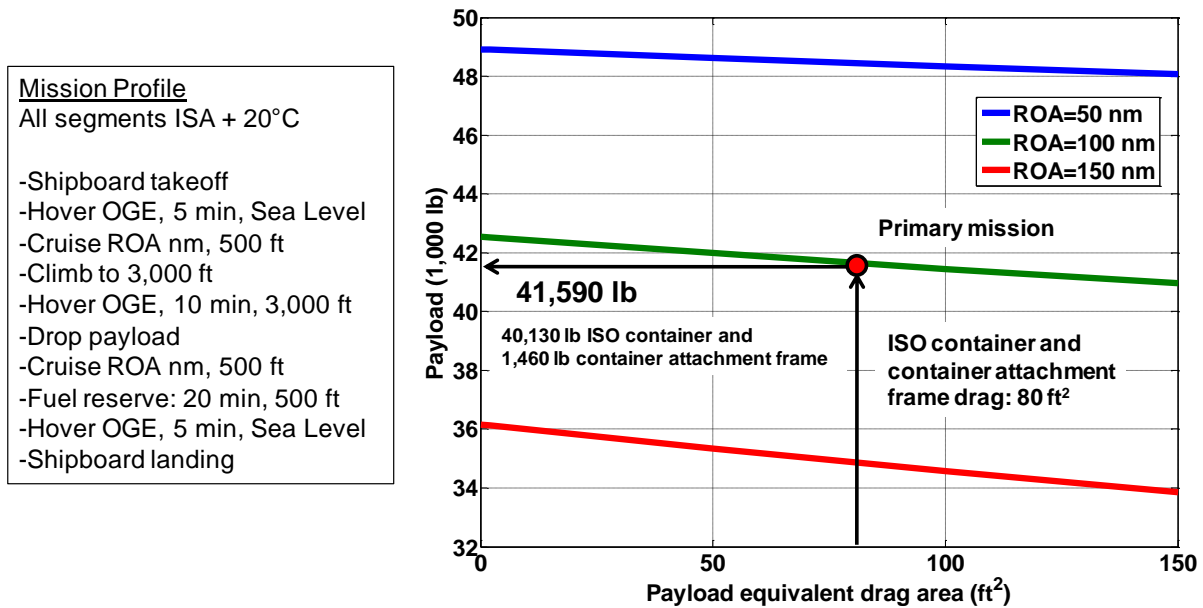


Figure 32: Sensitivity of maximum payload to radius of action and payload drag for generic payload

5.2.3 Payload sensitivity to outside air temperature

Payload-range sensitivity to ambient temperature conditions is shown in Figure 33. Increases in outside air temperature have a large effect on payload capability because of degraded performance of the CH-53E engines as well as increased rotor induced power requirements. Maximum range is slightly increased because the reduced air density decreases the effect of the large payload and structure drag. The *Goliath* capability at standard-day temperature conditions (ISA) becomes limited by the external payload weight limit of the individual CH-53E aircraft for ranges under 50 nm.

Mission Profile
 -Shipboard takeoff
 -Hover OGE, 5 min, Sea Level
 -Cruise ROA nm, 500 ft
 -Climb to 3,000 ft
 -Hover OGE, 10 min, 3,000 ft
 -Drop payload
 -Cruise ROA nm, 500 ft
 -Fuel reserve: 20 min, 500 ft
 -Hover OGE, 5 min, Sea Level
 -Shipboard landing

External drag
 -Payload: 70 ft²
 -Support structure: 116 ft²
 Support structure weight: 4,750 lb

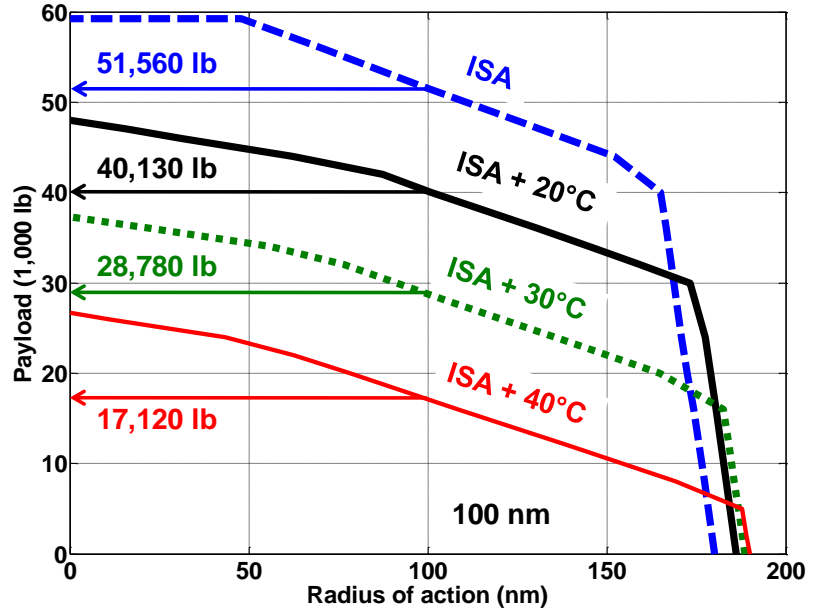


Figure 33: Payload-range curves for varying ambient temperature conditions

5.3 Performance summary

The *Goliath* twin-lift system was predicted to deliver **87% more payload** than the baseline CH-53E for the hot-day primary OMFTS mission profile with 100 nm delivery radius—which meets and exceeds the RFP requirement of a 75% increase. The 100 nm payload capability of 40,130 lb was shown to increase 5% to 42,000 lb when the two helicopters returned separately with the spreader bar structure and cables stowed internally. The payload-delivering capability was found to be relatively insensitive to payload drag area, but highly sensitive to increasing outside air temperature. Under standard-day conditions the *Goliath* can deliver a 51,560 lb payload 100 nm.

6 Twin-Lift Sling Load Dynamics

The addition of a sling load to a helicopter results in logistical problems in hover, and stability problems in forward flight. Solutions suggested to address these issues for a single helicopter are of great value to the twin-lift concept, since similar challenges must be addressed in the twin-lift system. It is, therefore, useful to review the major advancements in sling load operations of single helicopters and then, apply the knowledge gained from previous research. The following subsections presents a summary of previous work done on sling load operations and various twin-lift flight tests and analyses that have been performed. Problems encountered during flight tests and suggested solutions are discussed. The second subsection discusses the history of, and advancements made with the twin-lift concept.

6.1 Perspective on helicopter sling loads

Single helicopter sling loads: The addition of an external payload on a sling to a single helicopter introduces pendulous load motions to the helicopter during its flight. This motion is weakly damped in hover and also has large settling times, resulting in logistical problems during reposition maneuvers. The most appealing solution is the use of hook accelerations to suppress the load oscillations excited by strong gusts and pilot inputs during reposition maneuvers. This low-cost technique requires no external modifications to the helicopter and is adaptable to different platforms. This methodology will be used for the current configuration.

In forward flight, significant unsteady aerodynamic forces on the payloads (which are usually bluff bodies) have been known to cause dynamic instabilities [Simpson 1981]. This instability is characterized by large lateral oscillations coupled with a yawing of the payload. The rotorcraft must operate at reduced speeds to reduce the effect of these instabilities, resulting in performance degradations. Twin vertical fins mounted above the payload have been found to be effective in eliminating the instabilities over the speed range of interest, and appear to be at least one effective solution for the stabilization of the load in forward flight. The current design uses this solution for flight at a cruise speed of 90 knots. Figure 34 summarizes some of the advancements in single helicopter sling load operations.



Figure 34: CH-53E carrying a UH-60 on a sling

Twin-lift helicopter sling loads: The use of multiple helicopters to lift a common payload has been successfully implemented in the past, when heavy-lift helicopters are not available locally. For example, Figure 35 shows two CH-54B helicopters carrying a spreader bar. This exercise was carried out by the U.S. Army [Curtiss 1984]. Two helicopters have been used in synchronization to transport transmission cables in South America. Another example is the use of two Bell Jet Rangers to carry 2,200 lb utility poles at 60 knots. This is equal to 180% of the payload of a single Jet Ranger [Curtiss 1984]. The twin-lift is an emerging concept and has been investigated by various researchers. Instabilities associated with coupling two helicopters have restricted operational implementation until now. These instabilities have been identified in the current design, and appropriate control systems have been suggested to resolve these issues.



Figure 35: Ch-54B on a twin-lift mission

Table 15: Sling load literature summary

Author [Year]	Contribution
Dukes [1973]	<ul style="list-style-type: none"> Proposed use of a translating support point to eliminate load oscillations in hover.
Bisgaard [2008]	<ul style="list-style-type: none"> Delayed feedback and feed forward to suppress load oscillations using helicopter motions.
Gabel [1957]	<ul style="list-style-type: none"> Summary of sling load instability identification and resolution.
Ehlers [2002]	<ul style="list-style-type: none"> Active and passive stabilization of CONEX using vertical fins.
Cicolani [1998, 2009]	<ul style="list-style-type: none"> Frequency domain load aerodynamic modeling. Identification of fish-tail instability for certain vertical fin configurations. Spin stabilization of CONEX boxes.

Table 16: Twin-lift literature summary

Author [Year]	Contribution
Meek [1970]	<ul style="list-style-type: none"> • Feasibility studies and demonstration of twin-lift system. • Identification of high pilot workload levels. • Suggestion of control coordination.
Curtiss [1984]	<ul style="list-style-type: none"> • Modal analysis of twin-lift system in lateral-vertical plane. • Identification of inverted pendulum instability.
Rosen [2005]	<ul style="list-style-type: none"> • Modal analysis in forward flight for twin-lift system. • Identified role of turn coordination on system dynamics.
Walker [2006]	<ul style="list-style-type: none"> • Piloted simulation of twin-lift system. • Suggested vertical and lateral separation distance.
Kondak [2007]	<ul style="list-style-type: none"> • Implementation of multi-lift system using 3 UAVs (single MR/TR). • World's first multi-helicopter lift demonstration (small scale).

6.2 Dynamics of the isolated helicopter

The natural dynamics of a single helicopter was assumed to be represented by a linearized stability and control derivatives model. To obtain these quantities, an in-house analysis was developed in which the following features were implemented:

- Blade element based 2-d quasi-steady aerodynamics with linear inflow (Drees model).
- Finite element analysis for elastic flap bending, rigid in torsion and lag.
- Coupled aeroelastic trim using finite elements in time.
- Finite-difference stability and control derivatives.

The code was then validated by comparing the predicted stability derivatives with flight test data [Heffley 2005] for the CH-53D helicopter, as shown in Figure 36.

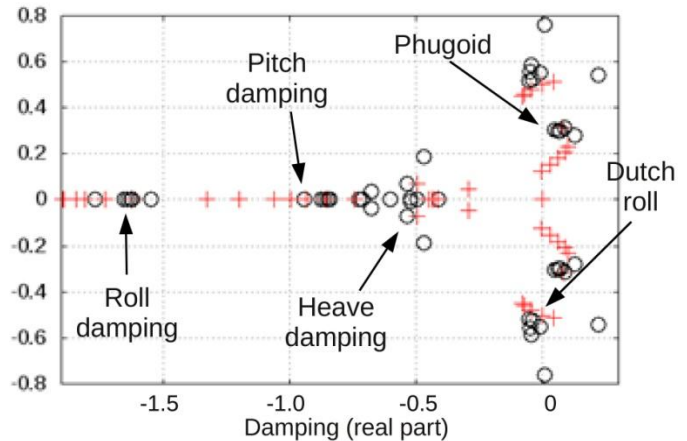


Figure 36: Prediction of CH53-D natural modes versus flight test data for various speeds: hover to 100 knots

The stability and control derivatives subsequently obtained were used for predicting the following:

1. Natural dynamics of the twin-lift system.
2. Handling qualities criteria with a sling load.
3. Simulation of the twin-lift system with a controller.
4. Selection of feedback gains.

6.3 Twin-lift dynamics

An analysis was performed to determine the stability characteristics of the twin-lift system in hover. The flight dynamics was subdivided into those in the lateral-vertical plane, the longitudinal-vertical plane, and the truss yaw dynamics. The model derived by Curtiss [Curtiss 1975] was used to obtain the system characteristics for the vertical-lateral plane motions.

6.3.1 Vertical-lateral plane

It was assumed that the helicopters are in hover with their fuselage reference lines normal to the span of the spreader bar. The planar dynamics may be further subdivided into symmetric modes and anti-symmetric modes. The symmetric modes involve vertical in-phase motion of the helicopters, as well as anti-phase roll and lateral motion. The anti-symmetric modes involve vertical out-of-phase motion, as well as the in-phase roll and lateral helicopter motion along with motion of the load. The various modes are described in the following subsections.

Symmetric modes: The symmetric modes are largely governed by the relative weights of the payload and helicopter and the distance from the center of gravity to the hook point. The symmetric modes are:

1. An inverted pendulum or tethered helicopter divergent mode, which is increasingly unstable for greater vertical offsets of the cargo hook from the center of gravity of the helicopter.
2. A mildly unstable oscillatory mode involving lateral translation of the helicopters when the hook is above center of gravity.

The presence of these divergent modes demonstrates the need for a feedback control when carrying sling loads with a spreader bar.

Anti-symmetric modes: The anti-symmetric modes are observed to be:

1. Motion resembling the lateral phugoid of the helicopters in hover.
2. A lightly damped pendulous mode of the payload and spreader bar.
3. A damped spring mode involving the relative vertical separation of the two helicopters. The differential cable tensions stabilize the vertical separation of the helicopters.

Therefore, utilization of a spreader bar for a twin-lift task leads to two important effects:

1. A stable damped mode restoring vertical separation.
2. A divergent “inverted pendulum” mode.

6.3.2 Vertical-longitudinal plane

The helicopters, spreader bar, and payload system form a double pendulum system in the vertical longitudinal plane. The support points are free to translate vertically and horizontally. The associated modes for the double pendulum are shown below schematically in Figure 39 and after the simulation in Figure 40 and Figure 41 respectively.

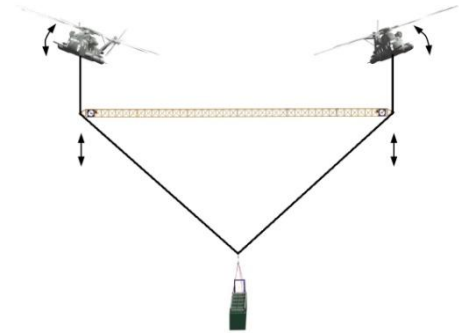


Figure 37: Twin-lift symmetric modes

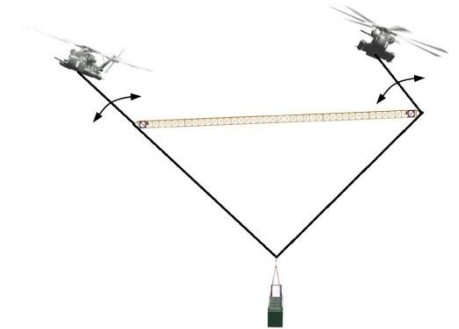


Figure 38: Twin-lift anti-symmetric modes



Figure 39: Double pendulum symmetric mode (left) and anti-symmetric mode (right)

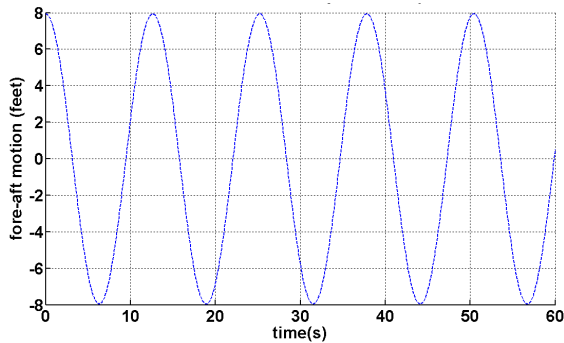


Figure 40: Double pendulum symmetric mode simulation

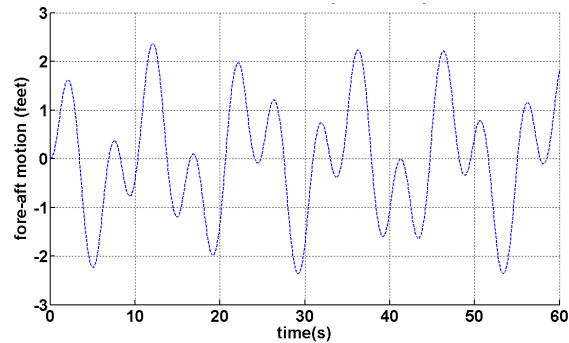


Figure 41: Double pendulum anti-symmetric mode simulation

In the symmetric motion, the truss and payload move in synchronization, and in the anti-symmetric mode the truss and payload execute motions opposite to each other.

The relative magnitudes of these modes are dependent on the mass ratio of the payload and the spreader bar. For a heavy payload, the lower mass is 3 to 4 orders of magnitude greater than the mass of the truss. Thus, the dominant response is the “single pendulum” motion (i.e., symmetric motion) with a small anti-symmetric component. This effect is shown in Figure 40. However, for a relatively light payload, which would be experienced during the return journey after payload drop-off, the magnitude of the anti-symmetric mode becomes significant, as shown in Figure 41. Both of these modes make it difficult to execute precision hover maneuvers with the sling load, and must be damped out before lowering or picking up the payload to prevent impact damage.

Symmetric mode: The symmetric mode oscillations can be eliminated through support point accelerations. Payload oscillations were reduced effectively by feeding back the payload swing rate to the hook accelerations. This technique is equivalent to moving the support point of a simple pendulum to reduce the load motions. The control inputs to introduce these accelerations are applied by the automatic stabilization system.

The natural frequency of the symmetric mode is shown in Figure 42 and Figure 43, respectively. It is seen that for the symmetric mode, the length of the cable from the helicopter to the spreader bar, as well as the vertical offset of the payload beneath the spreader bar, play an important role in determining the frequency, which is of the order of 0.1 Hz. It is this “slow” mode that can be damped out through the translational accelerations of the helicopter.

Anti-symmetric mode: The anti-symmetric mode cannot be eliminated by using hook accelerations. This mode can be damped out by applying control forces on the spreader bar, using feedback of the anti-symmetric swing rate, and is significant for light or no payloads. Stabilization is required to avoid structural impact damage to the lower spreader bar and so eliminate a potential safety hazard issue at the pick-up and landing site. The stabilization mechanism is

The anti-symmetric mode frequency is plotted in Figure 43 as a function of cable length from the spreader bar to the helicopters as well as various vertical offsets of the payload beneath the spreader bar. This frequency is a function of the mass ratio of the payload to the spreader bar and changes with the payload weight. The effect of payload vertical offset on this longitudinal mode was found to be negligible. Furthermore, for all vertical offsets of payload beneath the spreader bar, the mode frequency asymptotic limit is 0.3 Hz.

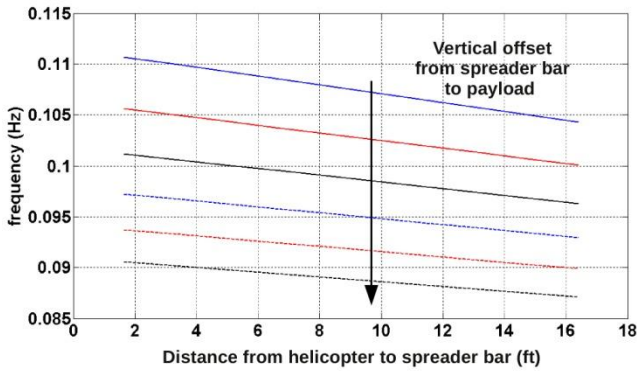


Figure 42: Symmetric mode frequency versus suspension length

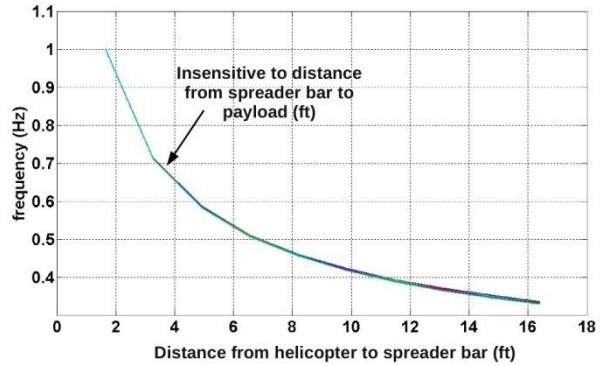


Figure 43: Anti-symmetric mode frequency versus suspension length

6.3.3 Effect of sling loads on helicopter modes

The addition of a sling load to a single helicopter has a significant effect on its natural dynamics. It was found that a sling load stabilizes the natural mode dynamics if the sling point is below the helicopter’s center of gravity. However, for a twin-lift configuration, the presence of the payload beneath the spreader bar, as well as the hook position beneath the center of gravity, results in the unstable inverted pendulum mode.

6.3.4 Spreader bar yaw mode

The spreader bar that is suspended from the two helicopters is susceptible to yawing oscillations when differential translational accelerations are imparted to the support points. This motion is shown schematically in Figure 44. As a result of this oscillation, the container attachment frame executes undamped vertical motion that results in logistical problems during load pick-up and at the payload delivery area. A counteracting control moment is required to damp out these oscillations and reduce the time required for securing the payload.

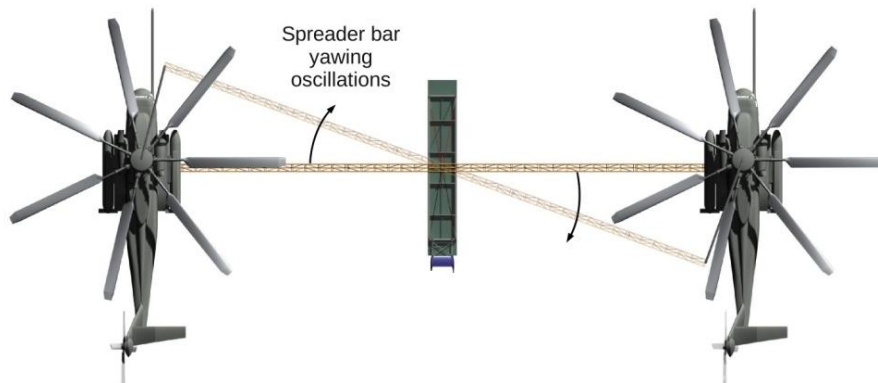


Figure 44: Spreader bar yawing mode

6.3.5 Spreader Bar Stabilization

To simultaneously stabilize the double pendulum anti-symmetric oscillations and the spreader bar yawing oscillations, the Goliath twin-lift design utilizes two ducted fans placed at the ends of the spreader bar. In-phase actuation of the thrusters are used to stabilize the double pendulum anti-symmetric mode, while differential (anti-phase) thrusts are used to damp out any yawing oscillations. The thruster design has been discussed in SECTION 4.2. A limiting force of 60 lb is found to be sufficient for stabilizing spreader bar oscillations for lightly-loaded configurations, as seen during the load pick-up and the return phases. Therefore, the thrusters improve system characteristics and reduce payload lock-in times, while ensuring complete operational safety.

7 Twin-Lift Handling Qualities

Pilot ratings of helicopters operating with external loads provide insight into the workload associated with specific piloting tasks. This situation is considered to be of particular importance to a twin-lift piloting task involving precision load maneuvering, where the “baseline” workload levels are already high. To alleviate these high workloads, a study of handling qualities of rotorcraft operating with sling loads may provide valuable information that may be refined to provide additional design constraints.

The first subsection (below) discusses the effect of adding external loads on rotorcraft handling qualities. The next subsections cover the development of an equivalent single helicopter model for the twin-lift configuration, followed by the application of this model and associated handling qualities constraints to the current design.

7.1 Surge response criteria

Flight tests [Heffley 2005] have shown that for rotorcraft operating with externally slung loads, pilot opinion correlates better with surge response criteria (i.e., longitudinal and lateral translational velocities) than with pitch or roll attitude response criteria. For a single rotorcraft with an external load, a detailed procedure to obtain the modified gain and phase bandwidth is outlined below [Heffley 2005]. These criteria provide insight into pilot opinions and are first-order predictions of handling qualities of a helicopter carrying an externally slung load. Bandwidth requirements to retain Level-1 handling qualities with sling loads are stated in Table 17.

Table 17: Surge bandwidth requirements for rotorcraft operating with external loads

Axis	Pendulum bandwidth (rad/s)	Surge bandwidth (rad/s)
Longitudinal	0.39	0.44
Lateral	0.73	0.59

The validity of this surge response criterion to the twin-lift configuration must be verified from flight tests, but it is considered that the surge response is a better measure of pilot opinion than the attitude gain and phase bandwidth-based ratings.

7.2 Evaluation of surge bandwidths

To evaluate the helicopter surge bandwidths with the sling load, the Bode plots are obtained from the transfer function from cyclic stick inputs to the lateral and longitudinal surge responses of the helicopter.

Pendulum bandwidth: The pendulum bandwidth is defined as the range of frequencies around the sling pendulum frequency over which the phase margin is 45° or greater because of the addition of the external load.

Phase bandwidth: Described in Figure 45, the load phase bandwidth is determined by:

- Obtain the highest frequency at which the phase margin is 45° and determine the magnitude at that frequency.
- Draw a horizontal line at that magnitude and note the lowest frequency at which the surge magnitude plot crosses this horizontal line.
- The frequency at this intersection point is the phase bandwidth of the helicopter-sling load system.

Gain bandwidth: Describe in Figure 46, the load gain bandwidth is determined by:

- Find the highest frequency at which the phase is -180° and read the magnitude at this frequency.
- Multiply this magnitude by 2 and draw a horizontal line.
- Obtain the lowest frequency at which the magnitude curve intersects the horizontal line; this is the gain bandwidth of the helicopter-sling load system.

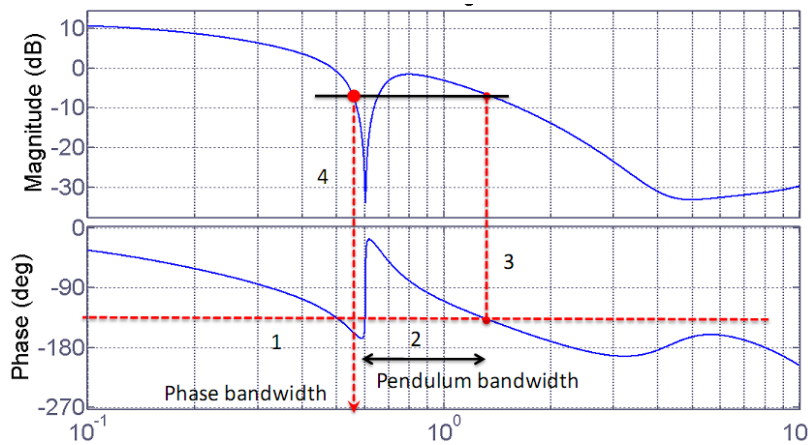


Figure 45: Finding phase and pendulum bandwidths from a bode plot

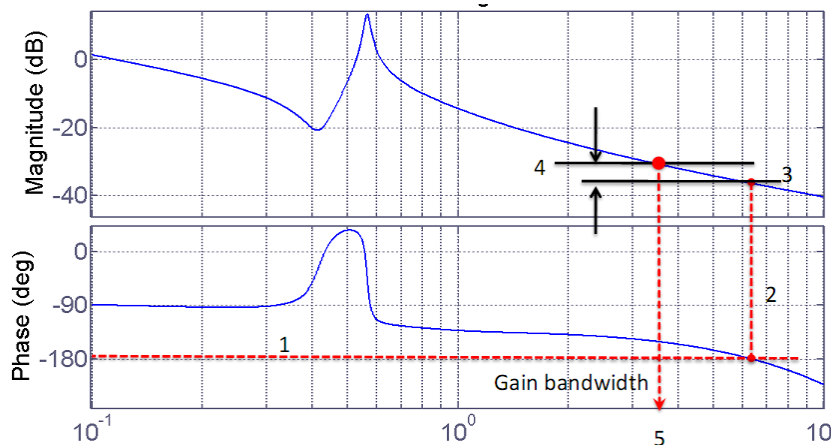


Figure 46: Finding gain bandwidth from a bode plot

7.3 Model description

In the current configuration, each helicopter supports half of the total system weight in hover (including the payload and spreader bars). For a control-synchronized configuration, both helicopters are controlled by a single pilot and move with a relatively small time lag. Therefore, an “equivalent” single helicopter model can be built as shown in Figure 47. For a single helicopter carrying a sling load, a linearized model about the trim condition was found to yield a sufficiently accurate measure of the system surge response.

Lateral mode: For the lateral mode, the pendulum length is considered to be the length of the cable from the helicopter’s hook to the spreader bar. The linearized model is given by:

$$\begin{aligned} \ddot{x}_H &= X_u u + X_q q + X_\delta \delta_{lon} + \frac{m_L g}{M_H} \theta_c \\ I_{yy} \ddot{\theta}_H &= M_u u + M_q q + M_\delta \delta_{lon} + \frac{m_L g r}{I_{yy}} \theta_c + \left(M_{\theta_H} - \frac{m_L g r}{I_{yy}} \right) \theta_H \\ \ddot{x}_H + r \ddot{\theta}_H + l_{c1} \ddot{\theta}_c &= -g \theta_c \end{aligned}$$

Longitudinal mode: For the longitudinal mode, the pendulum length is the vertical separation between the helicopter and the payload.

$$\begin{aligned} \ddot{y}_H &= Y_v v + Y_p p + Y_\delta \delta_{lat} - \frac{m_L g}{M_H} \phi_c \\ I_{xx} \ddot{\phi}_H &= L_v v + L_p p + L_\delta \delta_{lat} + \frac{m_L g r}{I_{xx}} \phi_c + \left(L_{\phi_H} - \frac{m_L g r}{I_{xx}} \right) \phi_H \\ -\ddot{y}_h + r \ddot{\phi}_H + l_{c2} \ddot{\phi}_c &= -g \phi_c \end{aligned}$$

From the surge response Bode plots, the gain and phase bandwidths were computed and checked against the requirements specified in Table 17.

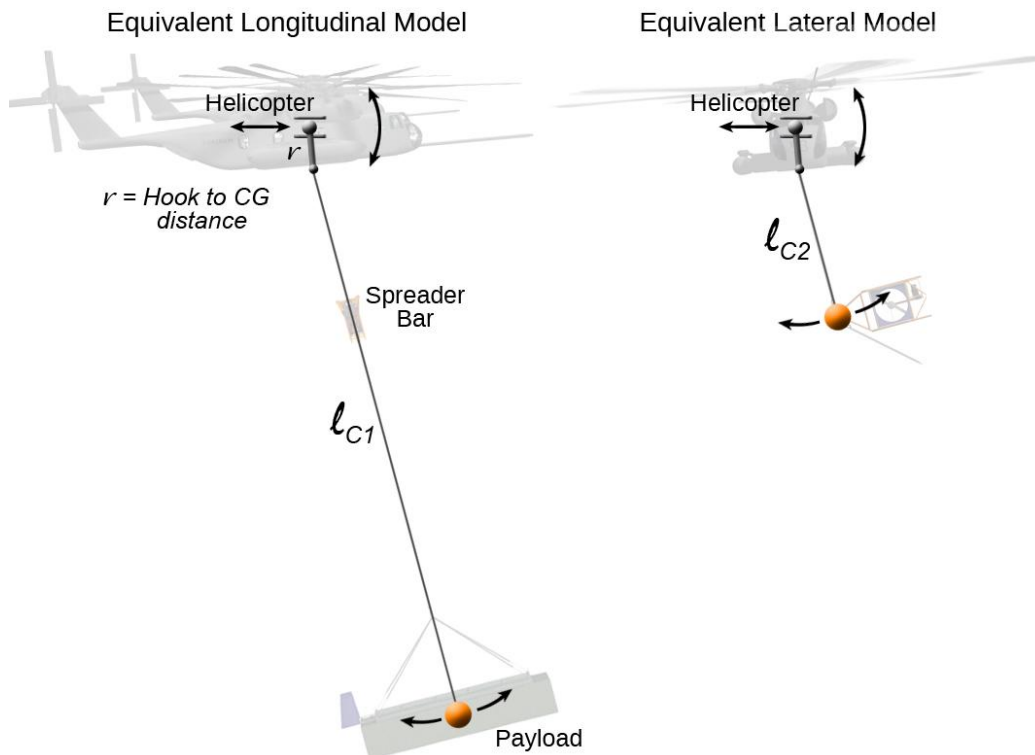


Figure 47: Equivalent sling load model for lateral and longitudinal modes

7.4 Results from analysis

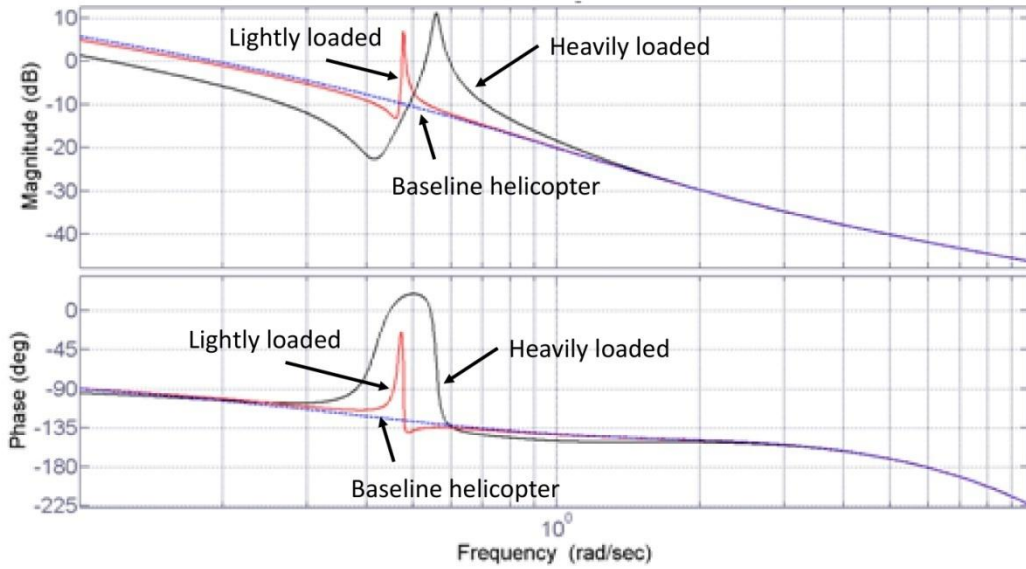


Figure 48: Longitudinal surge gain and phase

Based on the simplified models, the transfer functions for helicopter surge response were constructed and the bode plots drawn, as shown in Figure 48 and Figure 49. The three lines in the Bode plots represent the unloaded configuration (blue), carrying only spreader bars (“light double pendulum” in red) and the fully loaded configuration (black).

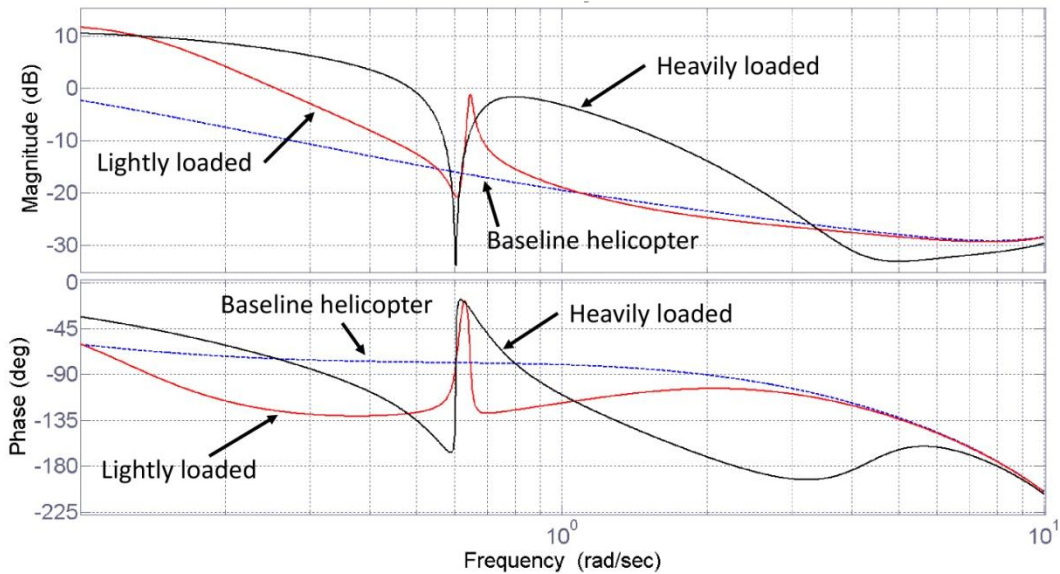


Figure 49: Lateral surge gain and phase

7.5 Conclusions

The following conclusion were drawn from the dynamic load analysis:

1. The phase bandwidth limits the allowable cable lengths (longitudinal).
2. The pendulum bandwidth, together with the phase bandwidth criterion, limits cable lengths (lateral).
3. A decrease in cable length shifts the pendulum bandwidth median to a higher frequency, resulting in a greater frequency range for an improvement in phase margin.

The effect of increasing relative payload to helicopter mass is to:

1. Significantly degrade the lateral axis phase and gain bandwidth.
2. Significantly widen the pendulum phase bandwidth for longitudinal and lateral surge.
3. Decrease the gain bandwidth in the longitudinal axis.

Based on these results, it was decided that to achieve acceptable handling qualities at for both the lightly-loaded and highly-loaded systems, the maximum cable lengths of the system were as follows:

1. Cable length from the helicopters to the spreader bar (lateral mode) must be less than 70 ft long.
2. Total vertical offset of the payload from the helicopters (longitudinal mode) must be less than 150 ft.

Additional constraints have been considered in SECTION 3 before finalizing the design.

8 Twin-Lift Control Coordination

When two helicopters are coupled to carry a common external payload, the workload of the trail pilot increases significantly [Kendrick 2006]. This is because the piloting task is not only to safely maneuver the rotorcraft, but also to maintain safe lateral and vertical separations. The existing control systems on the helicopters are designed to stabilize an isolated helicopter and by themselves are not adequate for the twin-lift task.

Pilot workload associated with maneuvering an isolated helicopter can be alleviated by using control augmentation systems that improve the handling qualities of the rotorcraft. The augmentation can alleviate the physical and mental workload of the pilot by favorably changing the natural response of the helicopter. These functions will be discussed in the following subsection.

Large values of attitude feedback gains are required to maintain lateral separations between the two helicopters and stabilize the divergent tether helicopter mode discussed in the SECTION 6. These gains are so high that the helicopter rotor modes might be driven unstable [Prasad 1989]. The vertical separation may be maintained by using the altitude hold functions of the Automatic Flight Control System (AFCS), but the accuracy obtained using the onboard sensors is insufficient for precise regulation of the relative positions. Simulations [Kendrick 2006] and flight demonstrations [Curtiss 1984] have shown that the pilot workloads associated with the twin-lift task are significant and need a stabilization system. The controller functions of the *Goliath* Twin-Lift System are described in this section, with particular focus on.

1. The available sensors and automatic stabilization modes of the CH-53E.
2. Utilization of these functions in the controller design.
3. Alleviation of pilot workloads through system synchronization.

8.1 Contributions of previous work

The solution for relative separation regulation between the two helicopters and the payload in a twin-lift system has been previously addressed in the literature. Table 18 summarizes the major contributions of researchers over the years.

Table 18: Summary of literature on twin-lift controls

Author [Year]	Contribution
Curtiss [1984]	<ul style="list-style-type: none"> Suggested attitude feedback for position regulation. Suggested cyclic feed-forward from one helicopter to another.
Prasad et al., [1989],[1990],[1991],[1992]	<ul style="list-style-type: none"> Developed 3d nonlinear model and controller of twin-lift system. Proved effectiveness over linear controller. Established adaptive control procedure. Comparison of role-assigned versus cooperative control for twin-lift. Comparison of pendant and spreader bar concepts.
Rodriguez [1992]	<ul style="list-style-type: none"> H_∞ control of twin-lift based on linearized model.
Bernard [2009]	<ul style="list-style-type: none"> Multi-UAV control coordination for lifting slung payload. Flexible algorithm to include additional helicopters in the system.
Bisgaard [2010]	<ul style="list-style-type: none"> Feed-forward anti-swing control for slung load oscillations. Delayed feedback for load oscillation damping.

8.2 CH-53E Automatic Flight Control System (AFCS)

The CH-53E features an automatic flight control system (AFCS), which is used to improve short term and long-term dynamic stability, and also to reduce pilot workload. The AFCS is subdivided into two parts: an inner loop and an outer loop. Components of the AFCS are detailed below in Table 19.

Table 19: CH-53E AFCS components

Component	Description
Sensors	Monitoring cockpit control settings and helicopter displacements and velocities.
Controls	Various cockpit switches available to the pilot, to enable or disable AFCS functions based on switching logic and sensor information.
Computers	Processing information gathered by sensors and generating signals based on switching logic.
AFCS Servos	Convert electrical signals generated by computers to mechanical motion (piston motion) that actuates the flight controls. The cockpit controls are also moved only if outer loop signals are generated.

AFCS sensors: The sensors onboard the CH-53E, and available to the AFCS, are shown schematically in Figure 50. This information is fed to the AFCS, and used to augment the pilot commands to maintain control and stability of the helicopter. The CH-53E AFCS sensors are:

1. Accelerometers (translational accelerations).
2. Air data transducer (velocities and altitude) .
3. Gyros (attitudes, angular rates and accelerations).
4. Radar altimeter (altitude).
5. Attitude and Heading Reference System (AHRS) .

The controller designed for the *Goliath* Twin-Lift system, leverages these sensors along with additional sensors on the spreader bar and payload, to completely determine the twin-lift component states in real-time. The controller developed for

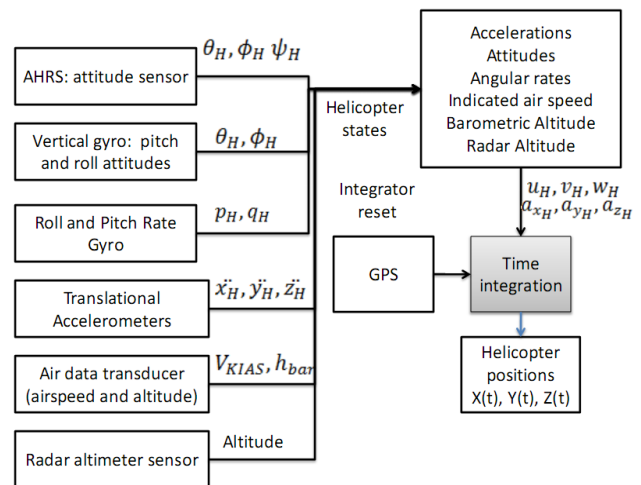


Figure 50: CH-53E onboard sensors available to AFCS

this system is then able to stabilize and control the twin-lift system.

AFCS controls: The controls and switches available to the pilot and copilot are the cyclic and collective levers, pedals and push buttons that initiate a number of the AFCS functions. The control paths from the pilot’s cyclic, collective and pedal provide inputs to the AFCS servos, through the mixing unit, and finally to the main rotor swashplate servos, as shown in Figure 51.

AFCS servos: When an AFCS function is engaged, the servos provide the following functions:

- Power boost for pilot stick and pedal control inputs.
- Electro-mechanical conversion of the inner loop signals into mechanical motion of main and tail rotor servos.
- Electro-mechanical conversion of outer loop signals into mechanical motion of the cockpit flight controls.

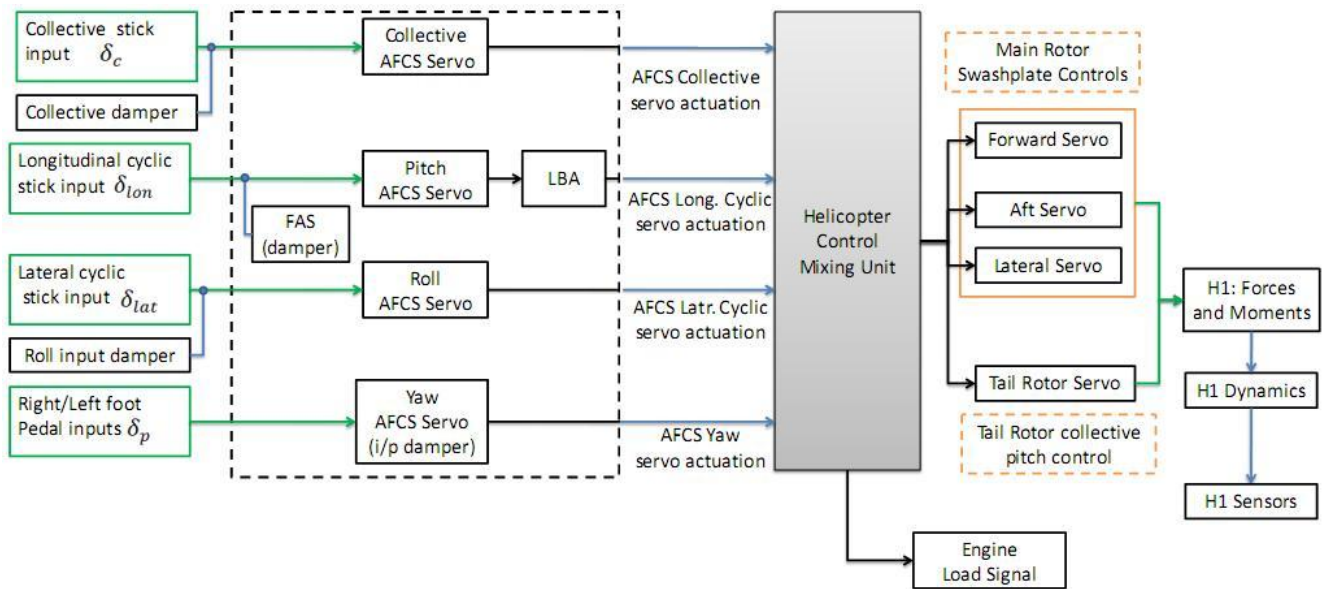


Figure 51: CH-53E control architecture

Longitudinal Bias Actuator (LBA): The LBA is an electrical screw jack that extends and retracts as a function of airspeed gradient and pitch rate. It provides positive static pitch trim gradient, decouples collective pitch from the longitudinal cyclic pitch channel, and improves the maneuvering stability.

Force Augmentation System (FAS): The FAS is an actuator that is placed in series with the longitudinal cyclic pitch input. It also provides input damping in the longitudinal channel. It provides cyclic pitch indent and gradient adjustment, pitch position trim, pitch autopilot functions (attitude/airspeed hold), and applies opposing stick forces proportional to g-loads to safe guard against over-stressing the airframe.

Mixing Unit (MU): The mixing unit is placed in series with the AFCS to counteract the effects of cross-couplings inherent in the helicopter. These cross-couplings arise from the presence of, and interactions between, rotor aerodynamics, forward shaft tilt, and tail rotor cant. The outputs of the mixing unit are then fed to the main rotor swashplate servos and to the tail rotor servo, which then provide collective and cyclic pitch inputs to the rotor. The functions of the mixing unit are summarized in Table 20.

Table 20: CH-53E control couplings

Coupling	Compensation description
Collective to yaw	Counters additional yawing moment generated by main rotor torque.
Collective to pitch	Counters additional pitching moment generated by main rotor thrust increase.
Collective to roll	Counters roll moment generated by tail rotor from collective to yaw coupling.
Yaw to pitch	Counters pitching moment generated by the tail rotor thrust due to cant.
Yaw to roll	Counters rolling moment generated by tail rotor thrust from vertical offset.

AFCS computers: Two AFCS computers are present and individually process signals generated by the onboard sensors. The AFCS computers generate electrical signals and then combine the signals through averaging. In the case of a malfunction, the appropriate computer signals are ignored. The electrical signals are converted to mechanical outputs by the AFCS servos. The computers also generate electrical inputs for the FAS for providing pilot force feedback, and for the LBA as described above. The capabilities of the AFCS are summarized in Table 21:

Table 21: CH-53E AFCS capabilities

Short-term (inner loop) dynamic stability functions	
Function	Description
SAS	<ul style="list-style-type: none"> Adds rate damping for attitude changes.
Hover augmentation and Gust alleviation	<ul style="list-style-type: none"> Opposes lateral and longitudinal accelerations.
Control desensitizers	<ul style="list-style-type: none"> Selective input attenuation at fuselage frequencies.
Turn coordination (SAS)	<ul style="list-style-type: none"> Feeds lateral accelerometer inputs to pedal servo.
Flight control damping	<ul style="list-style-type: none"> Damps out high frequency stick inputs. Hydraulic dampers built into Yaw Servo and FAS.
Long-term (outer loop) dynamic stability functions	
Function	Description
Trim	<ul style="list-style-type: none"> Holds cockpit controls at desired position.
Pitch / roll attitude hold, heading hold	<ul style="list-style-type: none"> Holds desired pitch/roll attitude. Holds desired heading.
Auto turn, auto bank	<ul style="list-style-type: none"> Improves turn coordination, re-references roll attitude.
Pilot stick force feedback	<ul style="list-style-type: none"> Force feedback to prevent airframe over-stressing.
Barometric altitude hold	<ul style="list-style-type: none"> Altitude hold with accuracy (greater of) 25 ft or 1%.
Radar altitude hold	<ul style="list-style-type: none"> Altitude hold with accuracy (greater of) 7 ft or 5%.

8.3 Twin-lift control description

A control system for the *Goliath Twin-Lift* system has been developed that takes advantage of the computing capability and autopilot functions already available onboard the CH-53E helicopter with minimum alterations to accommodate the twin-lift functionality. The additional capability is achieved without affecting the normal operation of the helicopter's flight controls. The controller algorithm works cooperatively with the existing AFCS architecture to provide stability, control, and safety of the twin-lift system. The challenge faced in the control of a twin-lift system lies in the coordination of two joined helicopters, which would ordinarily be under the control of two pilots. There are four possibilities that can be considered to achieve a satisfactory degree of control, as shown in Table 22.

Table 22: Twin-lift control comparison

Helicopter 1	Helicopter 2	Advantages	Disadvantages
Manual Synchronization Twin-lift Control (MSC)			
Pilot 1 and AFCS 1	Pilot 2 and AFCS 2	Pilot inputs unchanged.	High trail pilot workload.
Single Pilot Twin-lift Control (SPC)			
Pilot 1, AFCS 1 and twin-lift controller	Pilot 1, AFCS 2 and twin-lift controller	Automatic input synchronization.	System must take-off and land in twin-lift configuration. More hi-fidelity sensors required on helicopter – platform - specific modifications. Independent return option unavailable.
Independent Approach and Relinquish Single Pilot Control (IAR-SPC)			
Pilot 1, AFCS 1 and twin-lift controller	During approach: Pilot 2, AFCS 2 After Relinquish: Pilot 1, AFCS 2 and twin-lift controller	Automatic input synchronization. Independent operations: flexible approach and return options available.	Maneuvering clearance judgment critical in tight spaces.
Unmanned Twin-lift Control (UTC)			
Twin-lift controller	Twin-lift controller	No risk to human life. Automatic synchronization. Independent operations.	Fast transmission times required to track pilot inputs. Implementation possible only on rotorcraft with specific capabilities.

Of these concepts, the “Unmanned Twin-Lift Control” concept has the greatest advantages over all others, and appears to be the most advantageous concept. However, the *UTC* requires installation of unmanned piloting capabilities in the rotorcraft being considered, resulting in greater system implementation and maintenance costs. The “Independent Approach and Relinquish Single Pilot Control” concept, by comparison, has the most favorable cost-to-benefit ratio. It is this concept that is implemented for the Goliath Twin-Lift system.

8.3.1 Controller concept description

Twin-lift synchronization is engaged by the Master pilot, who is responsible for maneuvering the entire system. In forward flight, the Master pilot’s helicopter is offset laterally, and positioned behind and above the Slave pilot’s helicopter. The pilot in the lead helicopter, (the “Slave” pilot) is passive with no authority over the system. The Master pilot (referred to as pilot for the twin-lift system) maneuvers the twin-lift configuration by providing collective and cyclic stick inputs in his own helicopter. The Master pilot’s stick inputs are measured by the *AFCS* sensors and fed forward to the Slave helicopter to synchronize the helicopter motions. The avionics module integrates the sensor data from the Master helicopter, combines it with the state information of the Slave helicopter, spreader bar and payload. This information is processed by the control algorithm to determine the swashplate actuation required by both helicopters to maintain constant separation and reduce payload swings, as well as to coordinate maneuvers. The output signals of the controller are used to augment the helicopter *AFCS* servo signals to produce the desired actuations. The controller further generates actuation requirements of the thrusters, located at the spreader bar, to damp-out spreader bar oscillations initiated by strong gusts and system maneuvers. A detailed description of the controller is given in the following section. The system hardware is described in SECTION 4.5

8.4 Twin-lift state measurements

The system parameters are determined as detailed in Table 23 using information made available from the helicopter sensors, as well as sensors distributed on the load handling structure (see SECTION 4.5). This sensor scheme provides the information required to compute the system during various stages of the mission, as and when necessary, without the complexity of other methods e.g., adaptive algorithms.

Table 23: System parameter measurements

Parameter	Computed using	Sensors used
Helicopter mass	<ul style="list-style-type: none"> Swashplate control settings (hover). Trim attitudes. 	<ul style="list-style-type: none"> AFCS servo positions. Roll/pitch vertical gyro.
Spreader bar mass	<ul style="list-style-type: none"> Cable forces during pick-up. 	<ul style="list-style-type: none"> Load sensors at hooks.
Spreader bar length Cable length	<ul style="list-style-type: none"> Relative distances from ends of spreader bar to helicopter. 	<ul style="list-style-type: none"> RF sensor measurements.
Spreader bar inertia	<ul style="list-style-type: none"> Estimated using mass and length of spreader bar. 	
Payload mass	<ul style="list-style-type: none"> Cable forces during pick-up. 	<ul style="list-style-type: none"> Load sensors at hooks.
Payload drag and download	<ul style="list-style-type: none"> Cable angles during flight and force measurements. 	<ul style="list-style-type: none"> Swivel AHRS and RF sensor. Load sensors at hooks.

8.5 Twin-lift controller function

The twin-lift controller used to stabilize the system is shown in Figure 52. The functionality is divided into four subsystems, each designed to perform a specific task:

1. Stabilizing the anti-symmetric double pendulum oscillations for lightly loaded configurations.
2. Stabilizing the yawing oscillations of the spreader bar for lightly loaded configurations.
3. Regulating relative helicopter positions (safe separation).
4. Interpreting the commands of the controlling pilot to maneuver the twin-lift system.

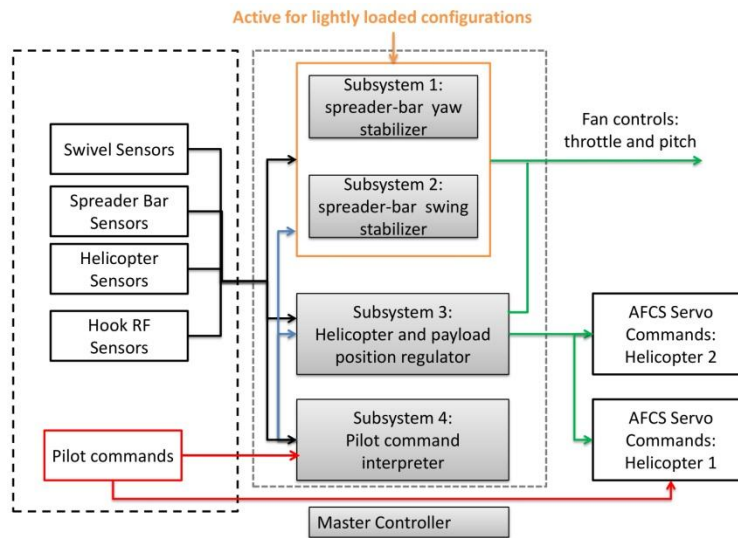


Figure 52: Controller for the twin-lift subsystems

8.5.1 Spreader bar stabilization

During the alignment process for the load pick-up and return flight, the load beneath the top spreader bar consists only of the lower spreader bar. Because of this light load (1,800 lb), the truss yaw mode is easily excited by relatively smaller perturbations (e.g., gusts and system accelerations) compared to the fully loaded case. This effect is of particular significance during pick-up, where the truss yaw mode results in a vertical oscillation for the lower spreader bar (load carrying device). The anti-symmetric double pendulum mode can result in translational swing (fore-aft motion) so some

stabilization mechanism is required to minimize the oscillations of the lower spreader bar. As previously described, this stabilization is provided through two thrusters placed on the upper spreader bar at each end. The double pendulum anti-symmetric mode can be eliminated by the in-phase actuation of the thrusters, while differential (anti-phase) thrust can be used to damp out spreader bar yawing oscillations. These mechanisms constitute the first and second subsystems of the twin-lift controller. These two subsystems are shown schematically in Figure 53.

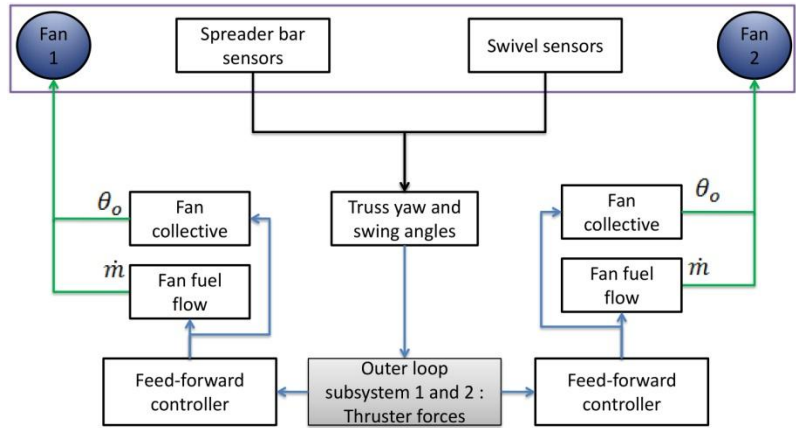


Figure 53: Spreader bar stabilization subsystems

Simulation results: anti-symmetric mode damping: The present analysis shows that feeding back the swing rate of the lower spreader bar relative to that of the upper spreader bar can efficiently damp out the anti-symmetric mode. Figure 54 shows fore-aft motion time-history of the lower spreader bar in response to an initial disturbance. The dotted line is the response in the absence of any stabilization, which is characteristic of a double pendulum. The associated time-history of the thruster is shown in Figure 55.

These thrusters effectively eliminate the anti-symmetric mode disturbance within about 30 seconds. This result is of particular importance during spreader bar positioning for payload pickup, where excessive oscillations of a load-carrying frame poses a risk to ground crew safety and damage to nearby equipment. This undesirable effect is reduced significantly by using dedicated anti-swing mechanisms.

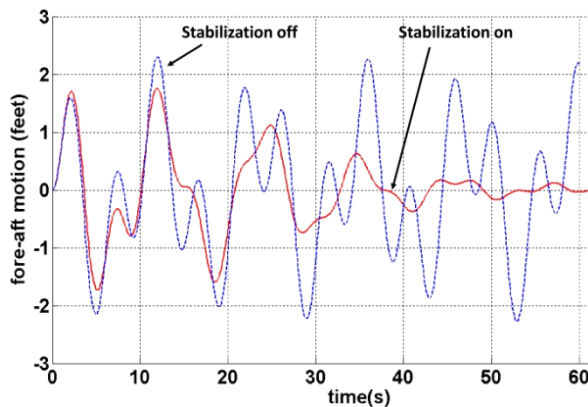


Figure 54: Longitudinal time-history of the lower spreader bar in response to an initial disturbance

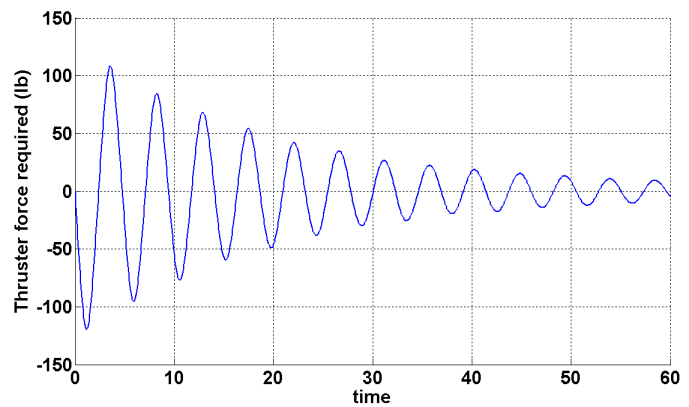


Figure 55: Thruster time-history for damping of pendulum asymmetric mode

Simulation results: spreader bar yaw damping: The present analysis shows that the feedback of the truss yaw rate to the differential thrust inputs is the most effective method of damping-out yawing oscillations. The differential forces from the ducted fans provide a counteracting moment to reduce the oscillation amplitudes. Feedback of the yaw rate of the spreader bar to the differential thruster force was effective in damping-out disturbances. In Figure 56, the red solid line shows the vertical position of the lower spreader bar when the stabilizing system is on, and the dotted blue line for when the system is off. The consequences of the yawing of the spreader bar on ground crew operations must be considered. When the truss yaws relative to the two helicopters, the entire spreader translates vertically upward, thus creating a vertical oscillation for the lower spreader bar (which is secured to the container). To lower the spreader bar over the container and lock it in place, vertical alignment is critical. This alignment may be accomplished through differential thrusts

to create a stabilizing yawing moment without exciting the asymmetric mode of the double pendulum response. Figure 57 shows the associated thruster time-history.

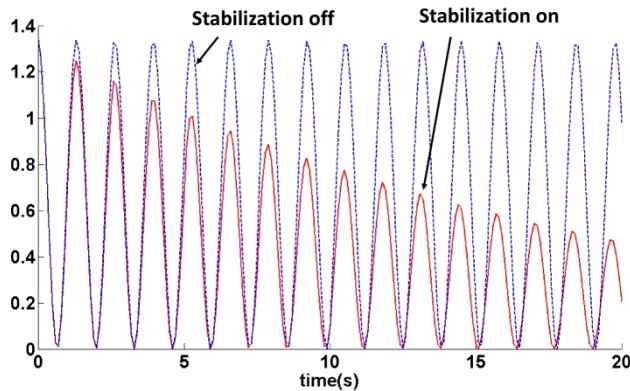


Figure 56: Vertical position of the lower spreader bar in response to an initial condition

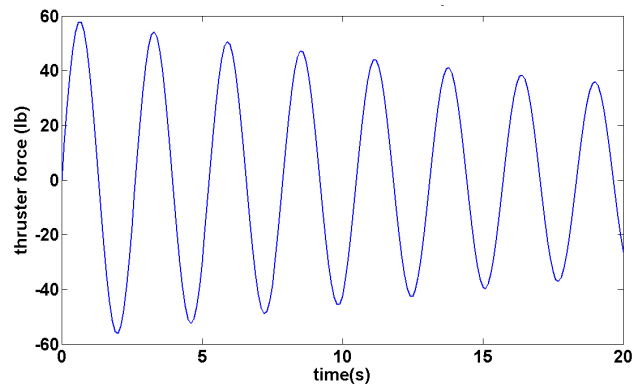


Figure 57: Thruster force time-history for yaw damping

Furthermore, a limiting thrust of 60 lbs was found to be sufficient to damp-out oscillations within a 45 second time interval.

Fan transient elimination: In the current design, a feed-forward controller is used in conjunction with the yaw angle and anti-symmetric swing rate time-histories to reduce the effect of thruster spin-up and spin-down transients. The limiting actuation frequency for the ducted fans is 0.4 Hz. Therefore, any residual spin-up and spin-down time lags produce insignificant changes to the augmented dynamics of the spreader bar.

8.5.2 Regulation of relative positions

To regulate relative positions of the helicopters, the controller obtains information from the AFCS sensors of both helicopters, and the sensor arrays on the load handling structure. These sensors measure the positions, velocities, attitudes, angular rates (of the helicopters) and the truss attitudes, swivel position beneath the spreader bar, the thrust being generated by each thruster on the spreader bar and the spreader bar position relative to the helicopters.

When the sensor measurements are combined with the calibrated spreader bar and cable lengths, as well as the vertical offset of the payload beneath the spreader bar, the controls required at the swashplates (to maintain the desired separation) of each helicopter are computed. In addition to these measurements, the controller obtains the pilot stick inputs, as detected by the sensors already present in the helicopter, to initiate system position changes

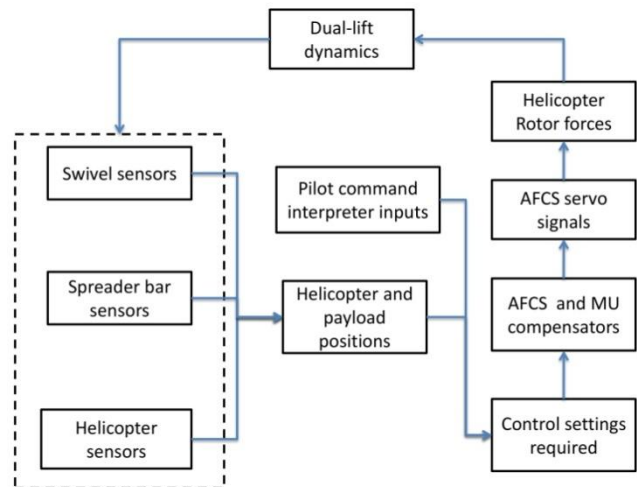


Figure 58: Separation regulation flow diagram

The third controller subsystem (relative position regulation) is operative as soon as the spreader bar is attached to the helicopters. Position regulation is considered to be essential to achieve safe payload pick-up with minimal pilot workload while conforming to safety standards. The method outlined by Prasad [Prasad 1989], based on input-output feedback linearization, has been adopted for separation regulation. Figure 58 shows the method flow diagram.

Inputs required: The helicopter positions, velocities, accelerations, angular rates, attitudes, angular accelerations; as well as the truss orientations, cable angles, cable lengths, payload position and swing rate are required as inputs.

Processing: Using the signals generated by the sensor suite, the relative positions and velocities of the helicopters and load are computed. These separations are then fed to a compensator that generates a set of pseudo-control variables. These pseudo-controls are converted into attitude orientations of the helicopters and rotor forces in the controller. To account for the system nonlinearities (from large attitude changes from trim conditions), the states (helicopter positions and orientations) are used to convert the pseudo-controls to forces and moments required at each helicopter rotor. Finally, these forces and moments are reduced to control changes required at the swashplate of each helicopter.

Outputs: Using the control angle changes generated by the processing unit, the electrical signals required to produce these actuations are computed and fed to the outer-loop channels of the helicopter AFCS servos.

Achieving control changes: The most efficient method for introducing control changes is through the addition of electrical signal inputs to the AFCS servos, as shown in Figure 60. This method does not require extensive hardware changes to the helicopters, which is the main motivation behind the choice of signal augmentation location. Once uncoupled from the twin-lift configuration controller, the AFCS servo displacements are obtained only by the onboard AFCS and the stick inputs, and can revert to the unmodified or uncoupled operation mode through a single switch.

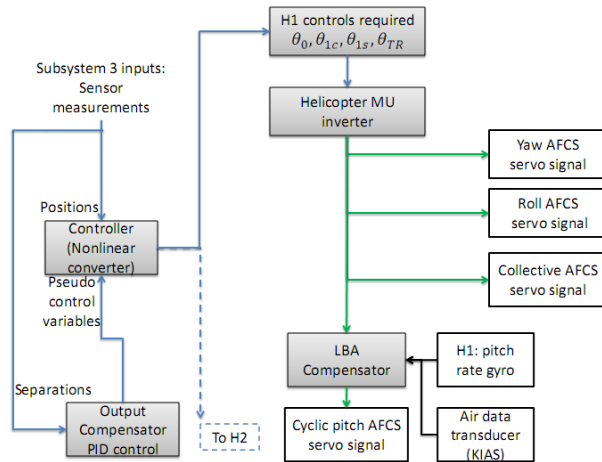


Figure 59: LBA and MU compensations

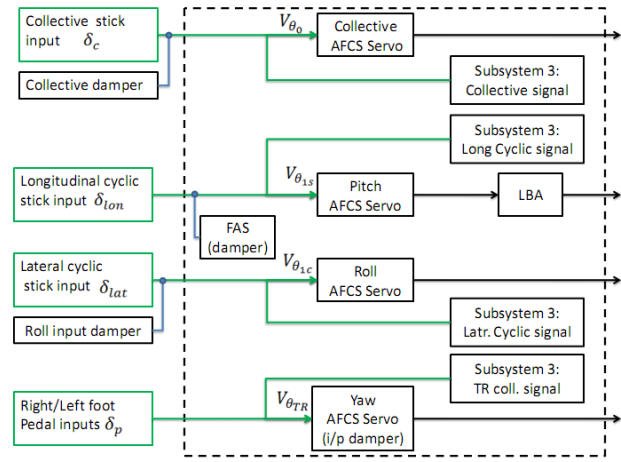


Figure 60: AFCS signal additions

Compensations for Longitudinal Bias Actuator and Mixing Unit: These are electrical compensations that are generated by the separation regulation subsystem and are shown in Figure 59. The necessity for these compensations is stated below.

The mixing unit present in the helicopter is meant to compensate for these couplings when the inputs are from the pilot controls and onboard AFCS. Because these couplings have already been accounted for in the controller analysis, it is necessary to introduce an inverter that, effectively, cancels out the role of the mixing unit for the augmented AFCS servo stroke displacements.

For the longitudinal channel, the Longitudinal Bias Actuator (LBA) is present between the AFCS servo and the mixing unit. This electrical screw jack extends and retracts with airspeed gradient and pitch rate, and must be accounted for in the control signals that are generated. Therefore, the pitch-rate gyro and air data transducer are used as inputs to the LBA Compensator.

8.5.3 Interpreting pilot commands

This feature allows one pilot to control the entire twin-lift system instead of the individual pilots having to manually synchronize their inputs. The collective, cyclic and pedal input signals from the Master helicopter are fed to the AFCS outer

loop servos on the Slave helicopter. Any transients that result in deviations from the preset separation distances will activate the third subsystem (separation regulator), ensuring that any intervention of the Slave pilot is unnecessary.

Simulation results: symmetric pendulum mode damping: For stabilizing the symmetric mode, the present analysis shows that feedback of symmetric pendulum swing rate to the helicopter translational accelerations is effective in damping out any oscillations. The helicopters are constrained to move forward only so as to avoid pilot disorientation.

Interaction with position regulation subsystem: The position regulation subsystem constrains the fore-aft oscillations of the helicopters and the payload. At the end of a reposition maneuver, the longitudinal position and velocity constraints are relaxed to allow the helicopters to translate. The payload swing rates are fed back to the helicopter accelerations, which are then tracked using the built-in accelerometers. The payload oscillations are as shown in Figure 61. Once the load swing is damped out, the separation regulation constraints are enforced and a reposition maneuver is initiated.

Control system modifications: In the case of low-speed flight operations, fore-aft accelerations of the helicopters can excite the double pendulum modes. To avoid pilot-induced oscillations, the cyclic stick feedback forces are increased to provide control cues to the pilot and so limit the allowable accelerations of the helicopter. This behavior is enforced through modifications to the Force Augmentation System, which obtains additional inputs from the translational accelerometers.

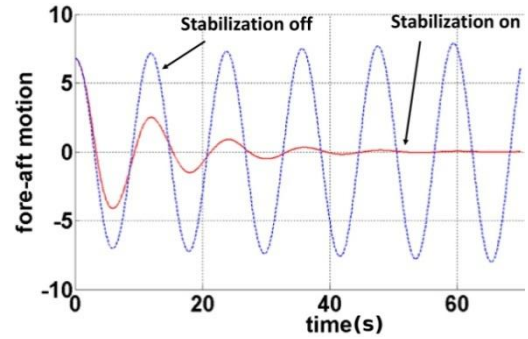


Figure 61: Oscillation time-history of container attachment frame

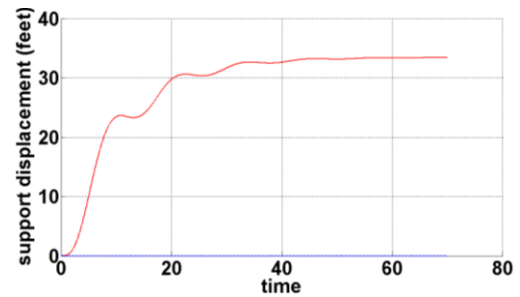


Figure 62: Support point motion time-history

Table 24: Separation regulation controller gains

State description	Proportional gain (K_P)	Derivative gain (K_D)	Integral gain (K_I)
Vertical separation	0.03	0.23	0.0033
Lateral separation	1.2	2.0	0.144
Payload lateral swing	0.1	0.5	0
Longitudinal separation	0.02	0.4	0.001
Payload fore-aft swing	0.25	0.4	0.001
Pitch attitude	0	10.0	0
Roll attitude	0	8.0	0
Yaw attitude	0	5.0	0

9 Twin-Lift Sequence of Operation

This section describes the complete operation of the twin-lift configuration when performing the design mission. This mission requires that the twin-lift configuration be assembled on a ship, without external assistance, from where the payload is collected, before being transported to a drop zone 100 nm further inland. The ship-based mission was chosen for discussion because there are detailed manuals for land-based sling load procedures; however, there is less data available for the more intensive ship-based operation. It was assumed that no special equipment is available to assist with load drop off. The mission then requires that the assembled configuration be returned to the ship, where it is disassembled. It is also assumed that any variants on this mission are a straightforward modification of these procedures. Finally, procedures specific to ground and aircrew operations pertaining to helicopter sling load operations are available in military field manuals. Only relevant modifications to these standards are mentioned here.

9.1 Assembly and payload pickup

9.1.1 Ship layout

Assembly of the spreader bar, layout of the helicopter approach path, and positioning of the ground crew and signalmen restrict truss use to large aircraft carriers and some amphibious assault ships. Two example ships with sufficient deck space are the LHD class USS Essex (length = 844 ft) or the aircraft carrier Nimitz (length = 1,092 ft). The ship layout given in Figure 63 is optimal for pilot workload and assumes a generic aircraft carrier with sufficient, unrestricted deck area. The applications of payload pickup where there is insufficient deck space, would necessitate the assembly of the twin-lift configuration either on a second larger ship or from a land station. The featured modularity of the spreader bar and components allows it to be easily transported in the cargo hold of a single CH-53E to a remote assembly point. Otherwise the procedures outlined will be identical.

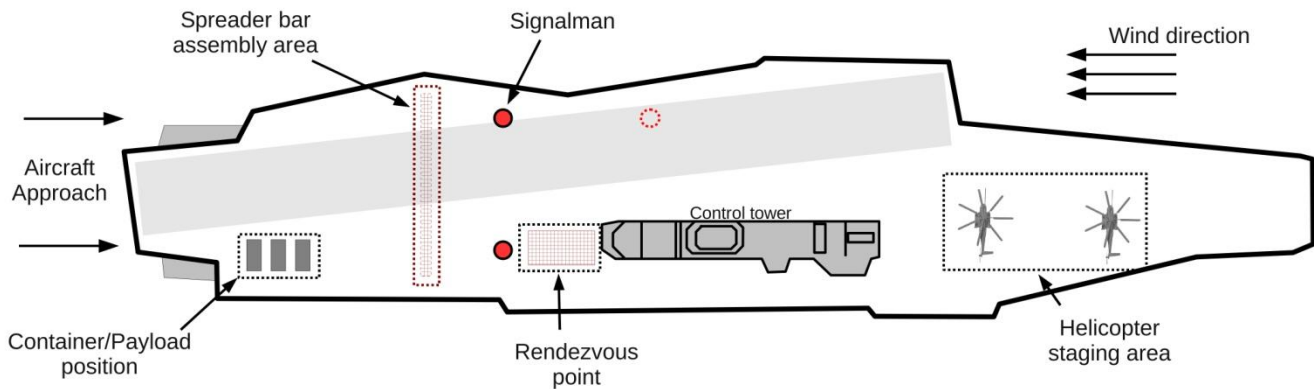


Figure 63: Aircraft carrier layout

- The helicopters approach from the rear of the carrier towards the spreader bar, which straddles the deck for reduced pilot workload.
- Two signalmen position themselves at both ends and 40 ft behind the spreader bar to guide in, and position each helicopter.
- The rendezvous point, where the ground crew position themselves before and after payload hook up, is located at a safe distance away from the pick-up point, as shown in Figure 63.
- The container/payload is positioned away from the spreader bar for safety.

9.1.2 Ground operations

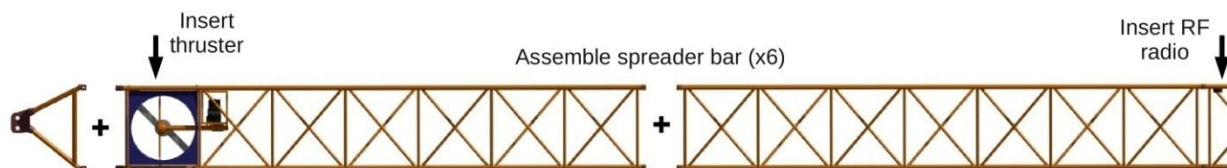


Figure 64: Assembly of spreader bar

- The spreader bar is assembled as shown in Figure 64. Each modular component is sized to be carried by a maximum of four personnel.
- Before clearing the helicopters for approach, one of the ground crew is responsible for diagnostics of the onboard sensors of the spreader bar. This diagnostic is carried out with a handheld wireless unit that receives the broadcast signals from each sensor to determine their signal strength, proper functionality, and battery life.
- Once all of the diagnostics are finished and the spreader bar is assembled, the signalman clears the helicopters in for approach.

9.1.3 Approach above the spreader bar



Figure 65: Approach of the helicopter to the spreader bar



Figure 66: Avionics box display during approach

- Figure 65 shows the approach of the helicopters. The pilots maneuver their helicopters under the direction of a separate signalman.
- The control box on board each helicopter is active and receiving transmissions from the spreader bar and the other helicopter so as to give positional awareness to the pilots. Figure 66 shows the pilot's display.

9.1.4 Positioning above the spreader bar

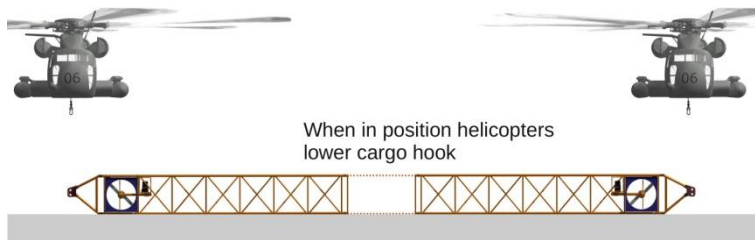


Figure 67: Positioning of helicopters before hook-up

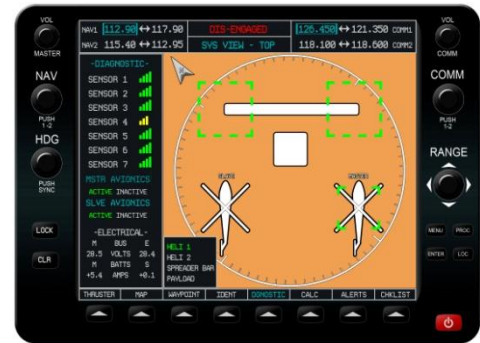


Figure 68: Avionics display before hook-up

- The helicopters will maneuver to reach a hover above each end of the spreader bar and engage the gust rejection and hover hold inner loop functions of the AFCS.
- Each pilot is directed by a signalman and assisted by on screen instructions from the control box. Figure 68 shows the display available to both pilots that indicates the current positions and the target positions of each helicopter. The display indicates the position and role of each helicopter on the screen.
- When both of the helicopters are in position, the cargo hooks are lowered, as shown in Figure 67.

9.1.5 Spreader bar hook-up

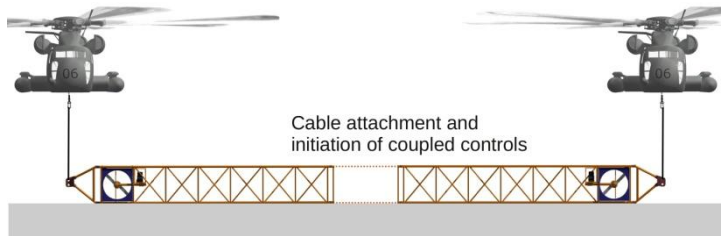


Figure 69: Spreader bar attachment

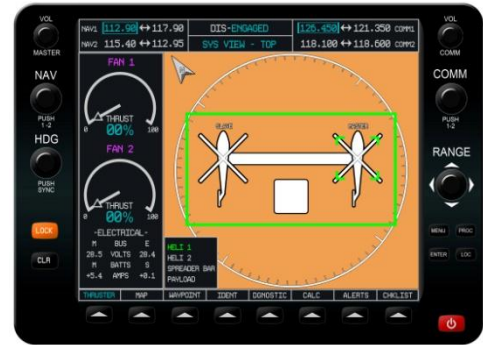


Figure 70: Avionics display for lock on

- When cleared by the signalman, two teams of ground crew approach each helicopter simultaneously.
- Static electricity is discharged before the spreader bar cables are attached to the helicopter’s cargo hook, as shown in Figure 69.
- The ground crews evacuate the area to the rendezvous point.
- On confirmation from the signalman, the pilots prepare to engage configuration lock and arm their control boxes.
- The Master pilot then presses LOCK, as shown in Figure 70, to initiate twin-lift mode, taking command of both helicopters. The outer loop control maintains helicopter relative position by providing swashplate commands to both helicopters.
- One signalman remains to direct the Master pilot for subsequent operations.

9.1.6 Load handling structure lift off

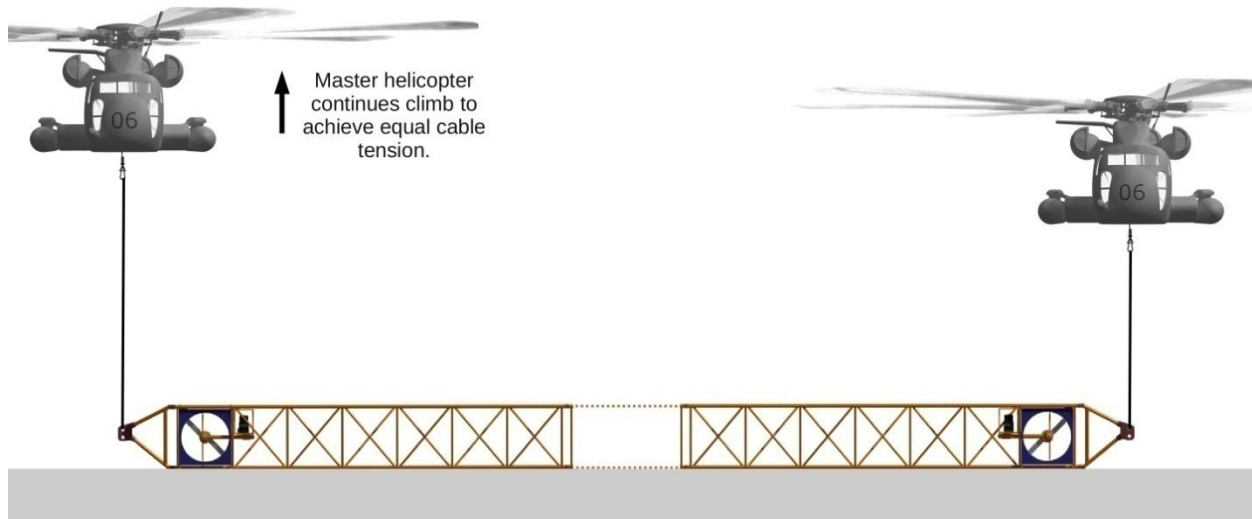


Figure 71: Coupled helicopters in climb

- The signalman gives the Master pilot an instruction to climb.
- Both helicopters climb at the same rate under pilot control until the cable on the Slave helicopter becomes taut. This point is determined by the load cell sensor on the instrumented cargo hook.
- Figure 71 shows how the autopilot commands the Slave helicopter to hold position while the Master helicopter continues to climb until the load sensor registers a cable tension.
- Once the spreader bar is clear of the deck, the control box calibrates the length of the cables and spreader bar using the RF radio measurements, and measures the weight of the spreader bar using the load cells.

- The pilot then continues to climb until the load handling spreader bar is clear of the deck.
- A second stage calibration determines the payload vertical offset from the helicopters to the load handling spreader bar and its weight.

9.1.7 Positioning above the payload

Two possibilities exist for payload pickup. One assumes that the load handling spreader bar is attached to the payload, in this case a container, before picking up the spreader bar. This is the simpler case, and should be attempted when feasible. However the general case, described here, assumes that the load handling spreader bar can only be attached to the helicopters.

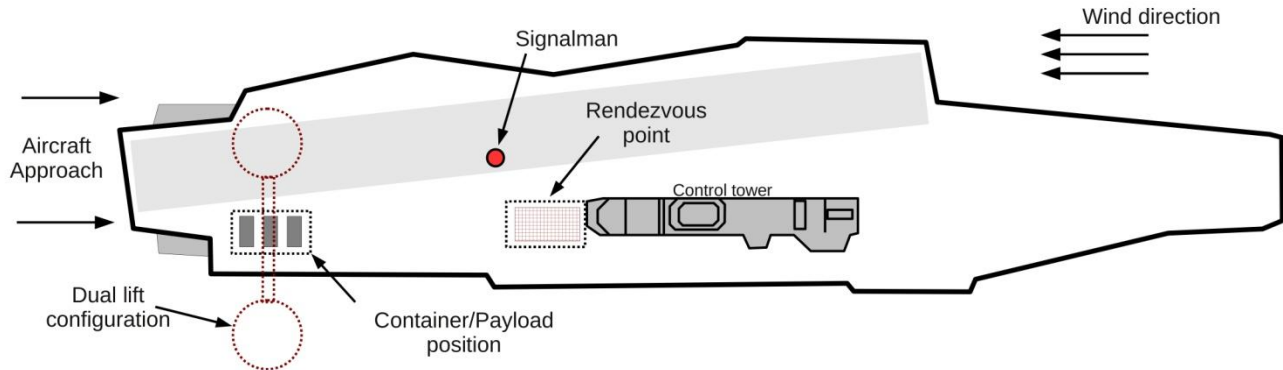


Figure 72: Configuration layout for payload pick-up

- The signalman repositions himself to provide a 45° pilot viewing angle (as shown in Figure 72).
- The Master pilot receives cues to position the load handling spreader bar above the payload.
- The controller actuates the thrusters on the spreader bar to stabilize any oscillations of the load handling spreader bar.
- When any oscillations are sufficiently damped, the signalman clears the ground crew to approach the payload, orient the load handling spreader bar, and ensure sufficient lower cable slackening to engage the automatic mechanical lock.
- The ground crew then returns to the rendezvous point, after which the Master pilot is guided by the signalman to climb and maneuver away from obstacles.

9.2 Forward flight

9.2.1 Orientation for forward flight

During load pick-up, both helicopters are oriented perpendicular to the spreader bar. Yaw control of the configuration in hover, with or without a payload, requires special attention. The pilot may need to “look around” after the twin-lift mode is engaged. It is important for safety and preserving pilot intuition that the response to control inputs in twin-lift mode mimics those of a single helicopter. This conflicts with yaw control in hover, where pedal inputs result in yaw attitude change for a single helicopter only. To retain the original control functions, the control box provides an interface to achieve a pure twin-lift turn about the payload. This maneuver requires large turn clearances and must not be initiated in confined areas.

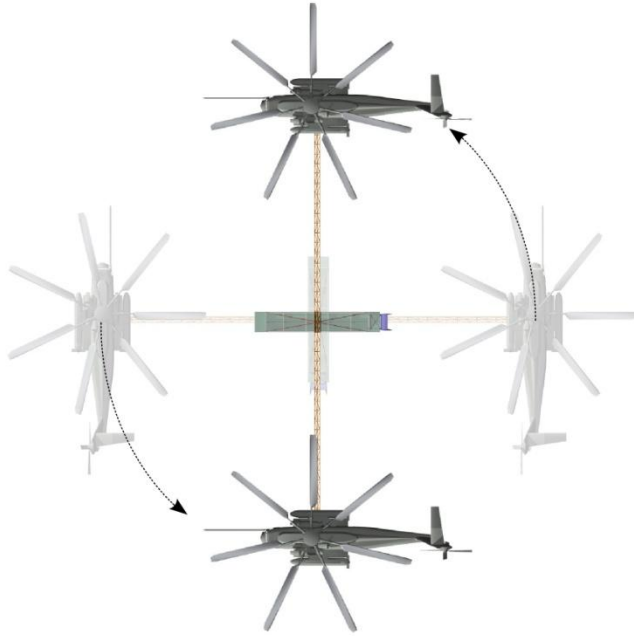


Figure 73: Twin-lift turn coordination in hover



Figure 74: Avionics display for turn coordination

- Figure 73 shows a left hand coordinated yaw maneuver in hover.
- A separate heading change dial is provided to avoid changes to existing control functions and to preserve pilot control intuition.
- Prior to engaging system turn, the heading hold settings on the helicopters are adjusted to orient the fuselage reference lines normal to the spreader bar axis.
- The Master pilot adjusts the heading dial on the control box shown as “HDG” in Figure 74, to the desired heading. The visual display shows the heading changes.
- Once heading is set the pilot engages the yaw command by depressing the “HDG” dial button.
- The control box generates swashplate commands to pivot both helicopters about the payload as indicated in Figure 73.
- Master pilot pedal inputs will cause yaw of the Master helicopter only.

9.2.2 Progression into forward flight

Once the desired heading changes have been achieved, the pilot applies longitudinal stick inputs to achieve the desired pitch attitude. The control inputs of the pilot (measured by the sensors available in the helicopter) are fed forward to the slave helicopter. The entire configuration then accelerates. To avoid exciting the symmetric pendulum mode, the acceleration is limited to 1.5 knots/s to restrict payload trail distances to 20 ft. Therefore, the minimum allowed time to reach 90 knots starting from hover is 60 seconds.

9.2.3 Configuration swing

To reduce drag on the spreader bar, the Slave helicopter swings ahead and the Master helicopter swings back, to orient the axis of the spreader bar at 30° to the flight direction. This swing takes place when the system maintains 30 knots or greater for 30 seconds, and is achieved over 60 seconds to avoid large accelerations. This time delay is imposed to avoid configuration swing during short reposition maneuvers. The air data transducers are used to measure the airspeed, and a time-history of the indicated airspeeds is used to initiate the swing using the controller. The separation distances are simultaneously reassigned to account for the forward flight configuration.

9.2.4 Calibrations

Using the steady-state cable trail angles, along with the calibrated cable lengths, the payload drag is computed.

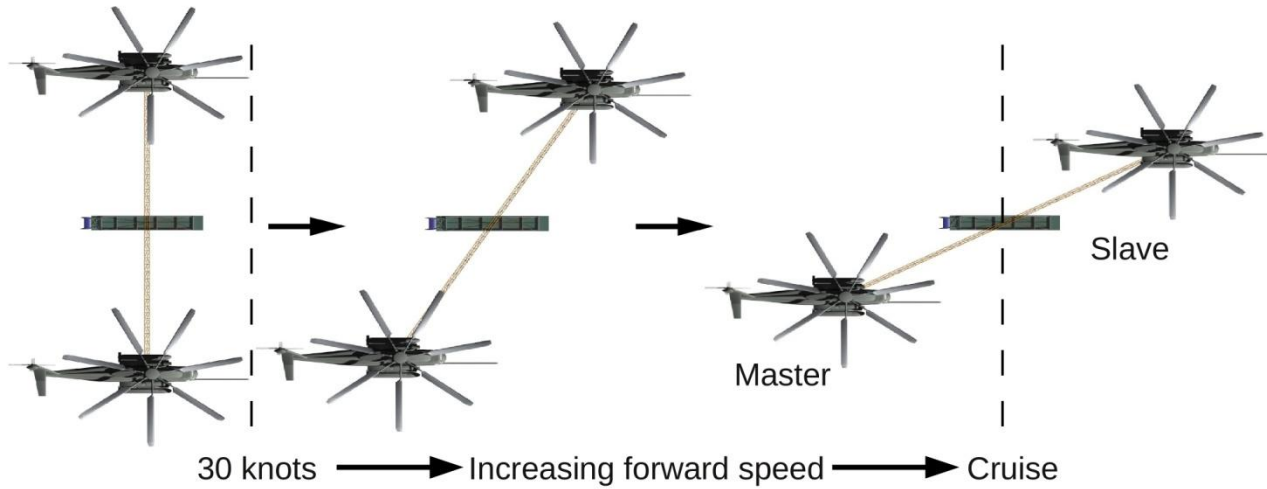


Figure 75: Illustration of swing maneuver

This swept configuration reduces the drag of the spreader bar and allows the Master pilot to observe the spreader bar and the tip-path-plane of the Slave helicopter.

Once the desired cruise speed is reached (which, in this particular case, is 90 knots) the primary pilot engages airspeed hold on the helicopter’s onboard AFCS. This AFCS, which is linked to the Master controller, ensures that the cruise condition is maintained. The configuration change is achieved by differential lateral and longitudinal cyclic pitch through the swashplates of both helicopters. The payload is chosen as the pivot point to avoid exciting the load swing.

9.2.5 System turn coordination

In forward flight, the twin-lift system may be required to execute a change of heading. The turn radius for this maneuver is restricted by allowable hook load limits. Rotor stall is not a limiting factor for system turn for the load specified. The minimum turn radius for various airspeeds is shown in Figure 76.

With increasing airspeed, the twin-lift system has to conduct wider turns because of two effects. At greater flight speeds, the aerodynamic drag as well as the centrifugal loads (for a given turn radius) increase as square of the airspeed. This is the reason for the quadratic curve for the lower limit of the turn radius, as shown in Figure 76.

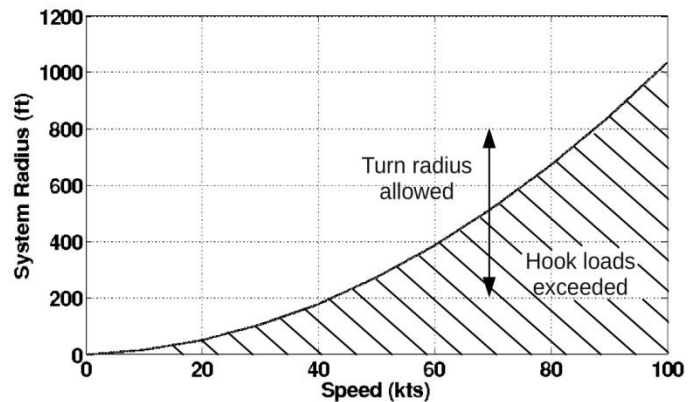


Figure 76: Minimum system turn radius versus airspeed

Turn coordination is activated in the helicopter AFCS at speeds of 60 knots or greater. However, in the twin-lift configuration, turn coordination is activated at all speeds so as to maintain nominally equal hook loads. Alterations to the AFCS must also compensate for the helicopter’s own turn coordination inputs.

For the isolated helicopter, turn initiation is recognized by lateral stick inputs during steady forward flight or changes to the heading dial. For the twin-lift system, the following procedure is proposed to achieve coordinated turns:

- The Master pilot makes the desired changes on the heading dial of the control box.
- The position regulator maintains the relative separations between the helicopters. Some allowance for load lateral swing (up to 10 feet) is permitted by the controller.
- It is the payload that is constrained to move in a coordinated turn. Allowance of 5 ft in the separation distances between the helicopters is considered to be reasonable to equalize the hook loads without exciting payload oscillations, while also maintaining safe separation distances.
- If the loads on any one hook exceed 95% of the allowable hook load, then the relative heights between the helicopters are varied during the turn to equally distribute the additional turn forces.
- If both hook forces exceed 90% of the allowable hook load simultaneously, then the controller instructs the system to increase the turn radius until the loads decrease to acceptable levels.

While a 5% hook load margin may initially seem insufficient, the loads encountered for the scale chosen are significant and a small percentage is, in fact, thousands of pounds of force. This is the justification for choice of load sharing margins.

9.2.6 Failure modes

During flight the safety of the crew is maintained as priority at all times. A number of failures modes are considered and redundancy is highlighted.

Sensor failures during payload pick-up: The remedy for a sensor failure during load pick-up is to disengage from twin-lift mode, land, identify and replace the faulty device and restart the mission.

Table 25: Sensor failure during payload transportation

Sensor	Measurement provided	Consequence of malfunction	Remedy
Swivel AHRS.	Payload position beneath the spreader bar.	Lower cable angle unknown.	<ul style="list-style-type: none"> • Evaluate angle using inclinometer (double pendulum ignored).
Spreader bar inclinometers (both sets).	Cable angles from helicopter to spreader bar.	Truss position unknown.	<ul style="list-style-type: none"> • Use RF sensors and cable forces to estimate truss position. • Truss dynamics not important with heavy payload.
Force sensors (one or both).	Cable forces.	Load sharing unknown.	<ul style="list-style-type: none"> • Obtain force estimate from cable angle time-histories and calibrated weights. • Increase allowed turn radius to 1000 feet to reduce hook loads during turns.
Helicopter vertical gyro (any one).	Helicopter pitch/roll attitudes.	Direct attitude measurement unavailable.	<ul style="list-style-type: none"> • Use time integration of rate gyros. Recalibrate using force sensors and other helicopter attitude.
Helicopter vertical gyro (any one) and corresponding rate gyro.	Helicopter pitch/roll attitudes.	Attitudes unknown during flight.	<ul style="list-style-type: none"> • Disengage outer loop immediately. Reduce speed to 30 knots, maintain radio contact and proceed to payload drop zone or base, whichever is closer. If fuel insufficient to reach destination at 30 knots, lower payload to ground, jettison spreader bars and RTB in isolated helicopter

			mode.
Helicopter rate gyros (one or both).	Helicopter pitch/roll rates.	Rates unknown during flight.	<ul style="list-style-type: none"> Use time-history from vertical gyro data and finite differencing to estimate rates.
Helicopter accelerometers.	Lateral and longitudinal accelerations.	Accelerations unknown during flight.	<ul style="list-style-type: none"> Anti-swing mechanism in outer loop controller disabled. Pilot cautioned to make slow steps for repositioning heavy loads.

Table 26: Sensor failure during return phase

Sensor	Measurement provided	Consequence of malfunction	Remedy
Swivel AHRS.	Payload position.	Lower cable angle unknown.	<ul style="list-style-type: none"> Evaluate angle using inclinometer and force sensor time-history.
Spreader bar AHRS.	Truss yaw attitude.	Active yaw damping no longer functional. Passive damping (via thruster heave damping) still operational.	<ul style="list-style-type: none"> Disassemble and transport spreader bar after payload delivery. Reduce speed to 60 knots. Increase separation distances to introduce spreader bar tension.
Spreader bar inclinometers (both sets).	Cable angles from helicopter to spreader bar.	Large spreader bar oscillations (return flight).	<ul style="list-style-type: none"> Disassemble and transport spreader bar after payload delivery. Reduce speed to 60 knots. Increase separation distance to introduce spreader bar tension.
(one set)			<ul style="list-style-type: none"> Use RF sensors, force sensors and other inclinometer readings to evaluate angles
Spreader bar RF sensors (one or all).	Spreader bar length and cable lengths.	Backup truss measurement system inoperative.	<ul style="list-style-type: none"> Use inclinometer measurements to obtain truss states.

Table 27: Actuator failure during return flight

Actuator	Function	Consequence of malfunction	Remedy
One or both thrusters.	Damping spreader bar oscillations.	Spreader bar motions may become dangerously large.	<ul style="list-style-type: none"> Reduce speed to 60 knots. Increase separation distance to introduce tension in the spreader bar.

Table 28: Communication loss

Situation	Function	Consequence of malfunction	Remedy
Wireless signal inoperative or both controllers (twin-lift synchronizing computers) inoperative.	Sensor information unavailable to controller.	All controller subsystems ineffective.	<ul style="list-style-type: none"> Disengage outer loop immediately. Reduce speed to 30 knots, maintain radio contact and proceed to payload drop zone or base, whichever is closer. If fuel insufficient to reach destination at 30 knots, lower payload to ground, jettison spreader bars and RTB in isolated helicopter mode.

Table 29: Controller malfunction

Situation	Function	Consequence of malfunction	Remedy
One synchronizing computer (control box) of the twin-lift controller malfunctions.	Primary processing unit inoperative.	Control commands cannot be generated in the Master helicopter.	<ul style="list-style-type: none"> Reroute all signals to second processing unit – utilize system redundancy. If transmission and processing time lag unacceptably large, interchange Master/Slave pilot roles.

9.3 Payload drop off and disassembly

9.3.1 Conversion to hover

The conversion from cruise flight to low-speed maneuvering flight is the reverse of the forward flight maneuver. As the helicopters make their approach, the Master pilot decreases air speed below 40 knots. Once the twin-lift configuration maintains this condition for 30 seconds, the configuration swing takes place and the fuselages of the helicopters are once again oriented perpendicular to the spreader bar. The reason behind using this configuration for low-speed maneuvering is has origins in pilot handling qualities for sling load operations, where load oscillations in the lateral direction present a greater difficulty than fore-aft motion of the slung load, as seen from the helicopter.

9.3.2 Orientation and positioning

- The signalman is positioned directly in line with the drop zone and 150 ft behind it in a similar way to the take off maneuver.
- The signalman directs the pilot towards the drop zone.
- When the load oscillations have damped sufficiently, the signalman directs the pilot to descend.

9.3.3 Payload reposition maneuvers

Once the twin-lift system has reached the landing site and is hovering close to the drop zone, the pilot has to identify the precise delivery point. Using visual cues from the signalman, the pilot will then maneuver the system until the payload is at the desired position. In this phase, load oscillations must not be damped out quickly to avoid damage to nearby objects or personnel. The following candidate maneuvers display the effectiveness of the controller in restricting payload oscillations.

Simultaneous lateral and vertical reposition: The following maneuver is representative of the twin-lift system moving laterally up an inclined surface, e.g., a small hillock. The target position is 165 ft to the right and 165 ft above the current position, as shown in Figure 77. The maneuver time allotted is 50 seconds. Payload oscillations are negligible during the

entire maneuver. The helicopter roll angle time histories are shown in Figure 78. The attitude changes required to perform the maneuver are small, synchronized and excessive oscillations are absent, which indicates efficiency of the controller. Shown in Figure 79 and Figure 80 are the helicopter position time-histories for the reposition maneuver. Excessive helicopter translational oscillations are absent. Therefore, the pilot seat motions from attitude changes are minor while the relative spacing is maintained, ensuring complete operational safety.

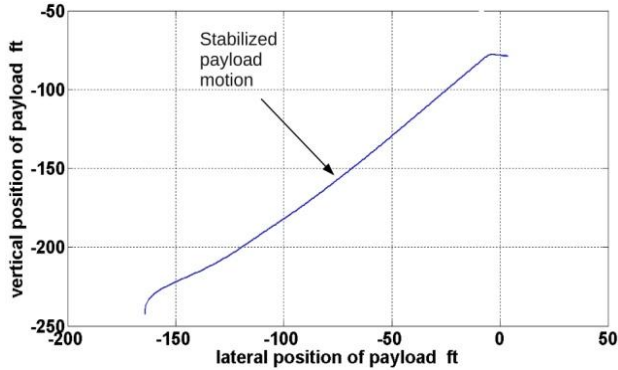


Figure 77: Payload path

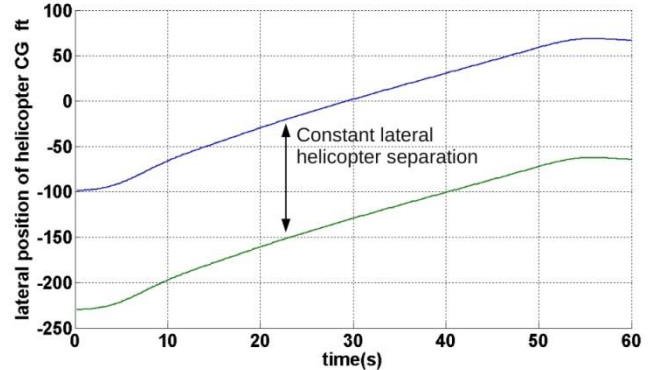


Figure 78: Helicopter lateral position time-history

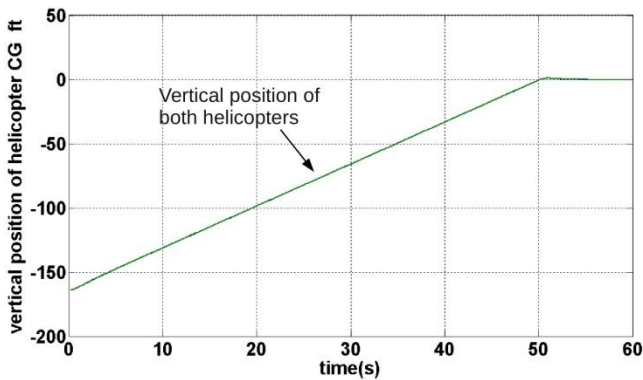


Figure 79: Helicopter vertical position time-history

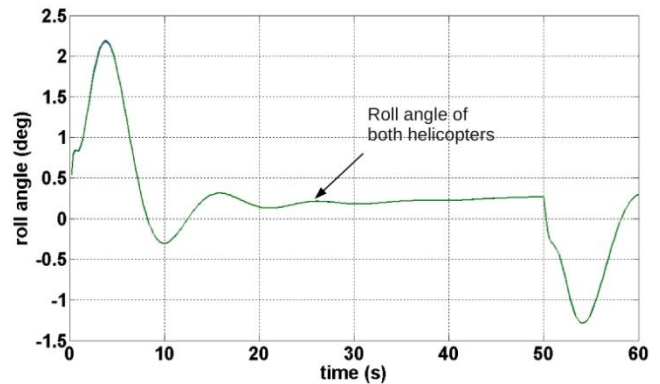


Figure 80: Helicopter roll angle time-history

Effect of altitude constraint: The performance of the control system was examined when the altitudes of the helicopters are not allowed to change. This constraint is representative of a situation where the pilot tries to maneuver the twin-lift system close to the ground, and the system is not allowed to decrease altitude any further to prevent payload damage.

A combined forward and sideways reposition maneuver was considered. The time limit for this maneuver was 15 seconds. This maneuver is considered representative of a situation where there are significant gusts acting from a head-on direction, and the pilot aims to reposition the payload without exposing the tail rotor to significant inflow fluctuations. Figure 81 shows the lateral position time-histories of the helicopters during the maneuver. The rotor separation, indicated by the distance between the two lines, is well maintained. It is seen in Figure 82 that the longitudinal helicopter positions are also well tracked without oscillations. Figure 83 shows the payload oscillations relative to an imaginary line joining the helicopters. The initial excitation of load the oscillation is small because the modal energy associated with the synchronized single pendulum is high. Load damping is realized through rate feedback of the symmetric pendulum mode to the helicopter accelerations. The oscillation time period is 8 seconds for the current configuration, resulting in larger settling times.

The effect of altitude constraint is best observed in Figure 84. When altitude is unrestricted, the lateral pendulum motion of the spreader bar and payload is coupled to the helicopter vertical translation through the well-damped spring mode, as

discussed in SECTION 6. However, when the helicopters are constrained to move at the same altitude, this mode is no longer available to provide damping to the lateral oscillations of the payload. The controller compensates for rotor heave damping, and eliminates payload oscillations at the end of the maneuver.

In conclusion, the control system proposed displays good performance characteristics in the presence of environmental constraints that limit the pilot from reorienting the twin-lift system.

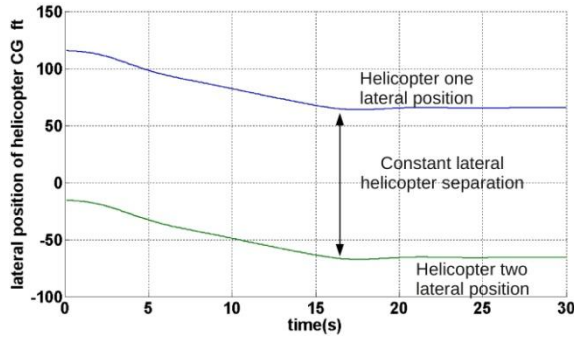


Figure 81: helicopter lateral position time-histories

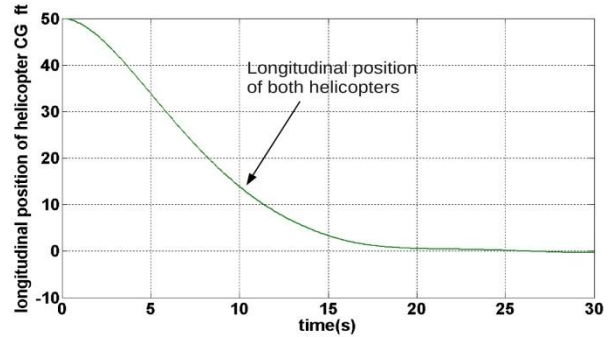


Figure 82: Helicopter longitudinal position time-histories

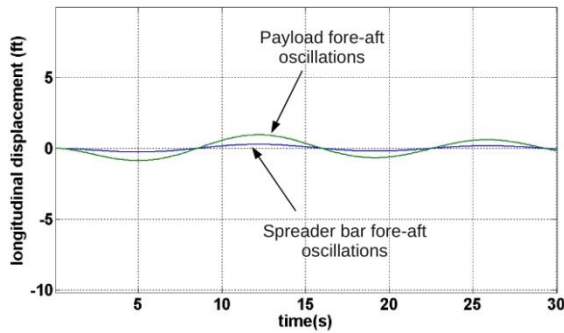


Figure 83: Payload fore-aft oscillation time-history

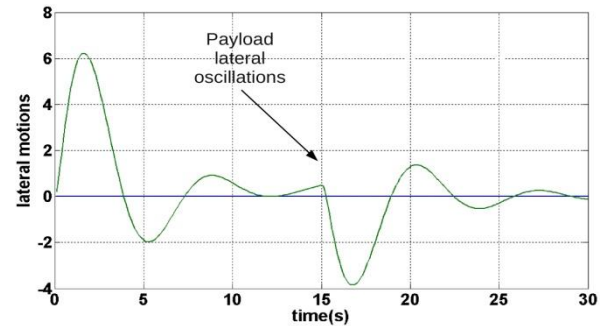


Figure 84: Payload lateral oscillation time-history

9.3.4 Payload drop off

- The drop zone should be clear of personnel.
- The signalman directs the Master pilot in a controlled vertical descent.
- After payload touchdown, the signalman directs the pilots to continue the descent until the cable tension drops and the container is automatically disengaged using the mechanical mechanism described in SECTION 4.3.
- If a mechanical failure occurs and the mechanical release does not work, then the ground crew must approach the container and manually release the load handling spreader bar. Another option is to actuate the remote cargo hook to release the load-handling spreader bar. The pilot in the Master helicopter can wirelessly release the cables from the remote cargo hook. However, this act necessitates that the lower spreader bar remains with the cargo container, which is considered to be an emergency procedure.

9.4 Return journey

The *Goliath Smart Truss* system has been carefully designed to maintain maximum flexibility with an emphasis on modularity and logistics. Taking advantage of this modularity gives the crew a number of options for the return journey of the mission.

- **Dropped load handling structure:** To maximize flight speed and gross payload throughput or range, the load handling structure can be dropped with the payload allowing the helicopters to decouple their controls and make an independent return. However, this latter procedure allows for a single delivery and requires a secondary mission to return the structure. This option offers maximum productivity and least pilot workload, but has a logistical handicap.
- **Disassembly of load handling structure:** A second option is ideally suited to infrequent deliveries that are not time restricted and takes particular advantage of the modularity of the spreader bar. The procedure is to land the configuration and disassemble the load handling structure to be stored inside one of the CH-53Es for the return journey, while the second helicopter carries the load handling spreader bar as a single slung load. The procedure for this is described in SECTION 4.1.7. This option offers reduced pilot workload in return and medium productivity performance, but at the cost of some time.
- **Coupled return:** The third option is most suited to missions that have time constraints, logistics requires the return of the load handling structure, or when the configuration is in frequent or repeated use. These situations may be encountered when offloading a ship to mainland without a port. However, of the three options compared, this option has the least payload or range flexibility and has the highest pilot workload and associated safety-of-flight risks.

The mission latter profile that is met by this design assumes the most demanding “Coupled return” return journey to a ship deck. This profile is described here, and mission variants are expected to be an adaption of these procedures.

9.4.1 Returning cruise flight

During the return phase, the lightly loaded configuration is susceptible to unsteady spreader bar oscillations. This situation places a greater dependence on the stabilizing thrusters to reduce potential oscillation amplitudes. The control system determines the changing loading conditions using sensor inputs, and generates appropriate correction signals for the first and second subsystems.

9.4.2 Return approach

- The twin- lift configuration will approach from the stern of the ship.
- The landing zone should be cleared to accommodate the 160 ft spreader bar across the ship breadth, if available. Otherwise two distinct landing zones are required to accommodate the lowering of the load handling spreader bar followed by the spreader bar.
- One signal man directs the Master pilot to position the load handling spreader bar above the landing zone.

9.4.3 Load handling structure release

- After reducing spreader bar oscillations, the signalman directs the pilot to descend until the lower cables become slack and the load handling spreader bar is firmly on the ground. The signalman directs to pilot to release the remote cargo hook to drop the lower cables.
- The signalman then directs the pilot to the area designated to receive the spreader bar.
- Two signalmen are stationed at the landing site of the spreader bar, in line with both ends and 40 ft behind it.
- The Master pilot is directed to descend until the spreader bar touches down.
- The outer loop autopilot then halts the descent of the slave helicopter and allows the Master pilot to continue the descent until their altitudes match.
- The two signalmen positioned at both of the spreader bar ends take responsibility for each helicopter.
- When cleared to do so, the Slave pilot prepares to take over control of his helicopter.

- The Slave pilot is responsible for disengaging the twin-lift mode to ensure readiness for reassuming individual helicopter control. This action is initiated by depressing the “LOCK” button on the control box, starting a five second timer that can be aborted by either pilot.
- At the conclusion of the countdown, the autopilot outer loop controller releases the slave helicopter into a hover hold (or airspeed and attitude hold when tracking a moving ship) that can be overridden by the pilot. The cargo hooks on both helicopters are simultaneously disengaged to release the cables to the spreader bar. This is a safety measure that doubles as a secondary emergency action that forces load jettison if the outer loop is disengaged in this manner.
- Both pilots are now free to climb out of hover, under direction of the signalmen, and then to land at the designated area.

10 Twin-Lift Cost Comparison

A significant measure of the practical feasibility of the *Goliath* Smart Truss system is the cost of using and developing the system. To this end, the baseline price of a system that could complete the RFP objectives was calculated, as well as assessments of various other cost considerations. A single vehicle that can meet RFP goals is currently unavailable, and if it were to be designed, it would require design and development costs stretching well beyond those of a twin-lift system.

10.1 Baseline price comparison

There are few helicopters that have the capability of lifting 1.75 times the load of a CH-53E and carrying it 100 nm. However, it is still possible to obtain an estimate of the baseline price of such a vehicle. Because acquisition costs can account for over 50% of the total life-cycle costs involved in owning and operating a helicopter, it is of benefit to estimate the cost of a single helicopter that can carry the same payload in comparison to utilizing the *Goliath Smart Truss* system. To this end, an estimate of the baseline price of a single rotor helicopter was achieved by using statistical data for comparison to the twin-lift concept. The costs were estimated by using the cost estimating formula of Harris and Scully updated to 2008 [Bush et al. 2008] [Harris 1998].

The price estimation equation is

$$\text{Baseprice} = \$345 \times H \times N_b^{0.2045} \times W_o^{0.4854} \times P^{0.5843}$$

or

$$\text{Baseprice} = \$345(H) \frac{N_b}{(550\sqrt{2})^{0.5843} r^{0.2922}} (UL)^{1.0697} \left(\frac{GW}{UL}\right)^{0.5843} \left(\frac{GW}{UL} - 1\right)^{0.4854} \left(\frac{DL}{FM}\right)^{0.2922} \quad (1)$$

In Equation 1, H is the influence of design decision on cost and is defined by values assigned to parameters such as engine type, number of engines, country, number of rotors, landing gear type, and pressurization. N_b is the number of blades, W_o is the empty weight, ρ is the air density, UL is the useful load, DL is the disk loading, GW is the gross weight, and FM is the hover figure of merit (Harris 1998).

To obtain a cost estimate for a single helicopter capable of satisfying the RFP requirements, a sizing estimate was undertaken and used in the baseline price equation. The gross weight of a helicopter capable of lifting 1.75 the payload of the CH-53E was estimated by using a statistical analysis based on historical data pertaining to useful load and gross weight. With this gross weight (129,000 lbs), an engine power to hover (16,469 hp) with a torque output of 648,530 ft-lb was obtained while maintaining the same disk loading. With disk loading held constant, a rotor radius of 52.3 ft was obtained. The base price of a helicopter that could complete the mission outlined in the RFP would cost about \$100M in 2008 or 2.2 times the price of a single new CH-53E (2008 price) using the same equation. The two parameters that contribute most to the significant increase in baseline price are the vehicle weight and the engine power.

The cost estimates for a single rotor mission specific helicopter are difficult to approximate because the ownership costs depend on a number interconnected design factors linked to mechanical complexity and systems sophistication.

In addition to the base price, there would be research, development, test and evaluation (RDT&E) costs associated with producing a new helicopter with the required capability. These costs are very difficult to estimate but based on the development costs of a CH-53K (US\$4B) and the V-22 (US\$12B) it is estimated that development of a completely new heavy lift helicopter would be in excess of these numbers. These are enormous costs that can be avoided with the use of the proposed *Goliath Smart Truss* system.

10.2 Goliath smart truss system comparison

The smart truss system is designed around two currently in-service helicopters, without modifications to the airframes. The main cost of such a system would be manufacturing the components of the truss system and integrating the components. The modular Smart Truss system is economically attractive because the concept can be shipped to locations where it is needed and where a heavy-lift helicopter may not be available. In comparison to the development of a single VTOL platform with the same capability, the price would be significantly less because of the leveraging of “commercial off the shelf” (COTS) technology. The COTS advantage includes availability, the avoidance of potentially expensive development and maintenance, and the use of mature/reliable/affordable technology. The trade-off in using COTS is a reduction in system development time versus an increase in costs related to component integration. Current sensors and transmitters can be employed to ensure that the system can be deployed safely and at an affordable price. In the area of safety, redundancies can be designed into the system to mitigate the risk of component failure. These measures also aid in reducing the insurance costs of the system. Manufacturing methods and materials were considered in the design process, including modularity and lean implementation of the system. Special attention was given to safety and cost.

Table 30: List of *Goliath Smart Truss* components and prices

Payload/Load Handing Components	Material	Cost (\$)
Truss materials	Aluminum	10,000
Spreader bar end connectors (2x)	Aluminum	1,000
Thrusters (2x)		5,000
Spreader bar	Aluminum	15,000
Cables	Steel	18,000
Cargo Hook (3x)		36,000
Onboard computer (2x)		10,000
Inertial measurement units (IMU)(3x)		2,000
Misc. (Welding, assembly, etc)		20,000
Sensor suite		
Totals		209,000

In Table 30, welding costs were assumed to be based on 2010 service and labor prices for welding the 470 joints in the truss assembly. The modularity of the truss system will reduce the operating costs of having a lifting device such as a crane to maneuver it into place. The fact that the truss system is stackable and fits into the cargo hold of a single CH-53E is an added benefit, especially for carrier-based missions where space may be limited.

In summary, the *Goliath Smart Truss* system provides an economical and efficient answer to the heavy-lift mission because of the availability of the CH-53E, the modularity of the truss system, and the practical versatility of the truss system. It is the obvious choice over developing a mission-specific vertical lift system.

11 Feasibility and Path to Production

A feasibility assessment process is used to provide analysis of the requirements and system concepts of the proposed RFP specifications. A path to production is outlined to provide an overview of research, development, test and evaluation with some attention paid to the manufacture and assembly process toward production.

11.1 Feasibility

During this analysis, the objectives of the system are defined based on the requirement functions described in SECTION 4 and the technical maturity required to execute each function is identified. Table 31 describes the high-level functional and performance objectives and constraints. For each variable, critical attributes and measures are defined and assigned a maturity order. The maturity indices are defined as follows:

1. Technology does not currently exist.
2. Technology is in its infancy.
3. Technology exists but requires design integration (i.e. cannot be purchased “off the shelf”)
4. Technology exists and is ready to use (i.e. can be purchased “off the shelf”)

Table 31: Feasibility assessment

System components	Attribute	Measure	Technology maturity	Comments
CH-53E Super Stallion.	Heavy lift helicopter.	External payload capability of 33,000 lb.	4	Proven and available technology validated with published data.
Container attachment bar.	Relieves tension forces on load.	Yield strength.	3	Requires fabrication however sizing and testing are necessary.
Load handling spreader bar.	Helicopter position, Relieves cable tension.	Yield strength.	3	Requires fabrication however sizing, testing, and control are necessary.
Thrusters.	Load stabilizing mechanism.	Reduced oscillation Requires a system check.	3	Requires a custom bidirectional variable pitch design that will accommodate dimensional constraints.
Vertical tail.	Stabilizing mechanism for the payload.	Payload oscillation damping.	3	Wind tunnel testing, CFD modeling.
RFPS.	Positioning sensor.	System check and calibration.	4	COTS however requires system integration.
AHRS/IMU.	3-axis sensors for orientation and rates.	Requires system and calibration checks.	4	COTS however requires system integration.
Wireless link.	Communication.	Requires system checks.	4	COTS however requires system integration.
Load cell.	Measurement of system forces.	Requires calibration checks.	4	COTS however requires system integration.
Thruster servos.	Control of the thrusters.	Requires systems check.	4	Must ensure response time within specification for thrust control via ducted fan.
Avionics module.	Control architecture.	Ground tests and flight tests.	3	Computer/programming and integration specialist required.

The concept of augmenting in-service helicopters to handle heavier containerized loads is novel in its concept, however it is achievable using today’s technology. Many of the system components *Goliath* are currently available however, must be skillfully integrated into the system. For example, SECTION 4.3 describes a container attachment frame that will accomplish the objectives of the RFP. However a COTS lower spreader bar can be acquired to suit a specific payload. Furthermore, components such as the avionics module and sensors are technology that will require a level of innovative system integration of reliable and available COTS technology. The culmination is a high-technology readiness level for developing this system. With this, the *smart-truss* technology becomes a versatile, efficient, and feasible concept that is marketable to the sector of the helicopter community interested in providing enhanced heavy-lift capability.

11.2 Path to production

The path to producing a technology demonstrator will require only a short RDT&E phase. It is difficult to estimate total time because there are several tests that must be approved and executed before the *helicopter community can leverage the smart-truss system*. Shown in Table 31, the high technology readiness levels reduce the development risk and time to production. This outcome is because many of the components require only a minimal level of integration. The development and testing of a safe technology demonstrator is estimated to take about 2-years, with system development items executed concurrently. Shown in Table 32, testing and evaluation will include ground and flight test.

Table 32: Timeline to production

Development item	Time (year)
System electronics development	1*
Software development	1*
Stabilizer thruster development	1*
Stabilizer fin development	1*
Truss structure development	1*
Lower spreader bar development	0.5*
Fabrication and assembly	1*
Ground tests	2*
Flight tests	1
RDT&E total	2

* Done concurrently

The fabrication and assembly of the truss system is estimated to take 1-year. Component fatigue testing of the *smart-truss* structure with special emphasis on joints and stress concentration areas is estimated to be 2-years and can be implemented concurrently during the development phase. Damage and tolerance test will also be performed in this time frame. The progression of the flight tests may proceed with evaluations of system hover, then transition from hover to forward flight with only the main spreader bar and lower spreader bar, then test with the empty ISO container, then tests carrying a lightly loaded ISO container, then tests carrying the fully loaded ISO container. The main emphasis will be on the control algorithms. However, transmitters, sensors, and thrusts will also be tested and proven.

12 Alternate Missions

The *Goliath* twin-lift system can be used for transporting large military vehicles, supplies, and equipment to the battlefield or for civilian construction, firefighting, and logging operations. Beyond ship-to-shore, there are missions pertinent to the smart truss system such as land-based and ship-to-ship based that can be performed.

12.1 Military missions

As shown previously, the system is capable of operating for extended periods in missions to replenish amphibious assault ships under the designation landing helicopter assault (LHA), landing platform helicopter (LPH), and/or landing helicopter

dock (LHD). The twin-lift system is also capable of operating from remote forward operating bases. Even though this *Smart Truss* has been optimized to the CH-53E, it is not platform specific. The *Goliath* twin-lift system can be adapted to expand the performance of several other helicopters such as the CH-47 or the CH53K by increasing the external lifting capability.

A routine mission for the CH-53E is the transport of light armored vehicles weighing about 26,000 lb. However, the mission can be expanded to carry various other payloads. Some essential tactical equipment that exceed the rated payload weight of a single CH-53E can be accommodated. The *Goliath* twin-lift system enables two CH-53E helicopters to transport or retrieve large ground vehicles or downed aircraft such as those shown in Table 33.

Table 33: Potential military payloads for CH-53E twin-lift concept

Payload	Weight (lb)
D7 caterpillar bulldozer	31,870
Downed V-22 or CH-53E	33,000
M-1070 heavy transporter truck	41,000
Buffalo MRAP vehicle	45,320
Stryker armored vehicle	44,000
USMC logistics vehicle system replacement (LVSr)	53,700

Ship-to-ship cargo transfer operations will benefit from the use of the twin-lift system, because the payloads need not be broken down into smaller segments and reassembled at the destination. More importantly, the *Goliath* twin-lift system enables the helicopters to transport heavy-assault ground vehicles (e.g., artillery batteries and associated ammunition), thus improving their perimeter defense while mitigating the need for assignment relief. Beyond ground missions, ship-to-shore, and ship-to-ship operations, various missions can be prescribed for the *Goliath* Twin-Lift System.

12.2 Civilian missions

Construction materials and equipment such as large bridge sections are prime candidates for the *Smart Truss* system. This is especially true in areas where track or wheel vehicles have limited access. Similarly, offshore oil rig support, disaster relief/humanitarian aid resupply, logging, fire fighting, or rooftop rescue would be potential civilian missions for the system. Table 34 shows several civilian payloads for which the twin lift control concept can be scaled.

Furthermore, several combinations of 2.5 ton Jersey Barrier, 5.5 ton Texas Barrier, 7.5 ton Alaska Barrier, or 9 ton Scud Bunker can be transported by the *Smart Truss* system to areas that are inaccessible by track or wheeled vehicles.

Table 34: Potential civilian payloads for CH-53E twin-lift concept

Payload	Weight (lb)
Tigercat wheel harvester 1135	33,000
Caterpillar 613G elevating wheel tractor-scraper	37,229
Tigercat forwarder 1045B	37,260
Tigercat forestry skidder 630D	37,250
Caterpillar wheeled excavator M322D	49,604

With the *Smart Truss* system, military and civilian missions are enhanced so that personnel and cargo can be transported without requiring a runway for takeoffs and landings. The key areas of mission enhancement for the system are improved external cargo and range capability, scalability for use on various helicopters, high reliability with low maintenance, modularity for ease of replacement and adaptability to various helicopters.

13 Baseline Helicopter Modifications

The Goliath twin-lift system has been designed to operate with minimal external modifications to the helicopters. The signals from the sensors of the helicopter are utilized to complete the system state information generated by the sensor suite mounted on the spreader bar. The helicopter AFCS servos are used by the avionics module to regulate relative positions and synchronize motions.

External hardware modifications: NONE.

Electronic modifications to helicopters

- AFCS servos
 - Enables avionics module to control and regulate twin-lift system.
 - Helicopter AFCS servo electrical signals augmented with analog signals generated by twin-lift avionics.
- AFCS sensors
 - Enables avionics module to use helicopter sensors to complete state measurements.
 - Helicopter sensor measurement fed to twin-lift avionics.
- FAS feedback
 - Provides force cueing to pilots during low-speed maneuvering to avoid load swing.
 - Longitudinal cyclic input resistance gradient triggered by fore-aft translational accelerations of 1.5 knots, at speeds less than 20 knots.

14 Conclusions

In response to the 2010 AMERICAN HELICOPTER SOCIETY Student Design Competition Request For Proposal “Lift! More Lift”, the University of Maryland’s graduate team entry, the *Goliath* twin-lift system, has been presented. The baseline helicopter selected to showcase the system is the *CH-53E Super Stallion*.

Optimized flight configuration for pilot situational awareness: In the submitted design, a 165-ft spreader bar is slung beneath the two helicopters, and the payload is suspended at a distance of 100 ft beneath the spreader bar from aramid cables. The lateral separation between the aircraft, as measured along the spreader bar, is one rotor diameter (80 ft) between rotor tips. Unequal cable lengths are used to offset one helicopter vertically above the other by 20 ft, for enhanced pilot situational awareness in forward flight. The limiting vertical separation between the helicopters and the payload, as well as between the helicopters and the spreader bar, are determined using surge response handling qualities criteria.

Light weight materials and drag reduction for extended performance: Utilizing high-strength aluminum alloys, optimized structural design and lightweight aramid cables, the *Goliath* twin-lift system exceeds the RFP-stipulated payload capacity by 2,500 lb (6%). The *Goliath* twin-lift also system incorporates an optimized container handling frame that provides 3,000 lb additional payload over OTS options.

The spreader bar is comprised of cylindrical tubes with roughened surfaces to minimize parasitic drag in forward flight. This drag reduction is achieved by increasing the effective Reynolds numbers over the surfaces of the cylindrical elements. The worst-case estimate for the total flat-plate area of the load-handling devices, including an allowance of 20% for interference effects, is 105 ft².

Modularity and reduced footprint for ship-based operations: The structure can be disassembled into six collapsible elements, each weighing 236 lb, without specialized equipment. These elements, once collapsed down, can be stowed in the cargo hold of a single CH-53E for efficient transport. This logistical flexibility and compact storage renders the *Goliath* twin-lift system especially suitable for shipborne operations.

Dual vertical fins for increased cruise speeds: Dual vertical fins mounted on the container attachment frame extend the forward flight speed range of the twin-lift system up to 90 knots.



Minimal hardware modifications for reduced implementation cost: The *Goliath* twin-lift concept requires no structural modifications to the airframes of the helicopters. Furthermore, cross-platform adaptability and system scalability allow for this system to be implemented on other types of helicopters.

Robust and redundant control system for complete operational safety: A doubly redundant, efficient, and flexible sensor and control network has been developed for the *Goliath*. This system utilizes proven technology, applied in a novel array to provide the avionics processors with precise measurements (greater than 99% accuracy).

The *Goliath* twin-lift system features an interactive avionics control and display unit that interfaces with the existing flight control systems of the helicopters. Dual-redundant processing modules, unique to the *Goliath* twin-lift system, provide accurate inputs to the twin-lift controller to ensure complete operational safety. Vehicle separation regulation and motion synchronization subsystems maintain relative positions with an accuracy of 99.5%, and even with 98% accuracy in the event of 20% controller signal error. Finally, the full retention of existing flight control functions preserves pilot intuition and reduces training time.

Dual ducted rotors for spreader bar stabilization: The *Goliath* twin-lift system utilizes two ducted rotors to actively stabilize all system oscillations within 45 seconds during the load pick-up phase. This feature facilitates streamlined ground crew logistics and ensures operational safety. An intuitive control interface reduces training time for pilots by preserving original control functions, further reducing implementation cost.

Proven technologies: The projected path to production, taking into account high technological maturity levels, is projected to be only 30 months from conceptual design to operational implementation.

Goliath is a revolutionary scalable twin-lift concept that, when fully implemented, would realize enormous advancements in both civil and military vertical-lift capability. The modular design of system components reduces implementation costs, while minimizing overall system footprint. The innovative use of proven technologies ensures complete operational safety, while robust and redundant sensor suites enable precision position control. Ultimately, it is the scalability of the *Goliath* to both heavy-lift and lighter helicopters, applicability to current and next-generation rotorcraft, and adaptability to a wide variety of payloads, that gives this versatile system an unrivaled edge over most, if not all, other vertical-lift platforms.

1 Introduction

The 2010 American Helicopter Society Student Design Competition “LIFT, More LIFT!” sponsored by Boeing and AHS included an experimentation task that involved hover testing of a commercial off-the-shelf (COTS) radio-controlled helicopter. The purpose of the task was to demonstrate an understanding of the needs of a flight test program.

The experimentation task requirements as outlined in the request for proposal (RFP) were as follows:

1. Measure the lift-to-power of the baseline COTS helicopter (with at least 30-inch rotor diameter).
2. Conduct analysis and correlate to the baseline results.
3. Design a modification that is predicted to provide at least 5% additional lift for a given power setting.
4. Apply the modification to the helicopter and measure the actual change in lift-to-power ratio.

The main focus of the task was to be placed on the design and efficiency of the testing process, as well as the safety measures and methods used throughout the program. The amount of improvement in rotor thrust was stated as not being a significant factor in the judging criteria.

A 46.5-inch rotor diameter COTS electric helicopter was purchased for this task. Instrumentation was installed to accurately measure main rotor thrust, torque, and RPM. A hover tower was utilized to elevate the main rotor out-of-ground effect and to ensure safety of the test operators. A rotor performance analysis was developed using blade element momentum theory and correlated to the baseline test results.

Five modifications to the baseline helicopter were tested for effect on rotor performance. All of the modifications were focused on the design of the main rotor blades.

- Increasing pitch-link bias for higher blade-loading coefficients and lower RPM operation of baseline blades.
- Applying geometric pre-twist to the wood baseline blades using a jig.
- Replacing the baseline blades with higher-performance off-the-shelf blades.
- Replacing the baseline blades with team-designed and constructed composite rotor blades.

Applying pre-twist by soaking and twisting the baseline wooden blades led to a decrease in performance. The remaining three modifications—operating at higher blade-loadings, using higher-performance COTS blades, and constructing custom-designed blades—all provided thrust increases for a constant power setting. The higher-performance COTS blades gave the largest increase in thrust over the baseline blades, namely a 21% increase at a constant power consumption of 0.6 hp. The custom-made University of Maryland blades increased rotor thrust by 15% over the baseline blades when compared at a constant power of 0.6 hp.

2 Baseline Helicopter Description



Figure 85: Century *Swift* ready-to-fly RC helicopter

The radio-controlled helicopter chosen for the experimentation task was a Century Helicopter Products *Swift* RTF (Ready-to-Fly) electric helicopter. This model is classified as a large, aerobatic, high performance helicopter. With a main rotor diameter of 46.5 in, this helicopter fulfills the RFP minimum diameter requirement of 30 in. the full list of specifications is given in Table 35. The RFP states that it is allowable to substitute major components of an off-the-shelf helicopter kit instead of a full-flying model. It was decided to preserve the helicopter in as close to a flight-ready condition as possible for testing so as to take into account losses and vibrations from all the components present. The tail rotor blades were also removed to eliminate counter-torque during testing. In this way the main rotor reaction torque could be measured while preserving transmission losses. The canopy fairing was also removed during testing, which permitted access to interior components and aided in motor cooling during testing.

The rotor system was driven by a brushless outrunner style electric motor with a 1470 kV rating (where the kV rating is defined as the ratio of motor RPM per unit of input voltage). Further specifications are listed in Table 36.

Table 35: Specifications of the Century *Swift* helicopter

Total weight (lb)	4.8
Main rotor diameter (in)	46.5
Nominal rotor RPM	1,600-2,100
Number of blades	2
Hover disk loading (lb ft ⁻²)	0.41
Tail rotor diameter (in)	8.5
Power system	Electric
Maximum continuous power (hp)	0.80

Table 36: Specifications of the Outrunner 550 Plus motor

Maximum voltage (V)	14.8
Maximum continuous current (A)	45
Maximum surge current (A)	65
Maximum efficiency	90%
Weight (lb)	0.45
kV rating (RPM/Volt)	1470
Gear ratio: Main rotor to motor	9.6:1

The motor was powered by a four-cell, 14.8 V, Lithium-Polymer (Li-Po) battery. With a capacity of 3,000 mAh (milliamp-hour) and a discharge rating of twenty times the rated capacity, the battery itself is able to supply approximately 60 A of current to the motor. At a fully charged voltage of 16.8 V (4.20 V per each of the four cells), the maximum output power of the battery was approximately 1,008 W. The on-board Electronic Speed Controller (ESC) was rated for 75 A continuous current, and 95 A burst current for short periods of time.

3 Experimental Setup

Hover tower test setup:

The main requirements for the testing location and model setup were as follows:

- Safety: Personnel and equipment should be shielded from debris during testing should parts catastrophically fail.
- Out-of-ground effect: The helicopter rotor should be far enough from the ground to be considered out-of-ground effect (at least 2 rotor diameters).
- Secure, stable mounting platform for the helicopter.
- Test operators can run data acquisition equipment while visually monitoring test.

The Hover Tower at the University of Maryland’s Alfred Gessow Rotorcraft Center was found to meet all of these critical requirements. The Hover Tower is a dedicated rotor test facility that ensured that any tests were performed in the safest environment possible. The tower height was about 13 feet above the floor level with the rotor at 14 feet (3.6 rotor diameters), ensuring that the helicopter tests would be performed well out of ground effect. At rotor level the tower was enclosed with heavy-gauge steel netting to contain potential rotor failures. The tower facility was constructed of a tubular steel post and provided a stable base for the helicopter mounting.

Adjacent to the hover tower test area was the control room where the test operators were stationed. The helicopter was monitored visually during testing through thick glass windows. The test operators could also hear the test being run, which helped in quickly identifying any problems.

Rotor thrust measurement:

- Precision bench scale: Adam Equipment *CPWplus*.
- Load rating: 75 lb.
- Accuracy: ± 0.02 lb, $\pm 0.2\%$ of 10 lb maximum expected thrust.

Rotor thrust was measured by securely mounting the helicopter on a precision bench scale and measuring the weight reduction as rotor thrust was increased. The scale had a 1 ft² surface plate that rested on four strain-gage load cells (Figure 86). This plate allowed sufficient area to create a stable platform for mounting the helicopter. The analog signals of the 4 load cells were identified, tapped, and fed into the LABVIEW™ data acquisition system for real-time data capture. As a backup, the force reading was also manually recorded from the LCD output display of the scale.

Rotor torque measurement

- Reaction torque cell: Transducer Techniques *TRT-50*.
- Torque capacity range: 50 in-lb.
- Accuracy: $\pm 0.1\%$.

The power consumption of the main rotor was determined by measuring the reaction torque and rotor speed during operation. This method of measuring rotor counter-torque required the disabling of the tail rotor, which was accomplished by removing the tail rotor blades. The lack of tail rotor power was not a concern because the modified rotors were compared at equivalent power consumption and rotor speed (which gives equivalent torque). Therefore the tail rotor thrust and power required for each configuration would be equal. Hence the relative comparison between concepts would still be valid, and would hold even for a full-flying configuration.

The reaction torque transducer was mounted between the helicopter and the supporting structure (see Figure 87). This created a load path for the reaction torque of the helicopter to pass through the torque cell. The weight of the helicopter and its thrust also passed through the torque cell. However, the maximum allowable thrust loading was 425 lb without an effect on torque, which was well under normal test loading. The torque cell analog output signal was recorded through the data acquisition system. Calibration data was provided by the manufacturer and also validated with a calibration conducted in-house.



Swift RTF RC Helicopter

Rotor Diameter: 46.5 in
Weight: 4.8 lbs

Main Rotor Shaft

Neodymium Magnets

Rotor RPM Hall-Effect Sensor

Steel Cable Safety Netting

Supporting Structure

Hover Stand Frame

Data Cables

Control Room

Rotor Height: 14ft
(3.6 x Rotor Diameter)
Out of Ground Effect

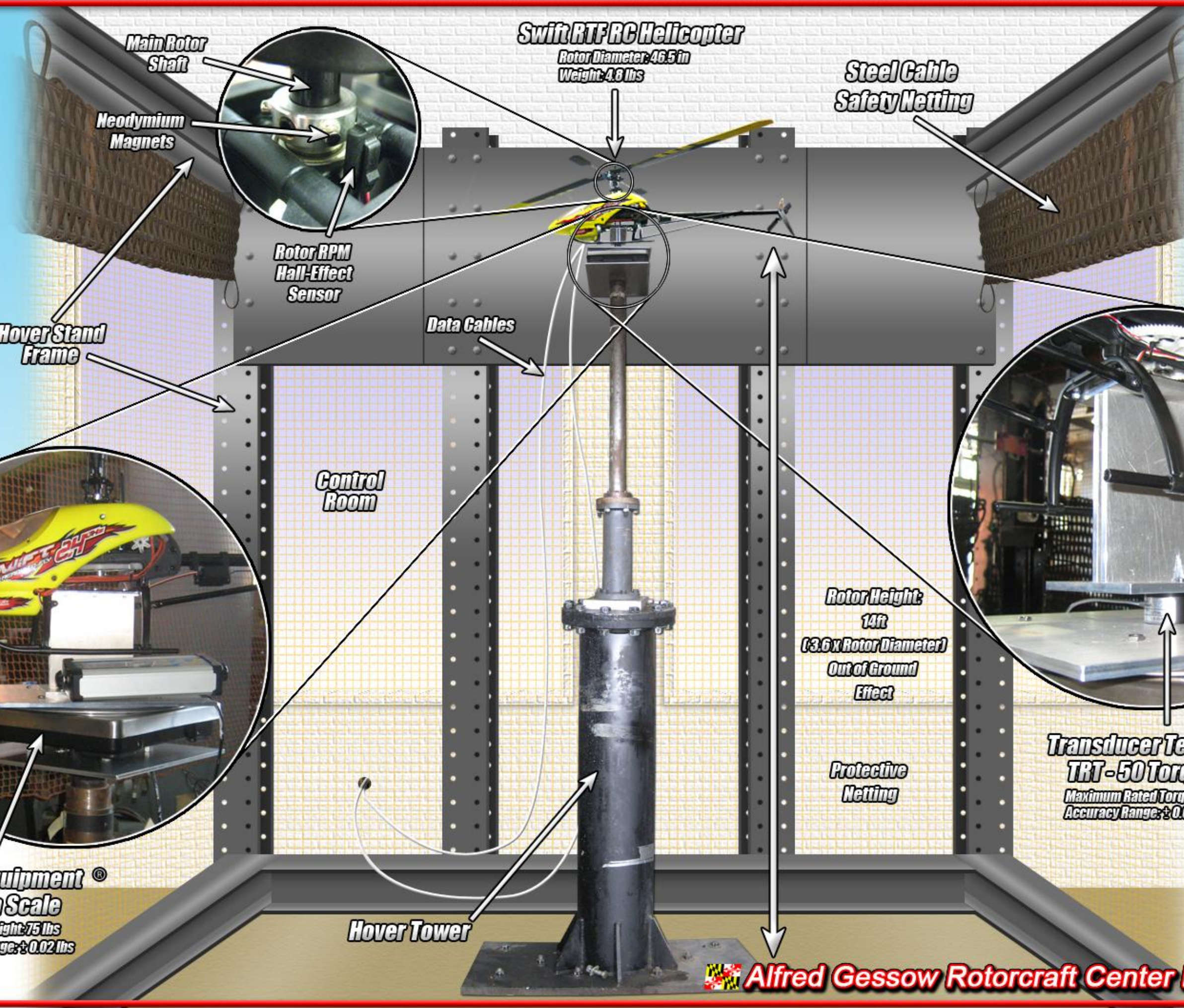
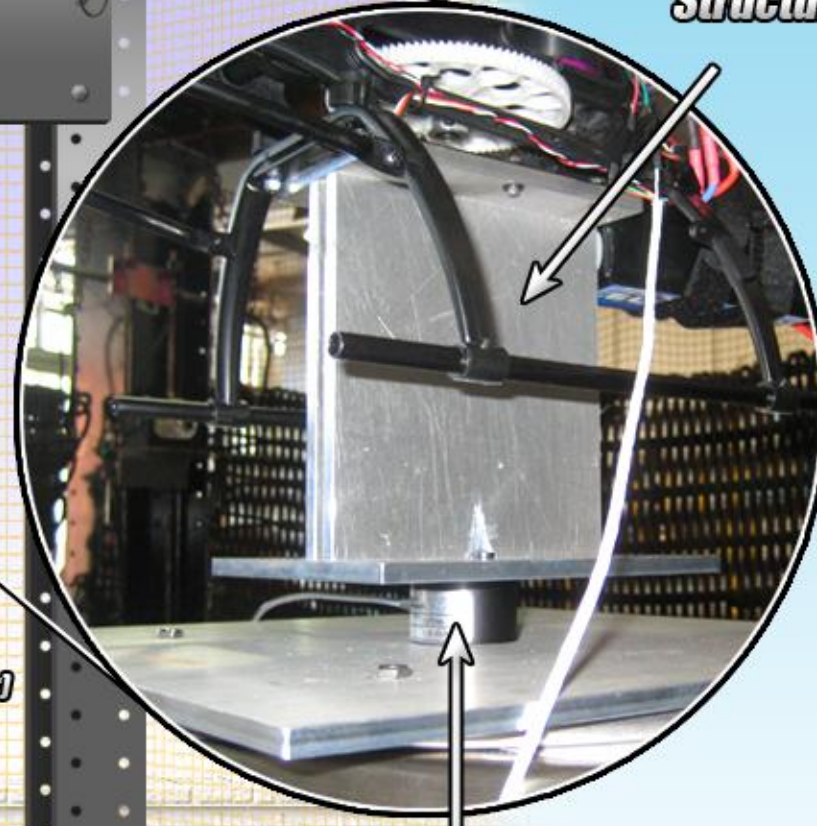
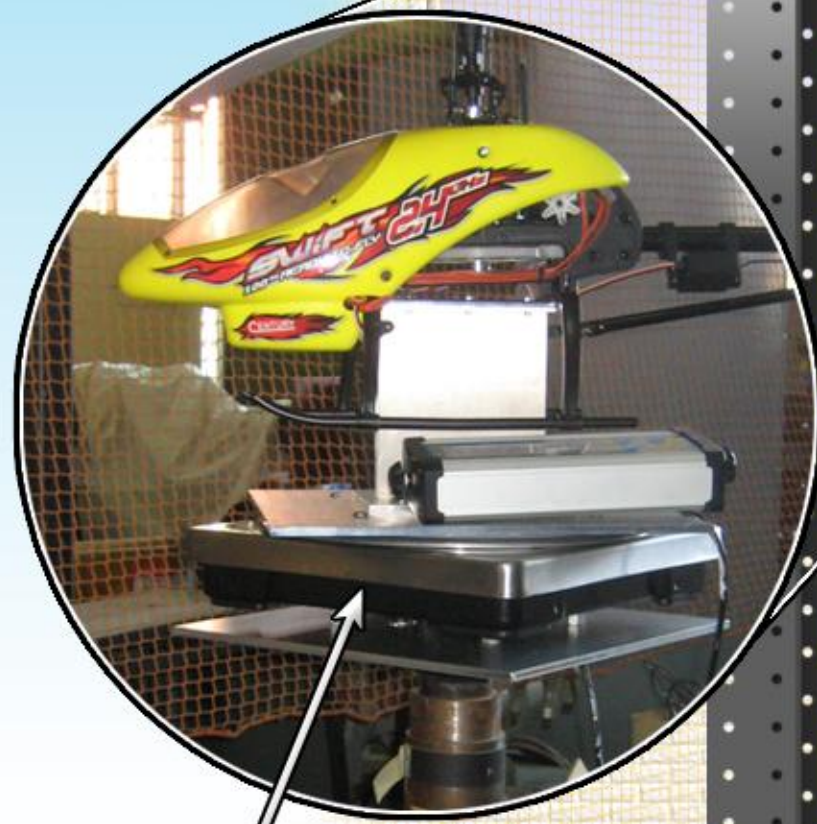
Protective Netting

Transducer Techniques®
TRT-50 Torque Cell
Maximum Rated Torque: 50 in-lbs
Accuracy Range: ±0.05 in-lbs

Adam Equipment®
Bench Scale
Maximum Weight: 75 lbs
Accuracy Range: ±0.02 lbs

Hover Tower

Alfred Gessow Rotorcraft Center Hover Stand



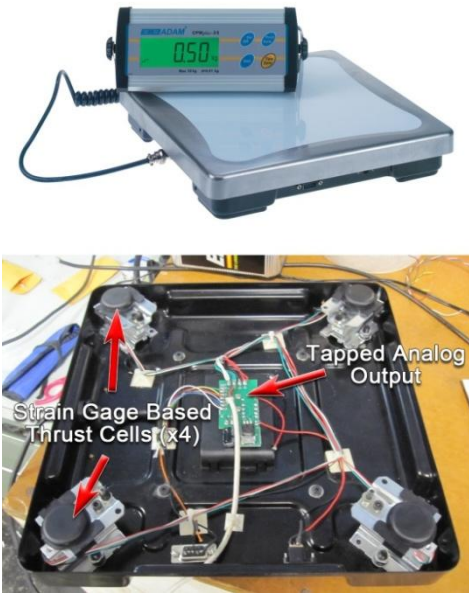


Figure 86: Adam equipment CPWplus bench scale modifications

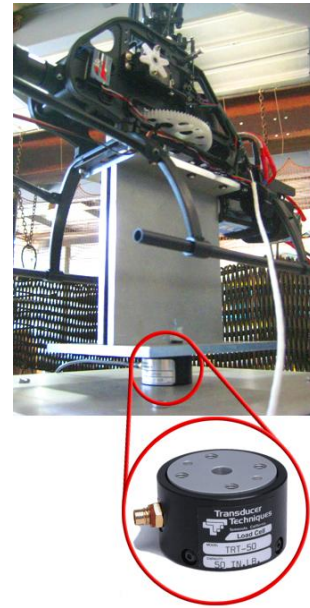


Figure 87: Torque cell mounted to capture reaction torque

Rotor RPM measurement

The rotor speed was measured using a Hall-effect sensor. A neodymium magnet was attached to the rotor shaft using epoxy adhesive. The Hall-effect sensor was attached to the non-rotating structure on the helicopter within 1 mm of the rotating magnets (see Figure 88). The signal peaks were counted in the data acquisition software over an interval of time to determine the rotor speed.

A backup method of rotor speed measurement was accomplished using frequency analysis of the thrust and torque analog signals. The strong frequency peaks in these signals occurred at integer multiples of the rotor speed. This approach provided a check on the Hall-Effect sensor readings in the case where the Hall-effect sensor failed to give a clean signal.

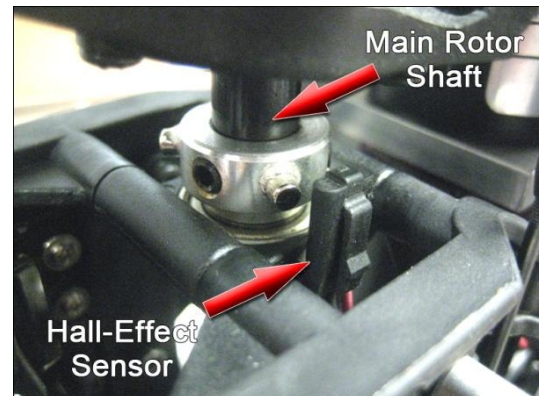


Figure 88: Hall-effect sensor to measure rotor speed

Data acquisition system:

The thrust scale, torque cell, and Hall-effect sensor (for rotor RPM) were analog signals that were processed through a National Instruments data acquisition system (NI-DAQ) system. The NI-DAQ system amplified the measurement signals with a voltage gain of 100 and a 1.6 kHz low-pass filter. The largest expected rotor speed was 35 Hz (2,100 RPM), therefore, the signal conditioning circuits had an appropriate bandwidth for this application. The signal conditioner also supplied the 10 V excitation voltage for the torque transducer and the Hall-effect sensor (the thrust scale had an on-board excitation source). The NI-DAQ system converted the analog signals into digital inputs at a user-specified sampling rate of 1,000 Hz. The data acquisition software interface was created in LABVIEW™. The signals were

displayed in the time-domain for real-time monitoring. The ambient temperature and pressure were manually input into the program before each run to calculate actual air density based on a standard atmospheric model.

4 Experimental Procedures

Pre-operation procedures and safety inspection:

Radio-controlled aircraft share many of the same operating procedures as full-scale aircraft. Two of these procedures are the pre-flight and post-flight check. In preparation for flight, a specific procedure is followed to ensure that all systems are functioning properly, and this applies for a radio controlled helicopter as well.

- Balance blades to minimize vibration
- Tighten helicopter fasteners
- Tighten support structure fasteners
- Clear test area of loose objects
- Check battery charge
- Check motor temperature
- Check data cables for load-path interference
- Check swashplate actuator motion

Test procedure

Tests were executed by a two person team consisting of the Pilot and the Data Operator. The Pilot's duties were pre-flight/post-flight checks and operation of the helicopter model. The Data Operator was responsible for the data acquisition hardware and recording data during testing. During operation, both the Pilot and the Data Operator observed the test from a separate control room through thick glass windows.

Pre-operation procedures and safety inspection

Radio-controlled aircraft share many of the same operating procedures as full-scale aircraft. One of these procedures is the pre-flight and post-flight check. In preparation for flight, a specific procedure is followed to ensure that all systems are functioning properly, and this applies for a radio controlled helicopter as well.

- Balance blades to minimize vibration
- Tighten helicopter fasteners
- Tighten support structure fasteners
- Clear test area of loose objects
- Check battery charge
- Check motor temperature
- Check data cables for load-path interference
- Check swashplate actuator motion

Test procedure

Tests were executed by a two person team consisting of the Pilot and the Data Operator. The Pilot's duties were pre-flight/post-flight checks and operation of the helicopter model. The Data Operator was responsible for the data acquisition hardware and recording data during testing. During operation, both the Pilot and the Data Operator observed the test from a separate control room through thick glass windows.

For each test run the following procedure was followed:

1. Data Operator supplies power to the thrust and torque cells to allow sufficient warm-up time (5 minutes).
2. Pilot performs pre-operation safety inspection of helicopter, mounting structure, and test area.
3. Data Operator records ambient pressure and temperature.
4. Pilot turns on transmitter and then connects battery to helicopter receiver.
5. Pilot clears test area of personnel and returns to control room.
6. Data Operator records thrust and torque readings as a zero level tare.
7. Pilot increases throttle to full, quickly passing through helicopter resonance frequency (300 RPM, 5 Hz).
8. Pilot alerts Data Operator when helicopter throttle/RPM is steady.
9. Data Operator records 5 seconds of thrust, torque, and RPM data.
10. Data Operator alerts Pilot to adjust throttle to next setting.

11. Pilot adjusts throttle to next setting on test matrix.
12. Steps 8–11 are repeated until battery is low (around 3 minutes).
13. Pilot reduces throttle to zero, allows rotor to spin down.
14. Data Operator records thrust and torque as an end tare (to compare against starting tare).
15. Pilot disconnects battery from receiver and then turns off transmitter.
16. Pilot performs post-operation safety and structural checks on helicopter.
17. Data Operator post-processes and checks data for quality.

5 Hover Performance Prediction Method

5.1 Tare profile power estimation

The helicopter model has rotating elements besides the blades that do not contribute to lift. Their power consumption is referred to as tare profile power in hover. The stabilizer bars, paddles, and blade attachment grips are included in this category. There is also inevitably a small power loss in the main rotor and tail rotor bearings. These losses were accounted for by measuring the torque on the helicopter without blades attached.

The blade grips were blocked-in to simulate an attached blade root and a normal test procedure was followed. The results showed that at operating rotor speed (1,500 RPM) the tare profile power was about 0.0115 hp, and the thrust from these elements was -0.07 lb. These results represent about 2% of full-scale power and less than 1% of full-scale thrust.

5.2 Validation of analysis method

As a check for the hover performance program, the analysis code was benchmarked against a classic hovering rotor experiment performed by NACA [Harrington 1951]. The results of the analysis were found to closely match the experimental results (Figure 89).

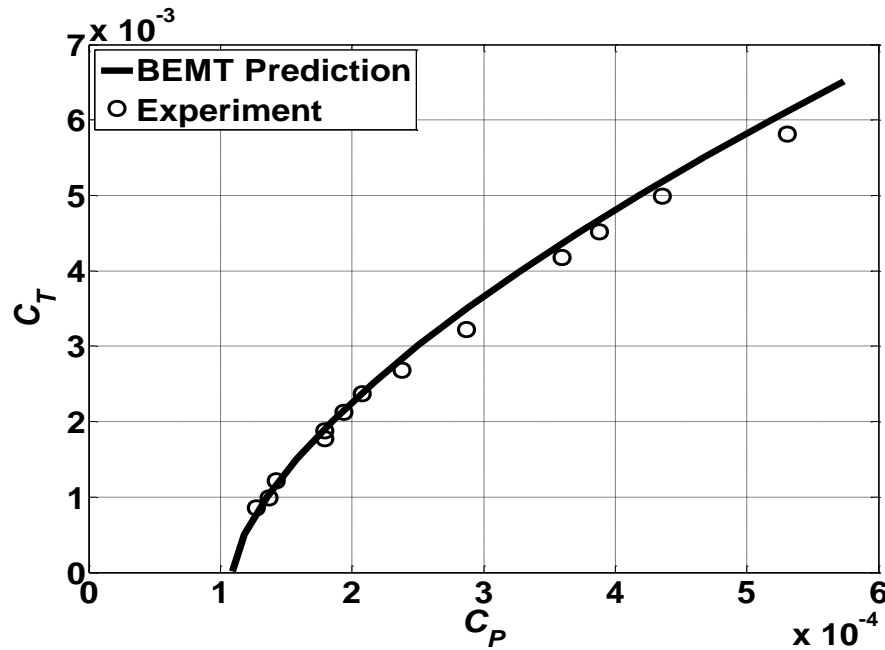


Figure 89: Comparison of hover theory with NACA experiment [Harrington 1951]

6 Baseline Rotor Testing

6.1 Rotor description

The baseline main rotor blades were constructed of laminated wood covered in a Mylar film. The airfoil thickness was measured to be 15% of the chord, and the airfoil closely resembled the NACA 0015. The blades were of constant chord and thickness along the span, with no pre-twist. The baseline rotor specifications are presented in Table 37.

Table 37: Baseline rotor geometry

Rotor diameter (in)	46.5
Number of blades	2
Blade chord (in)	1.71
Rotor solidity	0.047
Hover disk loading (lb ft^{-2})	0.41
Max airfoil thickness (inches, % chord)	0.25, 15%
Airfoil profile	NACA 0015
Tip Reynolds number (at 1,500 RPM)	275,000
Blade weight, per blade (lb)	0.14

6.2 Testing results

The RC helicopter was first tested in an unaltered “out-of-the-box” state. Five tests were performed over a five day period, with thrust, torque, and rotor RPM being recorded. Ambient pressure and temperature were also recorded to calculate air density. The power polar results are shown in Figure 90, with all results normalized to sea level standard day density conditions.

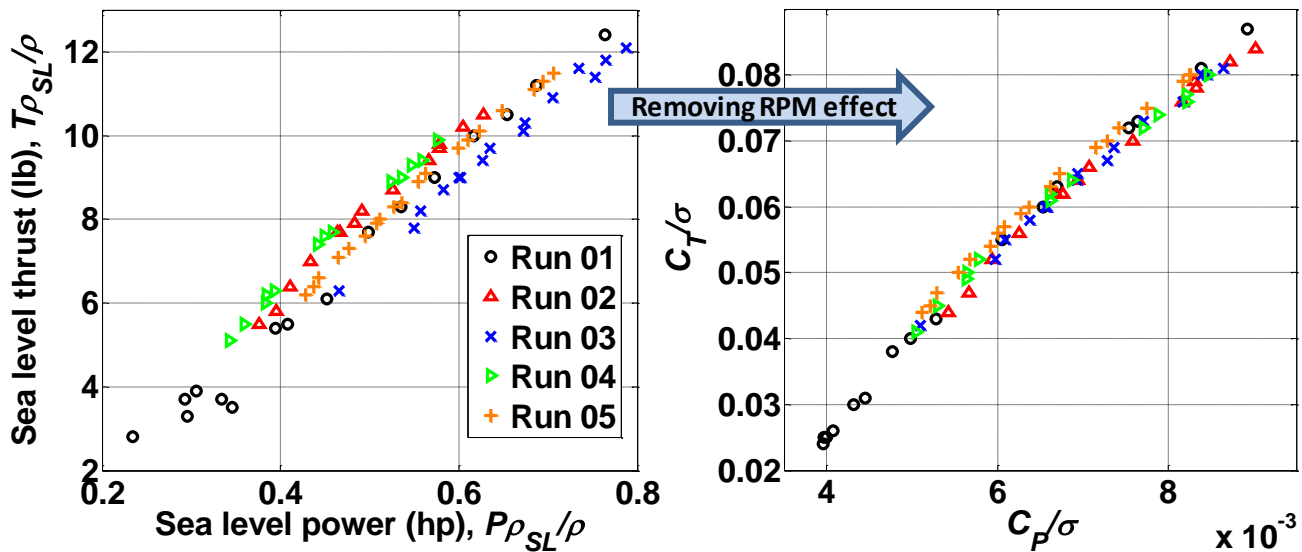


Figure 90: Baseline rotor power polars to show effect of rotor RPM

Each color/shape in Figure 90 represents a different test case, and within test runs the data is tightly correlated. The variation between tests was caused by rotor RPM variations; the throttle stick controls both collective pitch and rotor RPM in a pre-programmed manner by the manufacturer. RPM is also dictated by the voltage delivered from the battery. During different tests of the baseline rotor, the operating rotor RPM would vary depending on these factors.

To account for RPM variations the results were then plotted as blade-loading and power coefficients normalized by rotor solidity (Figure 90, right). The baseline test results are now collapsed into a tighter curve with a $\pm 2\%$ scatter. It shows that the differences in the dimensional plot were because of operating conditions and not because of experimental errors. This outcome increased confidence in the test setup, data acquisition system, and post-processing methods.

Baseline thrust and power benchmark:

The experimentation task goal was to increase the baseline lift of the helicopter by at least 5% at a given power setting. Therefore, a thrust and power setting benchmark was set by the baseline results, and used to evaluate the alternate configurations.

Because of the strong influence of RPM on rotor efficiency, the baseline benchmark was set at a specific rotor speed of 1500 RPM. All modified rotor results were compared to the baseline benchmark at the same RPM and power setting. Operation at identical RPM and power setting also ensured that the rotor torque was equivalent, and therefore tail rotor power consumption would not vary between rotor types in an operational flight situation.

The benchmark power setting was selected to be 0.6 hp, which was near the maximum power consumed by the baseline rotor for the 1500 RPM case. The baseline rotor at these conditions produced **10.1 \pm 0.2 lb thrust at 0.6 hp**.

6.3 Correlation

The BEMT analysis code was correlated to the baseline rotor system using the following assumptions and factors:

- Download factor = 0.11
- Tare power = 0.0115 hp
- Tare thrust = -0.07 lb
- NACA 0015 lift curve slope $C_{l\alpha} = 0.10 \text{ deg}^{-1}$
- NACA 0015 C_{d0} at 75% radius ($Re = 200,000$): 0.014

The results of the correlation are shown in Figure 91. The 75% radius zero-lift drag coefficient of 0.014 was found to under-predict power required. Increasing the zero-lift drag coefficient from 0.014 to 0.024 shifted the analysis curve to give a tight correlation with the experimental data over the entire operational range. This drag coefficient is an acceptable value for model rotors at Reynolds numbers in the transition range, especially for blades of this construction quality and material.

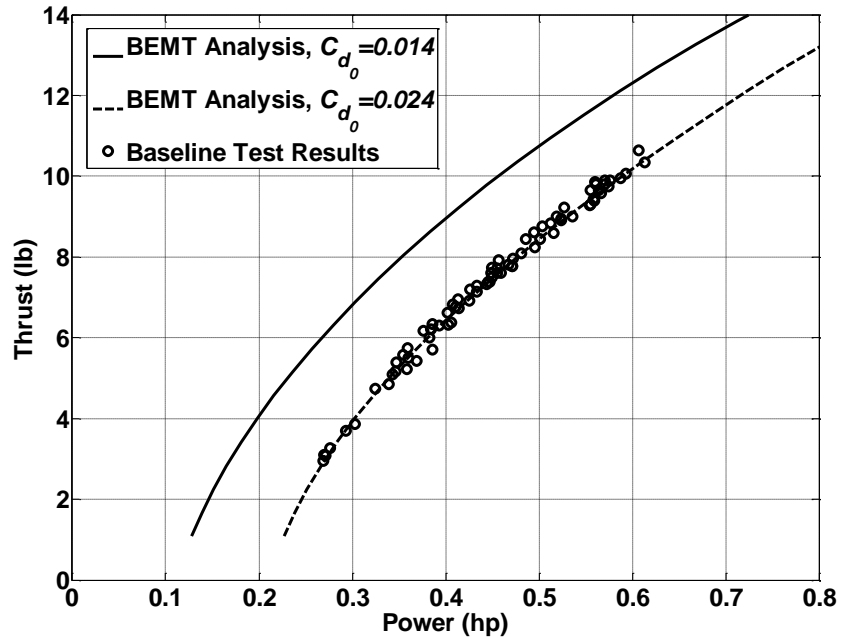


Figure 91: Correlation of baseline rotor results with predictions for sea-level density and 1,500 RPM rotor speed

7 Experimental Trade Studies

The RFP stated that a modification must be made that is predicted to increase the lifting capability by at least 5% for the same power setting. The extent and nature of the modification to increase lifting capability was not specifically defined or constrained in the RFP. The increase in lifting capability for a given power setting is most influenced by the main rotor efficiency. Helicopter rotor efficiency in hover is typically improved by adding blade pre-twist to provide more uniform inflow, incorporating blade taper to more optimally distribute lift, increasing rotor radius to reduce disk loading, and/or improving the blade airfoil sections to reduce profile drag.

These modifications were considered and used to varying extents in the four modifications that were implemented. The sensitivity of rotor performance to various potential modifications was explored using the correlated hover performance code. Each of the following sections contains experimental results from hover tower testing as well as the theory prediction/correlations.

7.1 Increased blade loading coefficient

After reviewing the baseline blade loading coefficient results (shown previously in Figure 90) it was determined that the rotor in its out-of-the-box configuration was operating with a fairly generous stall margin (i.e., at low blade loading coefficients). This significant margin allows RC helicopter pilots to perform aerobatic maneuvers without stalling the rotor. For the current heavy-lift application, large stall margins in hover are not required. Typically helicopter rotors can operate at blade loading coefficients in the region of 0.12 and beyond before approaching stall.

The implication is that the rotor can be made to produce the same thrust with less power required by increasing the collective pitch while reducing the rotor RPM. The profile power consumption scales approximately with the cube of the rotor tip speed, so reducing the RPM (while maintaining thrust via increased collective) will reduce the power required. Operating the rotor at higher collectives for similar thrust is additionally more efficient because the airfoil sections are operating closer to their maximum L/D ratio, and hence a better rotor figure of merit is expected.

7.1.1 Performance prediction

The correlated BEMT model from Section 6.3 was used to investigate the effect of lowering RPM on performance. The analysis shown in Figure 92 shows that lower RPM operation results in higher thrust for the same required power.

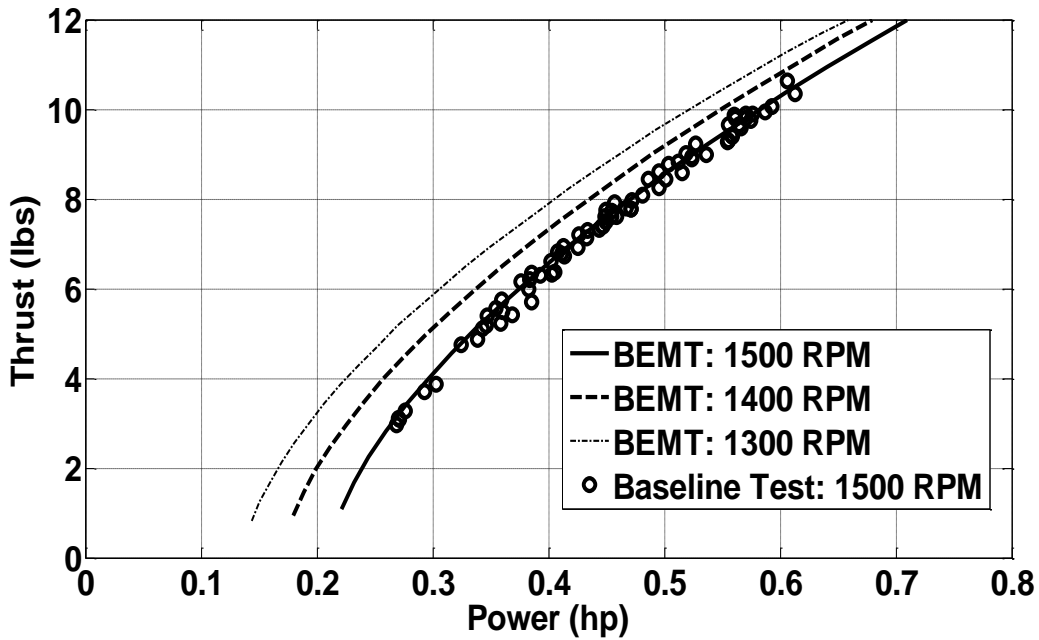


Figure 92: Predicted effect of rotor speed changes

At the benchmark power of 0.6 hp, decreasing the RPM from 1,500 to 1,400 was predicted to increase rotor thrust by 5%, with 10% gains at 1,200 RPM operation. It is apparent that reducing RPM when large stall margins are not required gives a significant reduction of rotor power required.

7.1.2 Implementation

Direct control over rotor RPM requires reprogramming the on-board speed controller and was not attempted. To increase the blade-loading coefficient of the baseline configuration, the control linkages were mechanically biased to operate at higher collective pitch angles for the same throttle stick range. In this manner the speed controller could be “tricked” into operating consistently at lower rotor speeds when it senses higher torque at lower throttle settings.

7.1.3 Results

The baseline blades operating at higher blade-loading coefficients produced 4% more thrust at a power setting of 0.6 hp. Results normalized to sea level density are shown in Figure 93. Two cases that were operating at similar rotor speeds (1500 ± 20 RPM) were selected for comparison.

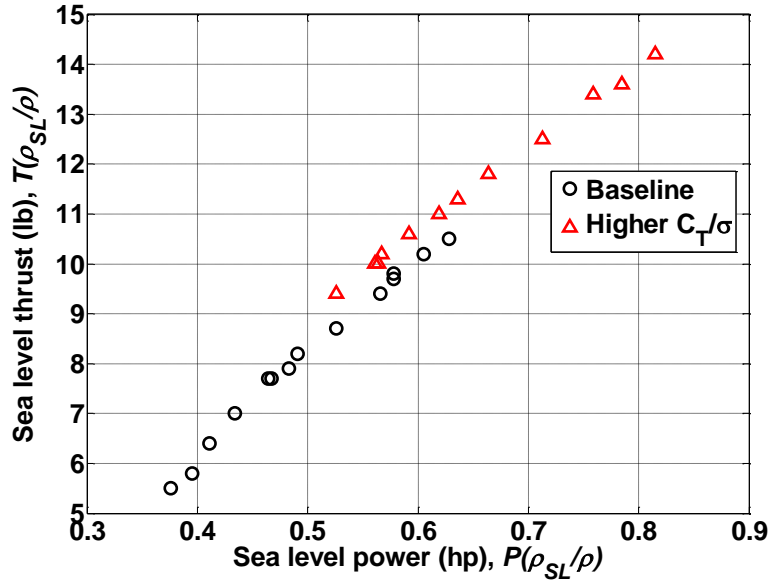


Figure 93: Results for the baseline rotor with increased blade loading coefficient at 1,500 RPM

Overall, it was clear that the rotor was now operating more efficiently. At the 0.6 hp power level, the rotor with slightly lower RPM (1,480 RPM compared to 1,510 RPM for the baseline) and increased collective pitch produced about 4% more thrust (10.55 lb compared to 10.12 lb). It was clear that if the speed controller could be reprogrammed to operate at a lower RPM, then the thrust could be increased even higher for the same power requirements.

The power polar plot in Figure 94 shows that the blade loading coefficients were greatly increased. Rotor performance began to degrade for blade loading coefficients around 0.14. This plot also shows that when the effect of rotor RPM is removed, the new data collapses into the same general trend for the baseline points.

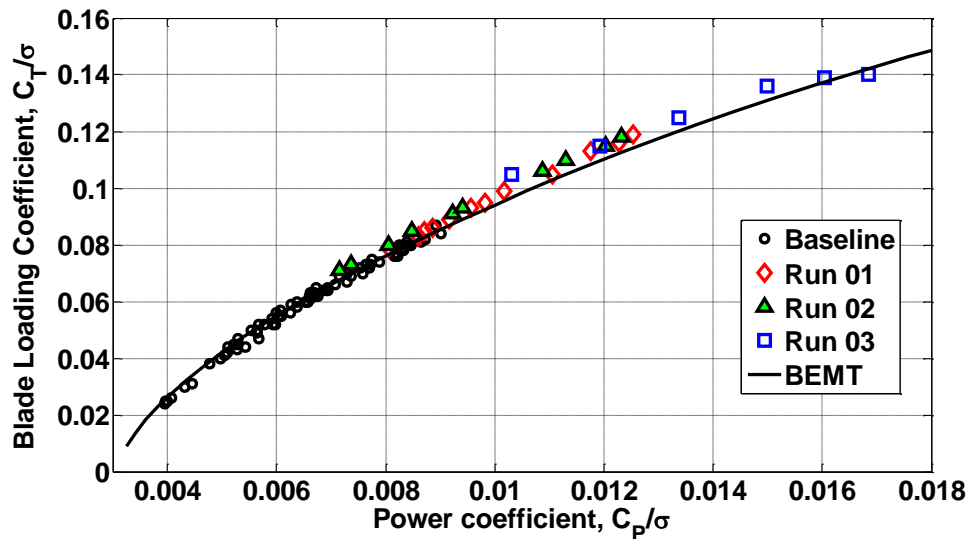


Figure 94: Blade loading coefficients for the baseline rotor with increased collective pitch biasing

7.2 Twisted baseline blades

Pre-twisted blades (nose-down at the tip) are used in hovering rotors to create a more uniform inflow to decrease induced power requirements.

7.2.1 Prediction

The BEMT code was run on the baseline blades for varying linear twist rates. Figure 95 shows the power required as well as the component powers (induced and profile). Higher twist rates reduce the induced power required, as expected, but at high twist rates the profile power term begins to increase. The performance gains at high thrust reached a maximum at around a -20° twist rate. Beyond that, the performance gains start to decrease and at low thrusts the twisted rotor performs worse than the baseline. Therefore a value of 20° nose-down twist was attempted. BEMT predicted a 6% increase in thrust at 0.6 hp for a -20° twisted rotor.

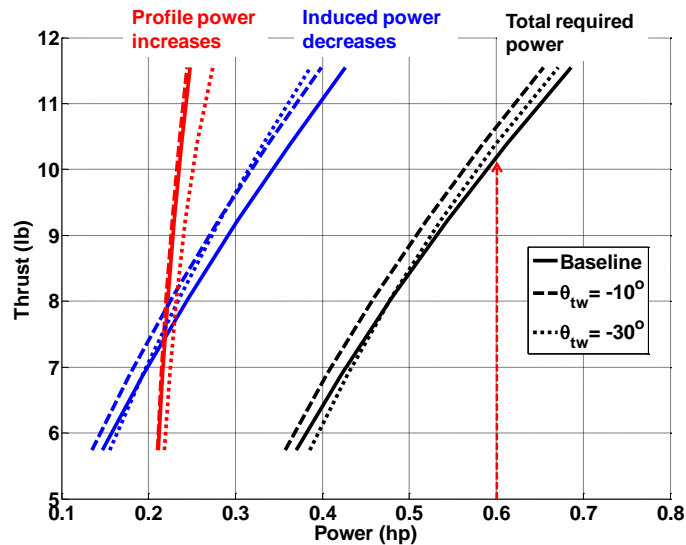


Figure 95: Effect of twist on hovering performance of baseline blades

7.2.2 Implementation

A custom jig was constructed to twist the baseline blades to a specific pre-twist angle (Figure 96). The baseline wooden blades were stripped of their factory installed Mylar covering and soaked overnight in water and then placed in the jig for approximately 12 hours. Because wooden blades experience spring-back once taken out of the jig, a -30° twist was introduced on the mold to arrive at a final twist of -20° . After the blades were dried and taken out of the jig, they were recovered with Mylar to match the surface finish of the baseline blades.



Figure 96: Jig built to impart nose-down twist to the baseline blades

7.2.3 Results

The twisted baseline blades produced less thrust at nearly all power settings tested compared to the unmodified baseline blades. There was a 9% decrease in thrust at 0.6 hp and 1,500 RPM. This result was counter to rotor theory and the BEMT predictions. Several reasons for this discrepancy were theorized:

- 1) The Mylar surface on the blades was noticeably wrinkled in certain locations, which could easily increase profile drag enough to account for the performance degradation.
- 2) The applied twist may have remained high enough to cause inboard sections (operating at higher angles of attack and lower Reynolds numbers) to operate in stall at high thrusts. As the local Reynolds numbers decreases below 200,000, airfoil stall angle and maximum lift coefficient decrease rapidly. This creates a situation where the NACA 0015 airfoil, while relatively thick, might exhibit thin airfoil stall characteristics such as laminar separation bubbles (abrupt leading-edge stall) [Leishman 2006]. The performance of twisted blades in low Reynolds number operation may therefore not behave as expected.

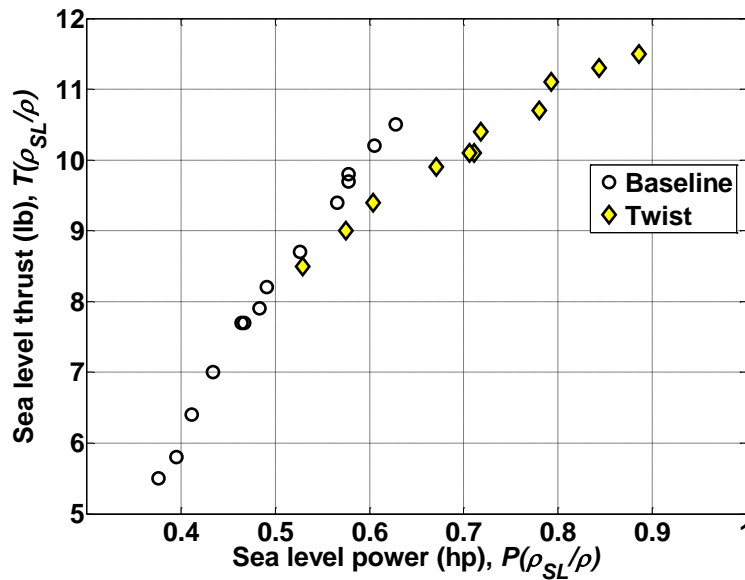


Figure 97: Results for baseline blades with added twist for 1,500 RPM

7.3 Alternate COTS blades

A set of “high performance” commercial off-the-shelf (COTS) rotor blades were purchased for testing and evaluation (see Figure 98). The blades had a larger radius, longer chord, blade tip taper, and a thinner airfoil compared to the baseline rotor. The surface finish and quality of the blades was also superior to the baseline blades, as was the bending and torsional stiffness. The specifications of the alternate COTS blades are given in Table 38.



Figure 98: Alternative OTS carbon fiber blades

Table 38: Alternate OTS rotor geometry

Rotor diameter (in)	49
Number of blades	2
Blade chord (in), root to 0.92 R	2.0
Tip chord (in) (tip taper)	1.25
Hover disk loading (lb ft ⁻²)	0.37
Rotor solidity, thrust-weighted	0.0498
Max airfoil thickness (inches, % chord)	0.28, 14%
Airfoil profile	NACA 0014
Tip Reynolds number (at 1,500 RPM)	338,000

7.3.1 Performance prediction

The following assumptions were used in the BEMT program to predict performance of the COTS blades:

- Download factor: 11% of thrust
- Tare power = 0.0115 hp
- Tare thrust = -0.07 lb
- NACA0014 lift curve slope $C_{l\alpha} = 0.10 \text{ deg}^{-1}$
- NACA0014 C_{d0} at 75% radius (Re = 250,000): 0.012

The BEMT prediction is shown correlated to the test results in the next section.

7.3.2 Results

The alternate COTS blades produced 25% more thrust than the baseline rotor at 0.6 hp. The predictions for the COTS blades agreed remarkably well with the test results. While the baseline rotor prediction required a shift of the zero-lift drag coefficient to obtain correlation, the COTS test results matched theory that used a smooth airfoil assumption. When re-running the COTS analysis assuming the same drag coefficient as the baseline blades, 0.024, the prediction correlates well with the baseline blades. This result further reinforces the significant effect of airfoil section profile drag on rotor performance above the small increase in radius or tip taper.

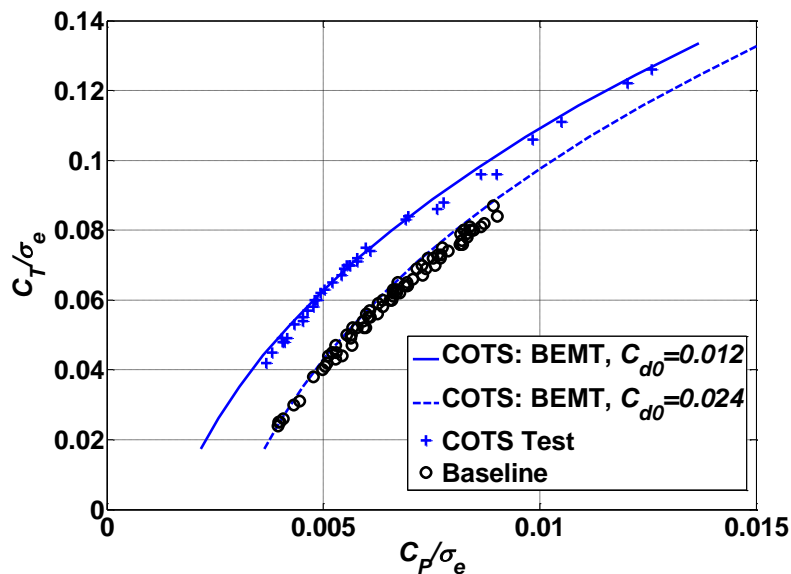


Figure 99: Power polar for the alternate COTS blades with BEMT correlation

8 Modifications: UMD Optimized Blades

Up to this point the test results have been for off-the-shelf blades, with the exception of the twisted blades. The alternate set of COTS blades far exceeded the RFP-required 5% lift improvement, and excellent correlations to analysis were obtained. However, it was decided that fulfillment of the RFP should involve the design and implementation of a custom modification, preferably not an off-the-shelf solution.

Therefore, the experience gained from the experimental trade studies and the capabilities of BEMT modeling were leveraged to design and optimize rotor blade geometry. The team realized the custom geometry through a wet lay-up composite blade fabrication process under high-standards of quality control to ensure high performance.

8.1 Blade geometry design studies

The modified rotor was kept to the same diameter as the baseline rotor. Increasing rotor area, holding all else constant, increases rotor efficiency by reducing disk loading and hence reducing induced power requirements. However, increasing rotor diameter is not always a practical solution for in-service vehicles due to operational footprint constraints and blade structure limits. Therefore, it was decided to match the baseline rotor diameter to remain in the spirit of the RFP goals.

The baseline airfoil profile was symmetric and had a medium thickness-to-chord ratio (nominally a NACA 0015). The Eppler 387 airfoil was selected as a replacement because of higher lift-to-drag ratio at the operating Reynolds numbers of the blades [Schroeder 2005].

Taper has a large effect on profile power and was shown to provide large performance improvements in figure of merit for small amounts of tip taper (see Figure 100). A tip taper ratio of 4:1 was used, which started at 80% radius. The equivalent thrust-weighted solidity of the rotor was kept equal to the baseline blades. Typically a lower solidity reduces profile power consumption; however, in this application lower blade chord decreases the Reynolds number further, which drives up the profile drag. Another reason not to decrease chord in this situation was that a certain size and thickness was necessary for blade bending stiffness and axial strength.

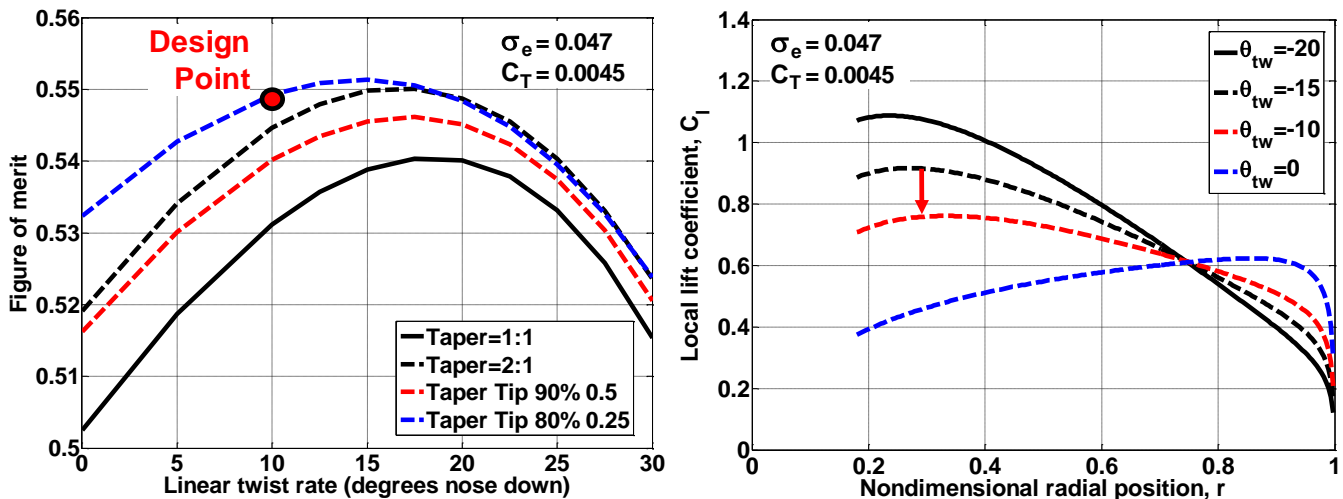


Figure 100: Twist and taper trade study results

Blade pre-twist was used despite the poor results of the twisted baseline blades. Analysis revealed that at twist rates beyond -15° the inboard sections of the blade may be operating in stall. The maximum lift coefficient decreases with Reynolds number and high values of negative pre-twist put the inboard sections of the blade at higher angles of attack. Therefore, a moderate amount of linear twist of -10° per radius was used to obtain the benefits of a more uniform inflow without keeping the inboard blade sections below stall angles (see Figure 100). The improvements in taper and twist were predicted to increase thrust by 9%, while the new airfoil and potentially superior surface finish has the potential for even greater gains (as evidenced by the previously-tested COTS blades). The BEMT code predicted a 22% increase in thrust for a constant power setting of 0.6 hp.

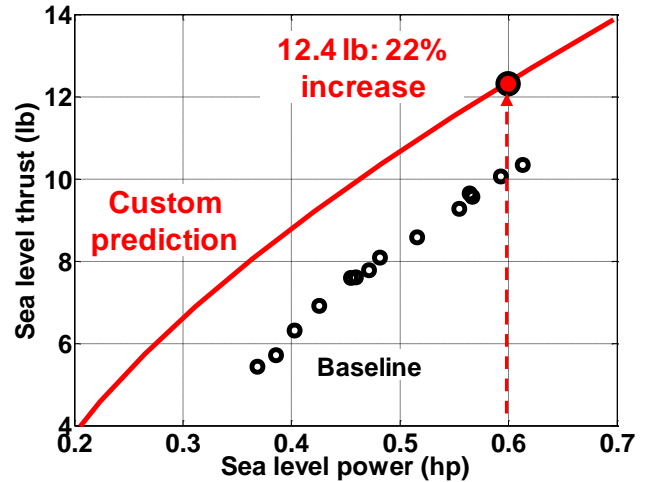


Figure 101: Prediction of custom optimized blade performance

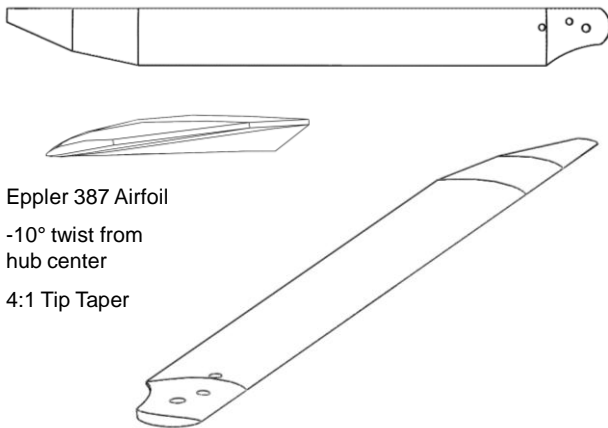


Table 39: UMD custom rotor blade geometry

Rotor diameter (in)	46.5
Number of blades	2
Blade chord (in), root to 0.80 R	2.16
Tip chord (in) (tip taper)	0.64
Hover disk loading (lb ft^{-2})	0.41
Rotor solidity, thrust-weighted	0.047
Max airfoil thickness (inches, % chord)	0.22, 10%
Airfoil profile	Eppler 387
Tip Reynolds number (at 1,500 RPM)	275,000
Finished blade weight, per blade (lb)	0.31

8.2 Manufacturing

Because of the complex blade geometry, the desired geometry was entered into a 3-D CAD model and constructed using a rapid-prototyping Stereolithography (SLA) process. The SLA material alone had insufficient stiffness or strength to support estimated blade bending and centrifugal root loads. Therefore the SLA blade was wrapped with a 1.5" carbon-fiber bi-weave sleeve using the SLA material core as a male mold (see foldout for manufacturing process).

The COTS blades appeared to be constructed using precision molds to obtain a uniform and hardened surface that does not deform during operation. Therefore attention in the manufacturing process was directed at ensuring a high-quality surface finish. The blades were placed in a female clamshell mold made of hard plastic to prevent the fiber weave texture from appearing on the finished surface.

A linearly-twisted female mold was created out of foam to enforce the blade twist during the wet lay-up curing process. The blades were then placed in a vacuum bag for 12 hours until cured solid. The carbon fiber bi-weave composite greatly increased the torsional



Figure 102: Blade root of optimized custom blades



IN-HOUSE DESIGN. OUT-OF-THIS-WORLD PERFORMANCE.

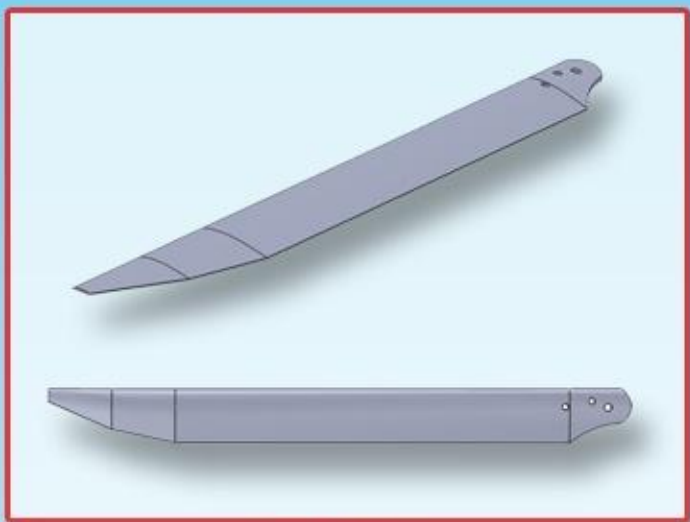


Design of Optimized RC Helicopter Blades

Airfoil: Eppler 387

Twist: -10°

Taper: 4:1 Tip Taper



CAD Design



Rapid Prototype Core and Plastic Clamshell Mold



Bi-Weave Carbon Fiber Sleeve

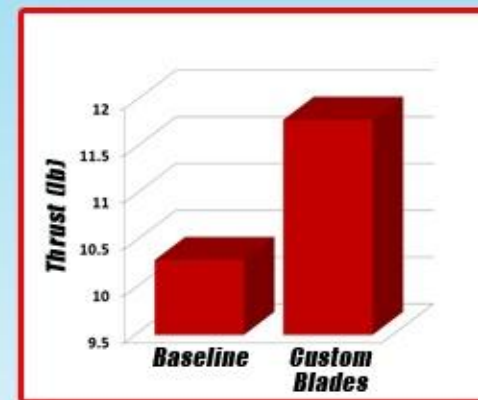
Provides Exceptional Torsional Rigidity

Wet Lay-Up Process



Mounting of Helicopter on UMD Alfred Gessow Rotorcraft Center Hover Stand

Result: 17% Increase in Thrust for Same Power Setting



Finished Blade Mounted on Helicopter



Removal from Vacuum Bag



12 Hours Under Vacuum



10° Linearly Twisted Female Foam Mold

Enforces Blade Twist

Custom Blade Design, Construction, and Testing

8.3 Testing results

The custom designed and manufactured blades produced a 17% increase in thrust over the baseline blades at 0.6 hp. The original BEMT prediction over-predicted the thrust gain at 0.6 hp. The surface finish of the blades was excellent considering they were in-house-built blades; but there were still some surface imperfections from the lay-up process, mainly a few small leading and trailing edge pits and voids. A sweep of drag coefficients found that right correlation was achieved with a zero-lift drag coefficient of 0.018. This is much lower than the baseline blades (0.024) but was higher than the COTS blades (0.012). This was considered a reasonable result.

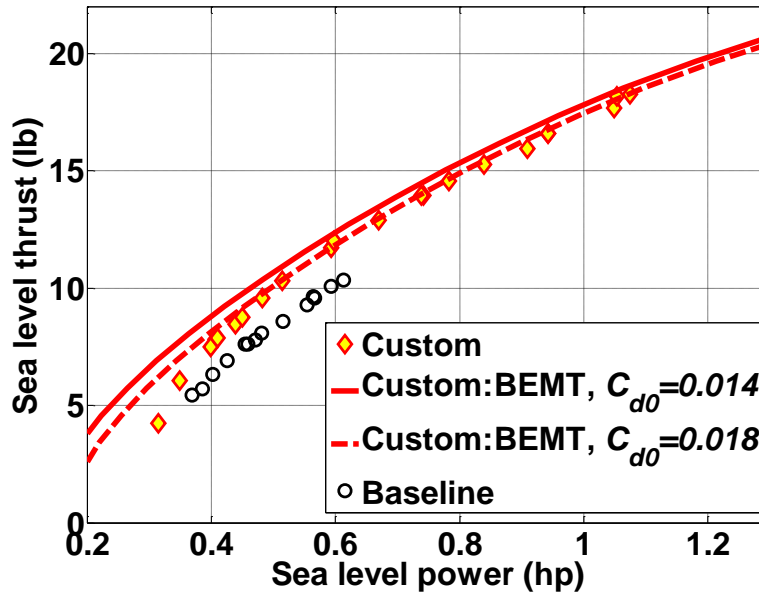


Figure 103: Custom blade results, sea level thrust vs. power

9 Test Program Conclusions

A COTS helicopter of 46.5 in rotor diameter was purchased and tested for thrust and power on a hover tower test stand. Guided by rotor performance theory, modifications to the main rotor were designed and implemented in an effort to increase baseline helicopter lift by at least 5% for a constant power setting of 0.6 hp. Several rotor blades were tested on the helicopter (see Figure 104) with the results being correlated to predictions to gain insight into the aerodynamic effects.

These results—along with rotor theory—guided the design and construction of custom optimized blades. The University of Maryland’s custom-designed and built blades incorporated lower-drag airfoil sections, blade pre-twist, and tip taper. The SLA core and composite skin construction methods ensured a smooth surface finish and a stiff construction, further increasing performance.



Figure 104: Baseline and modified rotor blades

10 Test Program Conclusions

The results of the optimized blades compared with the baseline rotor is shown in Figure 105. These blades increased rotor thrust by **17% at a constant power required of 0.6 hp**. Since the RFP specified helicopter *lift* being the criteria (not rotor thrust), the weight of the blades needs to be accounted for. The custom blades were made with a relatively heavy SLA core. A pair of UMD custom blades increase the weight of the helicopter by 0.34 lb over the baseline blades. Therefore, this extra weight decreases the percentage increase in lift over the baseline configuration. However, the RFP requirements of a 5% increase are still well-exceeded, with the **UMD custom optimized blades increasing net helicopter lift by 14%**.

Table 40: Lift increase of modified blades (0.6 hp)

	Rotor Thrust (lb)	Helicopter Lift (lb)
Baseline Blades	10.12	10.12
UMD Optimized Custom Blades	11.86 (+17%)	11.52 (+14%)

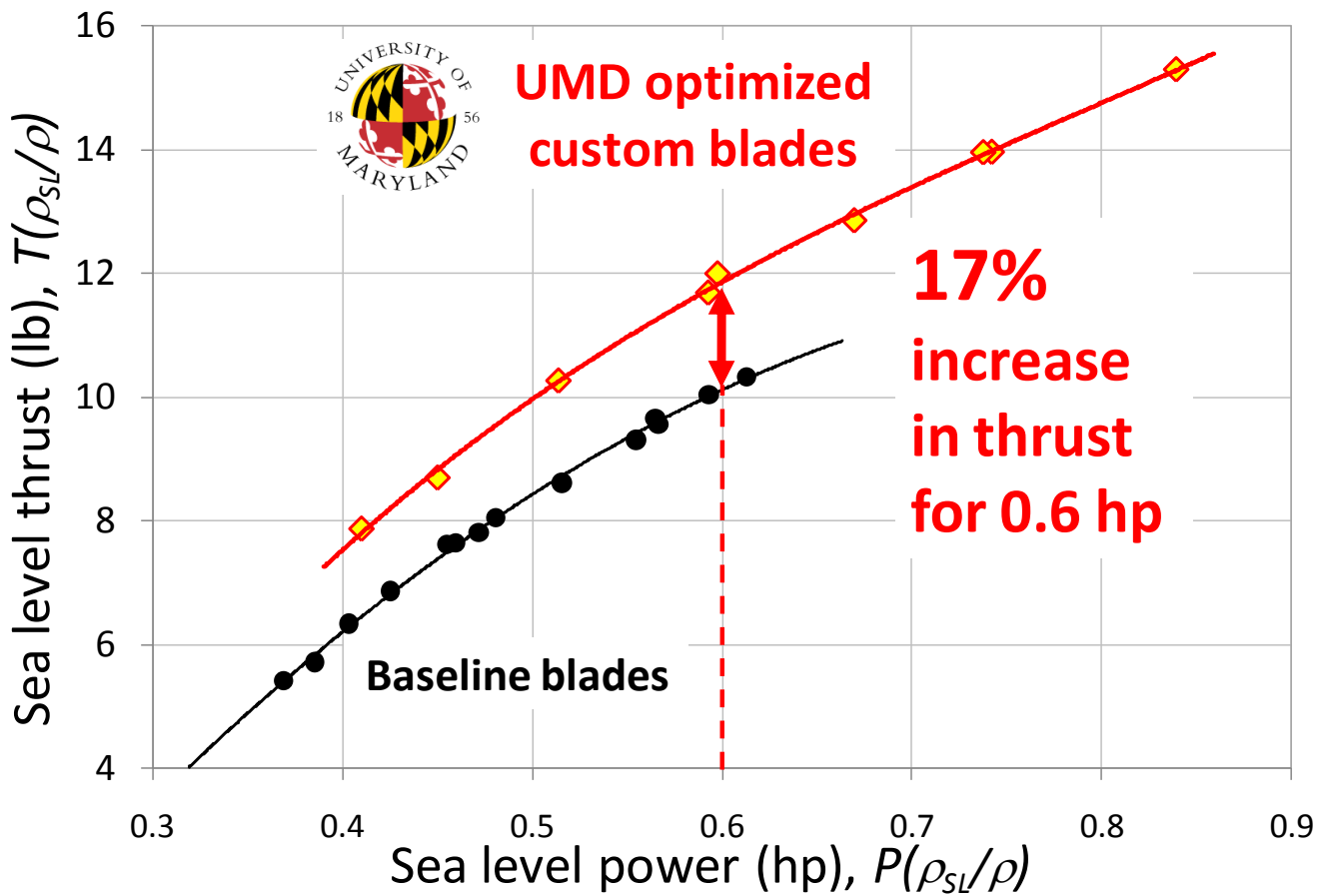


Figure 105: Power polar of the UMD optimized blades compared to the baseline blades

References:

- [Bisgaard 10] Bisgaard, M., Cour-Harbo, A. and Bendsten, J.D., "Adaptive Control System for Autonomous Helicopter Slung Load Operations", *Control Engineering Practice* (2010), doi: 10.1016/j.conengprac.2010.01.017
- [Bousman 03] Bousman, William G., "Aerodynamic Characteristics of SC1095 and SC-1094R8 Airfoils," NASA/TP-2003-212265 AFDD/TR-04-003, December 2003.
- [Bush et. al. 08] Bush, Brandon et. al., "The Volterra-Environmentally Friendly VTOL Concept Design: Volterra," American Helicopter Society Student Design Competition 2008.
- [Cicolani 02] Cicolani, L. and Ehlers, G., "Modeling and Simulation of a Helicopter Slung Load Stabilization Device", American Helicopter Society 58th Annual Forum, Montreal, Canada, June 11-13, 2002.
- [Cicolani 07] Cicolani, L., Cone, A., Theron, J. N., Raz, R., Gordon, R., Tischler, M., Lursadi, J. and Robinson, D., "Flight Test, Simulation and Passive Stabilization of a Cargo Container Slung Load in Forward Flight", American Helicopter Society 63rd Forum, Virginia, May 1-3 2007.
- [Curtiss 85] Curtiss, H.C. (Jr) and Warburton, F.W., "Stability and Control of the Twin Lift Helicopter System", *Journal of the American Helicopter Society*, April 1985, pp 14-23.
- [Dukes1 72] Dukes, T.A., "Maneuvering Heavy Sling Loads Near Hover Part I: Damping the Pendulous Motion", 28th Annual National Forum of the American Helicopter Society, May 1972.
- [Dukes2 72] Dukes, T.A., "Maneuvering Heavy Sling Loads Near Hover Part II: Some Elementary Maneuvers", 28th Annual National Forum of the American Helicopter Society, May 1972.
- [Gabel 68] Gabel, R. and Wilson, G.J., "Test Approaches to External Sling Load Instabilities", *Journal of the American Helicopter Society*, July 13, 1968, pp 44-55.
- [Harris 98] Harris, Franklin D. and Scully, Michael P., "Rotorcraft Cost Too Much," *Journal of the American Helicopter Society*, 43, 1, 1998, pp. 3-18.
- [Heffley 79] Heffley, R.K., Jewell, W.F., Lehman, J.M. and Van Winkle, R.A., "A Compilation and Analysis of Helicopter Handling Qualities Data: Volume One: Data Compilation", NASA Contractor Report 3144, August 1979.
- [Hoh 06] Hoh, R.H., Heffley, R.K. and Mitchell, D.G., "Development of Handling Qualities Criteria for Rotorcraft with Externally Slung Loads", NASA/CR- 2006 – 213488, October 2006.
- [Kendrick 06] Kendrick, S.A. and Walker, D.J., "The Modeling Simulation and Control of Helicopters Operating with External Loads", 62nd Annual National Forum of the American Helicopter Society, Phoenix, AZ, May 9-11, 2006.
- [Krulak 99] "Operational Maneuver From the Sea: A Concept for the Projection of Naval Power Ashore", General Charles C. Krulak, Commandant of the U.S. Marine Corps, 1999.
- [Leishman 06] Leishman, J.G., *Principles of Helicopter Aerodynamics*, Cambridge Press, 2006, pp.
- [Leishman 07] Leishman, J.G., *The Helicopter, Thinking Forward Looking Back*, College Park Press, 2007, pp. 16–18.
- [Lucassen 65] Lucassen, L.R. and Sterk, F.J., "Dynamic Stability Analysis of a Hovering Helicopter with a Sling Load", *Journal of the American Helicopter Society*, (10) April 1965, pp 6-12.
- [Mahaney 01] Operational Durability: The Marines and Operational Maneuver from the Sea, Major Michael P. Mahaney USMC, Jan 2001, School of Advanced Military Studies, US Army Command and General Staff College.

- [Maza 10] Maza, I., Kondak, M., Bernard, M. and Ollero, A., "Multi-UAV Cooperation and Control for Load Transportation and Deployment", *Journal of Intelligent Robotics Systems*, (2010) 57:417-449
- [Menon 88] Menon, P.K.A., Schrage, D.P. and Prasad, J.V.R., "Nonlinear Control of a Twin-Lift Helicopter Configuration", *Journal of the American Institute of Aeronautics and Astronautics*, 1988.
- [Mittal 89] Mittal, M., Prasad, J.V.R. and Schrage, D.P., "Comparison of Stability and Control Characteristics of Two Twin-Lift Helicopter Configurations", *Journal of the American Institute of Aeronautics and Astronautics*, 1989.
- [Mittal 90] Mittal, M., Prasad, J.V.R. and Schrage, D.P., "Nonlinear Adaptive Control of a Twin Lift Helicopter System", *American Control Conference*, San Diego, CA, May 23-25 1990.
- [Mittal 91] Mittal, M. and Prasad, J.V.R., "Input-Output Linearization of a Three-Dimensional Model of a Twin-Lift Helicopter System", *AIAA Guidance, Navigation and Control Conference*, New Orleans, LA, Aug 12-14, 1991, Technical Papers V.
- [Mittal 92] Mittal, M., Prasad, J.V.R. and Schrage, D.P., "Comparison of Nonlinear Controllers for Twin-Lift Configurations", *Journal of Nonlinear Dynamics*, 3: 199-223, 1992.
- [Navy 09] "Minimum Fuel Requirements", *NATOPS General Flight and Operating Instructions*, OPNAV Instruction 3710.7U, Section 4.8.5.1, Dept. of the Navy, November 23, 2009.
- [O'Keefe 92] "...From the Sea", *Navy and Marine Corps White Paper*, Naval Doctrine Command, Sean O'Keefe, Secretary of the Navy, September 1992 <http://www.globalsecurity.org/military/library/policy/navy/fts.htm#Operating>
- [Prasad 91] Prasad, J.V.R., Mittal, M. and Schrage, D.P., "Control of a Twin Lift Helicopter System using Nonlinear State Feedback", *Journal of the American Helicopter Society* 36, 57 (1991).
- [Poli 72] Poli, C. and Cromack, D., "Dynamics of Slung Bodies Using a Single-Point Suspension System", Paper 72-986, *American Institute for Aeronautics and Astronautics*, 2nd Atmospheric Flight Mechanics Conference, Paolo Alto, CA, September 11-13, 1972, pp 80-86.
- [Prouty 86] Prouty, R. W., *Helicopter Performance, Stability and Control*, R.E. Kieger, Malabar, 1986.
- [Raz 05] Raz, R. and Rosen, A., "Trim and Stability Analysis of a Twin-Lift System in Forward Flight", *Journal of the American Helicopter Society*, April 2005, pp 138-149.
- [Reynolds 92] Reynolds, K.H. and Rodriguez, A.A., " ∞ Control of a Twin Lift Helicopter System", *Proceedings of the 31st Conference on Decision and Control*, Tuscon, Arizona, December 1992, pp 2442-2447.
- [Schulz 03] Schulz W.E., Musatow M., Jiang C., Higgins C., Albus J., Bostelman R., "Skin-to-Skin Replenishment", *National Institute of Standards and Technology: Intelligent Systems Division*, NIST Report, 2003.
- [Sheldon 77] Sheldon, D.F., "An Appreciation of the Dynamic Problems Associated with the External Transportation of Loads from a Helicopter – State of the Art", *Vertica*, 1977, Vol I, pp 281-290.
- [Sikorsky 09] CH-53K Proposed OMFTS Mission, CH-53K Promotional Brochure, Sikorsky Aircraft, 2009.
- [Sturgeon 93] Sturgeon, William R., Phillips, James D., "A Mathematical Model of the CH-53 Helicopter," *NASA Technical Memorandum 81238* NASA Ames Research Center, Moffett Field, California, 1993.
- [Sullivan 09] Sullivan, Michael J. "V-22 OSPREY AIRCRAFT Assessments Needed to Address Operational and Cost Concerns to Define Future Investments," *Testimony Before the Committee on Oversight and Government Reform, House of Representatives United States Government Accountability Office*, June 23, 2009, pp. 8.

[Szustak 71] "Control of Large Crane Helicopters", Szustak, L.S. and Jenney, D.S., Journal of the American Helicopter Society, 1971, pp 11-22.

[Ugone 04] Ugone, Mary, L., "Acquisition of the CH-47F Improved Cargo Helicopter," Report No. D-2004-046, Department of Defense Office of the Inspector General, January 2004, pp. 4.

[USMC 1998] Marine Corps Doctrinal Publication 3: Expeditionary Operations, Department of the Navy, April 1998.

[Yeo 02] Yeo, Hyeonsoo, Bousman, William G., NASA, "Performance Analysis of a Utility Helicopter with Standard and Advanced Rotors," Ames Research Center Moffett Field, California American Helicopter Society Aerodynamics, Acoustics, and Test a